

# GLOBAL-SCALE ATTRIBUTION OF ANTHROPOGENIC AND NATURAL DUST SOURCES AND THEIR EMISSION RATES BASED ON MODIS DEEP BLUE AEROSOL PRODUCTS

Paul Ginoux,<sup>1</sup> Joseph M. Prospero,<sup>2</sup> Thomas E. Gill,<sup>3,4</sup> N. Christina Hsu,<sup>5</sup> and Ming Zhao<sup>1</sup>

Received 9 January 2012; revised 27 April 2012; accepted 4 May 2012; published 8 August 2012.

[1] Our understanding of the global dust cycle is limited by a dearth of information about dust sources, especially small-scale features which could account for a large fraction of global emissions. Here we present a global-scale high-resolution ( $0.1^\circ$ ) mapping of sources based on Moderate Resolution Imaging Spectroradiometer (MODIS) Deep Blue estimates of dust optical depth in conjunction with other data sets including land use. We ascribe dust sources to natural and anthropogenic (primarily agricultural) origins, calculate their respective contributions to emissions, and extensively compare these products against literature. Natural dust sources globally account for 75% of emissions; anthropogenic sources account for 25%. North Africa accounts for 55% of global dust emissions with only 8% being anthropogenic, mostly from the Sahel. Elsewhere, anthropogenic dust emissions can be much higher (75% in Australia). Hydro-

logic dust sources (e.g., ephemeral water bodies) account for 31% worldwide; 15% of them are natural while 85% are anthropogenic. Globally, 20% of emissions are from vegetated surfaces, primarily desert shrublands and agricultural lands. Since anthropogenic dust sources are associated with land use and ephemeral water bodies, both in turn linked to the hydrological cycle, their emissions are affected by climate variability. Such changes in dust emissions can impact climate, air quality, and human health. Improved dust emission estimates will require a better mapping of threshold wind velocities, vegetation dynamics, and surface conditions (soil moisture and land use) especially in the sensitive regions identified here, as well as improved ability to address small-scale convective processes producing dust via cold pool (haboob) events frequent in monsoon regimes.

**Citation:** Ginoux, P., J. M. Prospero, T. E. Gill, N. C. Hsu, and M. Zhao (2012), Global-scale attribution of anthropogenic and natural dust sources and their emission rates based on MODIS Deep Blue aerosol products, *Rev. Geophys.*, 50, RG3005, doi:10.1029/2012RG000388.

## 1. INTRODUCTION

[2] Mineral dust affects climate by absorbing and scattering solar and terrestrial radiation as well as by modifying

cloud properties [Forster *et al.*, 2007]. In addition, dust mediates carbon uptake by providing iron, a limiting nutrient in many ocean regions [Jickells *et al.*, 2005], and phosphorous to land surfaces (e.g., the Amazon forest [Swap *et al.*, 1992]). As one of the most abundant aerosols in the atmosphere, dust has also important implications regarding air quality [Prospero, 1999]. In order to estimate the impacts of dust on climate and air quality, the factors controlling dust emissions must be identified and quantified. This objective has been the focus of numerous studies based on field campaigns, laboratory measurements, satellite data, and model simulations. Still, there are large uncertainties regarding the impact of anthropogenic activities on modulating dust emission directly, e.g., by disturbing soils, removing vegetation

<sup>1</sup>NOAA Geophysical Fluid Dynamics Laboratory, Princeton, New Jersey, USA.

<sup>2</sup>Rosenstiel School of Marine and Atmospheric Science, University of Miami, Miami, Florida, USA.

<sup>3</sup>Environmental Science and Engineering Program, University of Texas at El Paso, Texas, USA.

<sup>4</sup>Department of Geological Sciences, University of Texas at El Paso, El Paso, Texas, USA.

<sup>5</sup>NASA Goddard Space Flight Center, Greenbelt, Maryland, USA.

Corresponding author: P. Ginoux, NOAA Geophysical Fluid Dynamics Laboratory, Princeton, NJ 08542, USA. (paul.ginoux@noaa.gov)

cover, or desiccating water bodies, and indirectly, by changing climate and the hydrological cycle. In addition, most of the existing studies focus on local or regional scale and rarely quantify their global impact. Present estimates of the anthropogenic contribution to global dust emission range from less than 10% [Tegen *et al.*, 2004] to a maximum of 50% [Mahowald and Luo, 2003]. Such large uncertainty may be attributed in large part to the lack of global detailed characterization of dust sources.

[3] The objective of the present study is to develop a new satellite product that has adequate resolution to detect and attribute natural and anthropogenic dust sources and to use this product to assess anthropogenic and hydrologic impacts on dust emission at the global scale. These results are evaluated against a wide range of observational evidence.

[4] Satellite data analysis by Prospero *et al.* [2002] showed that most major dust sources are located in arid regions in topographic depressions where deep alluvial deposits have formed by intermittent flooding through the Quaternary and into the Holocene. Although the sources are located in arid regions, the action of water is evident from the presence of ephemeral streams, rivers, lakes, and playas (ephemeral or desiccated lakes which contain deposits of clay, silt, and salts). In some of these depressions, the layer of alluvium is sufficiently deep to sustain dust emission without further replenishing, but others are regularly flooded, thereby forming new sediment deposits. Although within a basin ephemeral lakes provide ideal conditions for wind erosion, ephemeral riverbeds (e.g., wadis or arroyos) also have the potential to be active dust sources. Most recent field studies of dust sources have focused on ephemeral lakes, for example, Owens Lake [Gillette *et al.*, 1997] and Franklin Lake [Reynolds *et al.*, 2007] in the Great Basin of the USA, the Bodélé depression as characterized during the Bodélé Dust Experiment (BoDEx) field campaign [Washington *et al.*, 2006], the Etosha Pan in Namibia [Bryant, 2003], the Chotts of Tunisia and Algeria [Mahowald *et al.*, 2003], the Makgadikgadi pans in Botswana [Bryant *et al.*, 2007], the Lake Eyre basin of Australia [Bullard *et al.*, 2008], the Mar Chiquita of Argentina [Troin *et al.*, 2010], and Lake Ebinur of northwest China [Abuduwaili *et al.*, 2008]. They all show that dust emission depends on the interplay of characteristics of sediments, soil moisture, groundwater, and vegetation. Some show an increase of dust emission after inundations, which provide fresh deposits of fine sediments. But Mahowald *et al.* [2003] noted that the role of ephemeral lakes is unclear on a regional scale and even less clear at the global scale. The main reason cited by the authors is the difficulty in interpreting coarse-resolution satellite data.

[5] Source identification is even more difficult for small-scale sources (the “hot spots” defined by Gillette [1999]) such as floodplains, alluvial fans, rivers, and wadis. Using a global model, Zender *et al.* [2003] studied the importance of sediment availability and erodibility in reproducing dust distribution and deposition. They concluded that although evidence suggests that these were quite important, they could not support their conclusions with direct observations because of limited resolution over dust sources. These studies are

indicative of the growing recognition of the great spatial and temporal diversity of dust source environments. Thus, in order to understand the global dust cycle it is critical to quantify the relative importance of the different types of sources and the factors that affect emissions, as noted by Okin *et al.* [2011] and Bullard *et al.* [2011].

[6] Even more uncertain is the impact of human activities on dust mobilization. Mahowald *et al.* [2010], by constraining a dust model with observations, estimate that global dust loads have doubled in the twentieth century due to anthropogenic activities. A review by Gill [1996] documents many examples in numerous nations of the effects of anthropogenic land disturbance and the desiccation of playas. Neff *et al.* [2008] link the expansion of livestock grazing in the early twentieth century with a 500% increase of dust deposition in the western United States. Agricultural practices have long been recognized as a key factor in producing the “Dust Bowl” in the 1930s [Orlove, 2005; Cook *et al.*, 2009]. Cropland and rangelands are still the main sources of dust in the southern high plains of North America [Stout, 2001; Lee *et al.*, 2012]. Since the end of the nineteenth century, there have been reports of new dust sources created by water diversion for irrigation, Owens Lake [Gillette, 1999], the Aral Sea [Micklin, 2007], and Lake Ebinur [Abuduwaili *et al.*, 2008] being examples. On the other hand, restoration and mitigation of degraded land have reduced dust activity from Lake Texcoco, Kara-Bogaz Gol, and the Konya Basin [Gill, 1996]. In China, Ma *et al.* [2010] have shown that over the last half century 243 lakes have vanished, while 60 new lakes appeared, mostly due to human influence and global warming.

[7] Projections of atmospheric dust in response to climate change have been simulated using different general circulation models [e.g., Tegen *et al.*, 2004; Mahowald *et al.*, 2006]. The results of these simulations differ substantially not only in their projections but also in the present-day dust distributions. Huneeus *et al.* [2011], retrospectively comparing the results of 15 dust models for the year 2000, found very large disparities among models, especially in their emissions. These model studies emphasized the need of satellite observations to better characterize dust loads over source areas.

[8] Satellite instruments are the most useful tool to locate dust sources as they provide near-daily global observations. Ginoux *et al.* [2010] discussed various satellite products, including Moderate Resolution Imaging Spectroradiometer Deep Blue (MODIS DB) Level 2 (henceforth M-DB2) aerosol products, and demonstrated their use to identify dust sources in West Africa. The advantages of M-DB2 products as retrieved by Hsu *et al.* [2004] are their high resolution ( $\sim 10$  km), daily near-global coverage, and spectral information (aerosol products at multiple wavelengths). A limitation of these products is that they can only be retrieved over bright surfaces in the visible, a restriction that consequently excludes forests and ocean surfaces which, in any event, are not significant dust sources. However, we are aware of at least two regions where M-DB2 cannot retrieve dust sources. One is in Iceland, where dust sources identified

by Prospero *et al.* [2012] are associated with active glacial outwash plains, which are too dark to be retrieved from M-DB2. The other is in Alaska, where dust plumes are emitted within the solar terminator, which necessitates special treatment of satellite backscatter radiances to effectively retrieve dust sources [Crusius *et al.*, 2011]. Another limitation of polar orbiting satellites is the lack of continuous measurements as they measure backscattered radiances of an area only once a day. Ginoux and Torres [2003] have cautioned that by using polar orbiting satellite products, one might miss sources that become active after satellite overpass. This has been clearly shown with some case studies based on geostationary satellite data [Schepanski *et al.*, 2007]. However, Smirnov *et al.* [2002], using multiple years of Sun photometer data, show that the variability of aerosol optical depth in dusty environments is typically less than 10% over the course of a daylight day.

[9] Here we extend the work of Ginoux *et al.* [2010] to the global scale. In addition, we assess our results through comparison with other data sets and estimate the contribution of each source type to dust emissions. In section 2, we provide a summary of our methodology. We briefly describe in section 3 the gridded M-DB2 data. In section 4, we first present the method to derive dust optical depth (DOD) from M-DB2 products and compare it to Aerosol Robotic Network (AERONET) Sun photometer data. We then analyze the spatial and frequency-of-occurrence (FoO) distributions of DOD. In section 5, the detection of dust sources is described and the resulting distribution is compared with inventories from other satellite instruments: the Total Ozone Mapping Spectrometer (TOMS) and the Ozone Mapping Instrument (OMI). Next we classify the sources according to land use and hydrologic origin, and we examine in detail dust sources in different continental regions. In section 6, we calculate the contribution of dust emissions from bare ground, vegetated areas, ephemeral water bodies, and land use. In section 7 we discuss the implications of our results on climate, air quality, and health. Finally, we present our conclusions in section 8.

## 2. METHODOLOGY

[10] For clarity, we summarize the five main steps of our methodology.

[11] *Dust optical depth.* After mapping daily M-DB2 aerosol products on a Cartesian  $0.1^\circ$  latitude-longitude grid, DOD is derived from the aerosol optical depth (AOD) using criteria based on size distribution and optical properties. The results of this technique are tested against AERONET Sun photometer data.

[12] *Background DOD.* The frequency distribution is analyzed and used to determine a minimum  $\text{DOD}_{\text{thresh}}$  that could be ascribed to background aerosols.

[13] *Source detection.* The FoO distribution of  $\text{DOD} > \text{DOD}_{\text{thresh}}$  is used to identify active dust sources, and the results are compared to similar analyses derived from TOMS and OMI satellite data.

[14] *Source attribution.* Source areas are attributed to an anthropogenic or hydrological origin based on, respectively,

the degree of land use and the presence of ephemeral water bodies.

[15] *Source emissions.* The contributions of anthropogenic and hydrological sources to dust emissions are calculated using wind speed from a high-resolution model.

## 3. GRIDDED MODIS DEEP BLUE DATA

[16] The M-DB2 algorithm employs radiances from the blue channels of MODIS instruments. At these wavelengths the surface reflectance is very low so that the presence of aerosol is detected by an increase of total reflectance and enhanced spectral contrast [Hsu *et al.*, 2004, 2006]. The values of AOD and single scattering albedo ( $\omega$ ) at 412, 470, 550, and 670 nm and the Angstrom exponent ( $\alpha$ ) between 412 and 470 nm are retrieved at the pixel level over bright surfaces (reflectance at 550 nm greater than 0.15) and then averaged over a  $10 \text{ km} \times 10 \text{ km}$  grid. The data are aggregated into granules which comprise the level 2 data. Ginoux *et al.* [2010] used collection 5.0 level 2 products from MODIS on the Aqua platform. For the present study, we use data from the same instrument but with the improved collection 5.1 data from 2003 to 2009. The improvements include updated characterizations of the surface bidirectional reflectance distribution function and cloud screening techniques. All aerosol products are interpolated on a regular  $0.1^\circ$  latitude-longitude grid using the algorithm described by Ginoux *et al.* [2010].

[17] The number of M-DB2 retrieval per  $0.1^\circ \times 0.1^\circ$  grid cell and per season (averaged from 2003 to 2009) is shown in Figure 1. Some regions yield no data because either their surface reflectance in the visible is below 0.15 (oceans and forests) or they were not considered in this study (Central America and Southeast Asia). Other regions yield reduced data due to the presence of clouds. These are mostly areas influenced by the monsoon (for example, in India) or located along the Intertropical Convergence Zone (ITCZ). Over arid and semiarid regions the number of valid retrievals is on average higher than 30 days per season, i.e., more than 30%.

## 4. MODIS DUST OPTICAL DEPTH

[18] After all the data have been gridded, a screening method is applied to extract scenes of AOD dominated by dust. The screening protocol applies three conditions that are based on size distribution, absorption of solar radiation in the green (550 nm), and the contrast of absorption between the red (670 nm) and deep blue (412 nm) channels.

[19] Dust size distributions are characterized by the presence of a prominent coarse mode (particle size greater than  $1 \mu\text{m}$  radius) in contrast to urban and biomass burning aerosols, which yield abundant fine-mode aerosols (particle size less than  $1 \mu\text{m}$ ) [Dubovik *et al.*, 2002]. Gravitational settling efficiently removes large particles, and consequently, the dust size distribution shifts to smaller radii with increasing transport time. Eck *et al.* [1999] show that the dominance of one mode over the other can be measured with the Angstrom wavelength exponent  $\alpha$ . The  $\alpha$  values range from  $-0.5$  to  $0.5$  in dusty environments; they are greater than  $0.5$

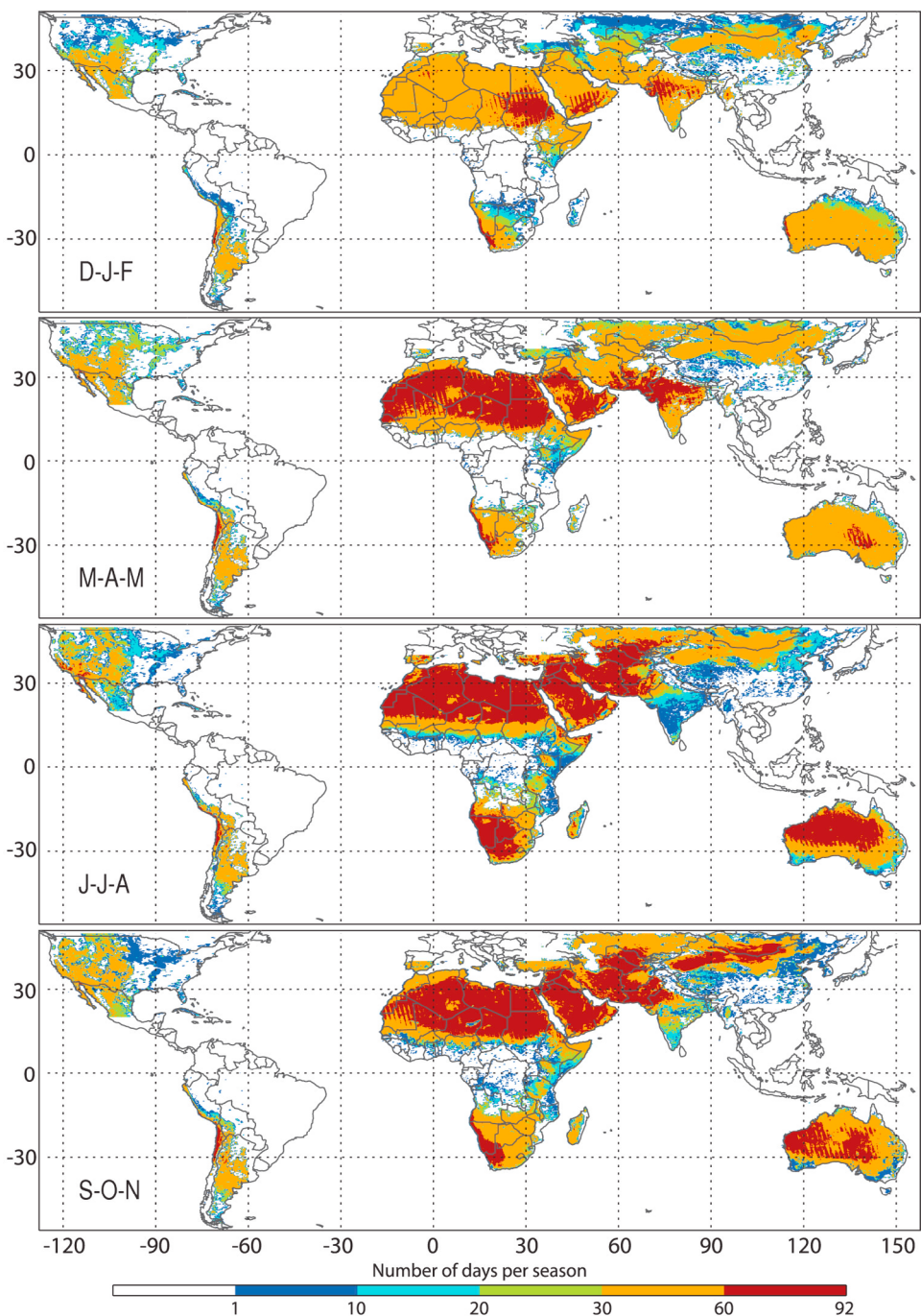


**Figure 1.** Global distribution of the number of MODIS DB AOD retrieval per  $0.1^\circ \times 0.1^\circ$  grid cell and per season, averaged from 2003 to 2009.

in polluted regions. *Schepanski et al.* [2007] have imposed  $\alpha < 0.6$  to detect dust using the infrared channels of the Spinning Enhanced Visible and Infrared Imager instrument on the Meteosat Second Generation satellite. However, we would like to apply a more stringent criterion so as to screen out all scenes with any significant amount of fine-mode particles, either from other aerosol types or aged dust. Many measurements in dusty environments yield negative  $\alpha$  during dust outbreaks and near dust sources: from  $-0.2$  to  $0.04$  (during three flights) in Niger [*Osborne et al.*, 2008],  $-0.06$  (three events) in Delhi [*Singh et al.*, 2005],  $-0.5$  (one event)

in Spain [*Cachorro et al.*, 2000], less than  $0$  at Birdsville (many events mostly in summer but also in fall) in the Lake Eyre basin [*Radhi et al.*, 2010], and  $-0.24$  (typical during dust storms) in Tengger Desert in northern China [*Xin et al.*, 2005]. *Cheng et al.* [2006] reported negative values 11.4% and 6.7% of the time over 5 years of measurements near Chinese dust sources at Dunhuang and Yulin, respectively.

[20] *Schuster et al.* [2006] show that for a monomodal distribution of coarse particles,  $\alpha$  is negative for effective radius greater than  $1\text{ }\mu\text{m}$ . Typically, for coarse-mode dust the effective radius is about  $2\text{ }\mu\text{m}$  [*Dubovik et al.*, 2002;

*Osborne et al.*, 2008]. Based on these various observations we impose as our first dust criterion that  $\alpha < 0$ .

[21] Although M-DB2 products are retrieved only over bright surfaces in the visible (to not be mistaken with brightness in the deep blue, which is always small), thereby excluding oceans, there may be scenes in coastal regions where sea salt concentrations are high. Because sea salt has a significant amount of coarse-mode particles, low  $\alpha$  values could result. To avoid this situation, we require that the single scattering albedo  $\omega$  at 412 nm is less than 0.95. For scattering aerosols such as sea salt  $\omega$  is near 1. This second criterion efficiently eliminates sea salt-dominated scenes. We should note that some dust sources contain a large percentage of salt, for example, the Aral Sea [Rudich *et al.*, 2002]. Internal mixing of dust and salt will affect the optical characteristics of pure dust, but it is not clear how it could affect our results. The mixture will still absorb shortwave radiation, although more weakly. In the following sections, we will show that our scheme successfully detects dust near salty sources such as the Aral Sea, Owens Lake, and Great Salt Lake, among others.

[22] Another specific optical property of dust is the sharp increase of absorption from red to deep blue. This translates into a positive spectral variation of  $\omega$  with wavelength. Internal mixing with nonabsorbing sea salt should theoretically not change the sign of dust spectral variation of absorption. This is also true for nonabsorbing sulfate aerosols. The third criterion requires a positive difference of  $\omega$  between 412 and 670 nm ( $\omega_{670} - \omega_{412} > 0$ ). Using these three criteria based on the physical and optical properties of aerosol, we extract the global distribution of daily DOD from the retrieved AOD over the period 1 January 2003 to 31 December 2009.

#### 4.1. Comparison With AERONET

[23] To evaluate our screening method using M-DB2 products, we apply it to the direct measurements of AOD made in the AERONET Sun photometer network. AERONET is a federated worldwide network of Sun photometers that are monitored and maintained at NASA Goddard Space Flight Center [Holben *et al.*, 1998]. We use aerosol optical depth and the Angstrom exponent (440–670 nm) level 2 data, which are cloud screened and quality assured; these are available at <http://aeronet.gsfc.nasa.gov>. From all measurements collected between 2003 and 2009 and from all sites, we extract AERONET data between 12:00 PM and 3:00 PM local time. This provides a 3 h window centered at 1:30 PM, the local passing time of the MODIS instrument on Aqua. We only use M-DB2 data within a 30 km window centered on the AERONET site. The spectral values of single scattering albedo are also retrieved by inversion of almucantar measurements [Dubovik and King, 2000]. The almucantar measurements are performed by keeping the same solar zenith angle while varying the azimuthal angle of the Sun photometer over 360°. However, the level 2 quality assured inversion products are computed only for AOD greater than 0.4. This condition would severely limit the number of

collocated measurements. Therefore, the only dust criterion that we require of the AERONET data is that  $\alpha < 0$ .

[24] Figure 2 (top) shows the comparison between the spatially and temporally collocated mean AOD (550 nm) measured by AERONET and retrieved by M-DB2 algorithm, as well as, in Figure 2 (bottom), the mean DOD (550 nm) extracted from AERONET and M-DB2 data. We found 195 and 13 AERONET sites with collocated measurements of AOD and DOD, respectively. There is a significant correlation between AERONET and M-DB2 for AOD as well as DOD. The root-mean-square differences are 0.11 and 0.26, while the mean absolute differences are 0.07 and 0.24 for AOD and DOD, respectively. Although AOD sites are widespread and include polluted regions with aerosol dominated by fine-mode particles, the screening method selects only sites known to lie nearby to dust sources. The largest biases in AOD and DOD are in California and Australia. In Africa, M-DB2 AOD is slightly overestimated while DOD is systematically underestimated by 25%–50%. The largest DOD value in Figure 2 corresponds to the Kanpur (India) site.

[25] Table 1 gives the mean AOD and DOD values and the number of days with collocated measurements at the 13 AERONET sites. While there are hundreds of AOD measurements per site, the number of days with collocated measurements satisfying DOD conditions is dramatically reduced, ranging from 104 days in Agoufou (Mali) to a minimum of 8 days in Rogers Lake (California). Table 1 shows that at all sites the mean DOD is significantly larger than the mean AOD, with the highest mean DOD (1.5 for M-DB2 and 1.4 for AERONET) at Kanpur (India). The lowest DOD values are observed at the Tinga Tingana and Birdsville sites, both of which are in the Lake Eyre Basin of Australia. The annual AERONET DOD is 0.16 for both sites; M-DB2 values are higher, 0.34 for Birdsville and 0.19 for Tinga Tingana. These data show, as expected, that the imposed condition  $\alpha < 0$  effectively serves to identify dust events and to discriminate against air parcels containing fine-mode pollutants.

#### 4.2. Seasonal Distribution

[26] Comparisons between monthly mean and standard deviation of AOD from AERONET and M-DB2 and DOD from M-DB2, calculated from measurements between 2003 and 2009, are shown in Figure 3. For this comparison, all M-DB2 data are selected within a 30 km window centered on the location of the AERONET sites but without restricting local passing time between 12:00 PM and 3:00 PM. The values in Figure 3 are calculated by averaging all valid AERONET level 2 measurements and M-DB2 retrievals. M-DB2 monthly AODs are within the standard deviation of AERONET data in Africa, Arabian Peninsula, and India but largely overestimated in California, Australia, and Israel. These discrepancies were already apparent in Figure 2. Most sites in Africa are located within or approximate to the Sahel, one of the most active dust sources in North Africa (Dakar, Agoufou, Cinzana, Banizoumbou, and Soroa). The

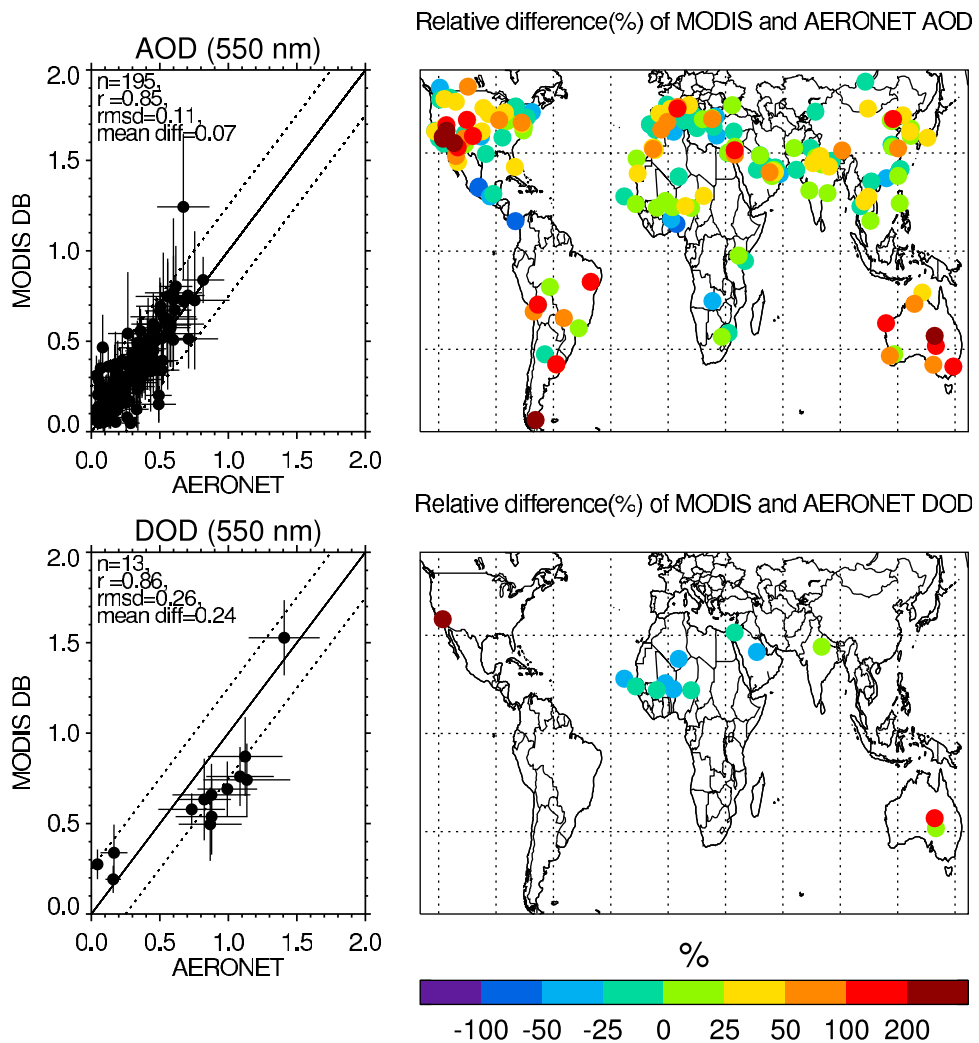


**Figure 2.** Comparison between AERONET and M-DB2 (top) aerosol optical depth and (bottom) dust optical depth at AERONET sites with collocated data between 2003 and 2009. (left) The standard deviation is added to the mean values. (right) The percent relative difference between M-DB2 and AERONET values, given using colored circles. The number of sites (n), correlation coefficient (r), root mean square difference (rmsd), and mean absolute difference (mean diff) are provided in the top left corner in Figure 2 (left).

Cape Verde Islands site is located off the west coast of North Africa, under the path of much of the dust that emerges from North Africa. Tamanrasset is a mountain site (1377 m above sea level) located in the Sahara. At the Tamanrasset site, there is a distinct peak of M-DB2 DOD in June, in agreement with the measurements taken in 2006 by *Cuesta et al.* [2008] at that location. The seasonal cycle at the Sahel sites differs from Tamanrasset in that dust is a significant contributor to AOD from January to July. The M-DB2 seasonality is supported by measurements made by *Rajot et al.* [2008] at Banizoumbou during the African Monsoon Multi-disciplinary Analysis field campaign in 2006.

[27] In Solar Village (Arabian Peninsula), there is a pronounced maximum of M-DB2 DOD in April-May; dust activity weakens rapidly in summer, reaching a minimum in winter, in accordance with observations of *Sabbah and Hassan* [2008]. At Kanpur (India), large amounts of dust are observed during the premonsoon season with M-DB2

DOD reaching 0.8 in May-June; in contrast, M-DB2 DOD shows no dust during the other seasons. The greatest discrepancies are seen at Sede Boker (Israel), Birdsville (Australia), and Rogers Lake (California), where M-DB2 AOD is largely overestimated.

[28] The 7 year mean seasonal variation of M-DB2 AOD and DOD at 550 nm is shown in Figure 4. DOD distribution is plotted for all values of DOD greater than 0.1; elsewhere, AOD is plotted so that the relative distribution is made visible. The Northern Hemisphere is clearly much more dusty than the Southern Hemisphere both in terms of the absolute values of DOD and the spatial coverage. The same is true for AOD. In both hemispheres, fall is the season with the lowest DOD values: September, October, and November (SON) in the Northern Hemisphere and March, April, and May (MAM) in the Southern Hemisphere.

[29] There are many regions with DOD > 0.1 all year long. The most widespread dust activity is seen in North Africa,

**TABLE 1.** Collocated Mean Aerosol (AOD) and Dust (DOD) Optical Depth at 550 nm Measured by AERONET and Retrieved From M-DB2, at 13 AERONET Sites<sup>a</sup>

Name	Country	Site		AOD			DOD		
		Latitude	Longitude	N	AERONET	M-DB2	N	AERONET	M-DB2
Agoufou	Mali	15.34°N	1.47°W	1207	0.51	0.51	104	1.13	0.74
Banizoumbou	Niger	13.54°N	2.66°E	1351	0.55	0.62	50	1.1	0.76
Birdsville	Australia	25.89°S	139.34°E	648	0.06	0.28	24	0.16	0.34
Cape Verde	Sal Island	16.73°N	22.93°W	314	0.43	0.36	10	0.99	0.69
Dakar	Senegal	14.39°N	16.95°W	1117	0.45	0.5	44	0.88	0.66
Maïné-Soroa	Niger	13.21°N	12°E	482	0.41	0.5	12	0.73	0.58
IER Cinzana	Mali	13.27°N	5.93°W	917	0.47	0.5	44	1.12	0.87
Kanpur	India	26.51°N	80.23°E	927	0.6	0.73	24	1.41	1.53
Rogers Lake	California	34.92°N	117.88°W	549	0.35	0.07	8	0.04	0.27
Sede Boker	Israel	30.85°N	34.78°E	1538	0.17	0.35	16	0.82	0.63
Solar Village	Saudi Arabia	24.9°N	46.39°E	1287	0.34	0.31	55	0.88	0.54
Tamanrasset	Algeria	22.79°N	5.53°E	381	0.21	0.21	12	0.87	0.54
Tinga Tingana	Australia	28.97°S	139.99°E	857	0.06	0.14	12	0.16	0.19

<sup>a</sup>The number of days with collocated measurements (N) of AOD and DOD are provided for each site. IER, Institut d'Economie Rurale.

especially within the Sahel, a region that is broadly defined in terms of rainfall as the zone lying between the 100 and 500 mm isohyets [National Research Council, 1983], which in West Africa lies roughly between 14°N to 20°N. This region encompasses three phytogeographical divisions: the northerly Sahelo-Saharan zone (grass steppe), between the 100 and 200 mm isohyets; the Sahel proper (tree steppe), between the 200 and 400 mm isohyets; and the southerly Sudano-Sahelian borderlands (shrub savanna), extending to the 500 mm isohyet. The Sahel has been the focus of much interest because of the great increase in dust activity that occurred following the onset of prolonged drought in the early 1970s [Prospero and Lamb, 2003].

[30] In West Africa, DOD is consistently higher in the Sahel (including Senegal, Mauritania, Mali, Niger, and Chad) than in the Sahara, although most studies of dust activity have focused on major sources in the Sahara [Prospero et al., 2002; Schepanski et al., 2007]. However, Maurer et al. [2009] pointed out that the Sahel region is one of the Earth's most wind erosion-prone zones because these soils, which largely overlie sand sheets, are intensively developed for agriculture and thus become vulnerable to wind erosion. The region is influenced by the dry Harmattan winds from the north and the monsoon flow from the Gulf of Guinea. These two flows converge at the surface along the Intertropical Discontinuity (ITD) and in the free troposphere along the ITCZ. There does not seem to be any seasonal variation of these hot spots in Figure 4 despite the fact that the ITD shifts from 5°N in winter to around 18°N in summer [Bou Karam et al., 2008]. This quasi-permanent maximum DOD in the Sahel may be a result of the combination of both emissions from local sources and transport from other upwind regions. Klose et al. [2010] analyzed weather reports from 1983 to 2008 and found the existence of a zone of frequent dust events and high dust concentration in the Sahel. The dust events are reported as mostly dust in suspension, which suggests that transport from the Sahara to the Sahel is more important than local emissions. Nonetheless, weak dust sources in the Sahel may be significant

as pointed out by the modeling study of Guelle et al. [2000].

[31] It is interesting to note that most models do not produce a large amount of emissions from the Sahel. Among the 15 global dust models analyzed by Huneeus et al. [2011], few reproduce the most southward displacement of the Saharan dust cloud in winter. This disparity may be related to the resolution of these models. Indeed, Bou Karam et al. [2008] observed haboob-type dust events during the passage of a density current that originated from a mesoscale convective system situated on the leading edge of the monsoon flow. Using a 20 km resolution model, Bou Karam et al. [2009] suggested that emissions driven by strong surface winds associated with these density currents may contribute significantly to the total dust load over West and North Africa. However, using a model with similar resolution (25 km), Haustein et al. [2012] had difficulty simulating an observed dust storm in the Sahel associated with intense moist convection. Using a higher-resolution (7 km) regional model, Tegen et al. [2006] could reproduce a heavy dust plume over the Bodélé depression, although the model underestimates wind speed over the region. Similar resolution will be necessary to confirm the importance of down-drafts from convective storms over the Sahel, as well as other monsoon regions.

[32] Some of the most intense hot spots are in the northern part of the Sahel. The best example is the much studied Bodélé depression (17°N, 18°E, 170 m) in Chad [Koren et al., 2006; Washington et al., 2006; Todd et al., 2007] which yields an annual mean DOD value greater than 0.75. This high value is in agreement with the mean AOD = 1.1 retrieved from Multiangle Imaging Spectroradiometer (MISR) and reported by Koren et al. [2006]. One of the few studies measuring DOD in this region [Osborne et al., 2008] reported values up to 0.8 during dust events over Niger.

[33] Over North Africa, there are regions where DOD < 0.1 and AOD > 0.25. They are mostly located in the Sahara where sulfate emitted by fossil fuel burning and transported from Europe [Lelieveld et al., 2002] may contribute

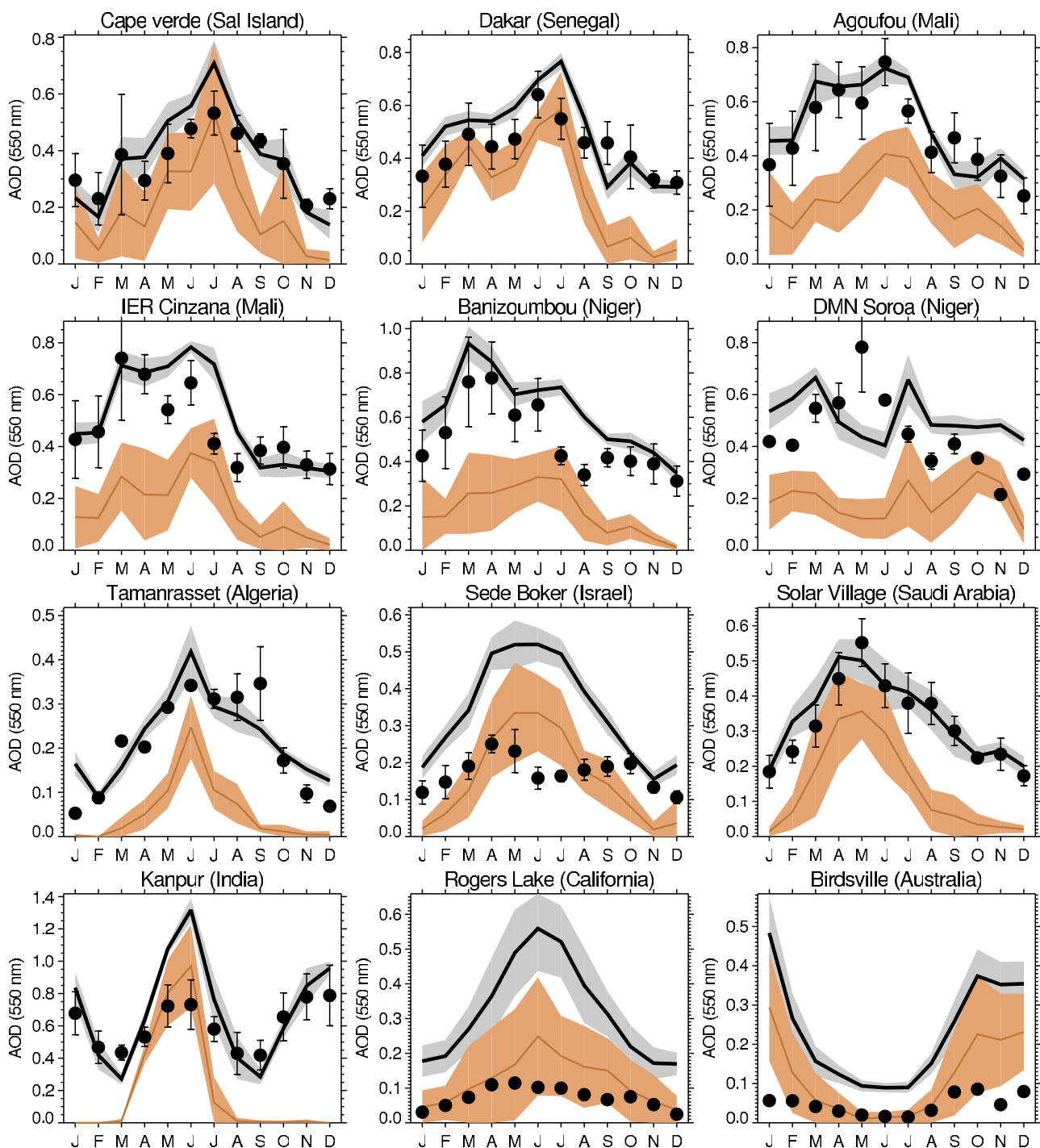


**Figure 3.** Monthly AOD from AERONET (mean, black dots; standard deviation, vertical line) and M-DB2 (mean, black bold line; standard deviation, grey shading) and DOD from M-DB2 (mean, brown line; standard deviation, brown shading) at 12 sites whose locations are given in Table 1.

significantly to AOD. Also along the southernmost areas of the Sahel, we expect carbonaceous aerosols from biomass burning to contribute significantly to AOD, especially in winter [Crutzen and Andreae, 1990].

[34] Over the Middle East, the regions with the highest and most widespread FoOs of  $\text{DOD} > 0.1$  are in Mesopotamia and along the Persian Gulf in MAM. There are also a

few local spots in the coastal regions of Yemen and Oman with mean DOD greater than 0.25, mostly in MAM and June, July, and August (JJA). In central Asia,  $\text{DOD} > 0.1$  is found over the east Aral Sea, the southeast coastal region of the Caspian Sea, the eastern parts of Uzbekistan and Turkmenistan, and the southwest corner of Afghanistan, all of which are known sites of highly active dust sources.

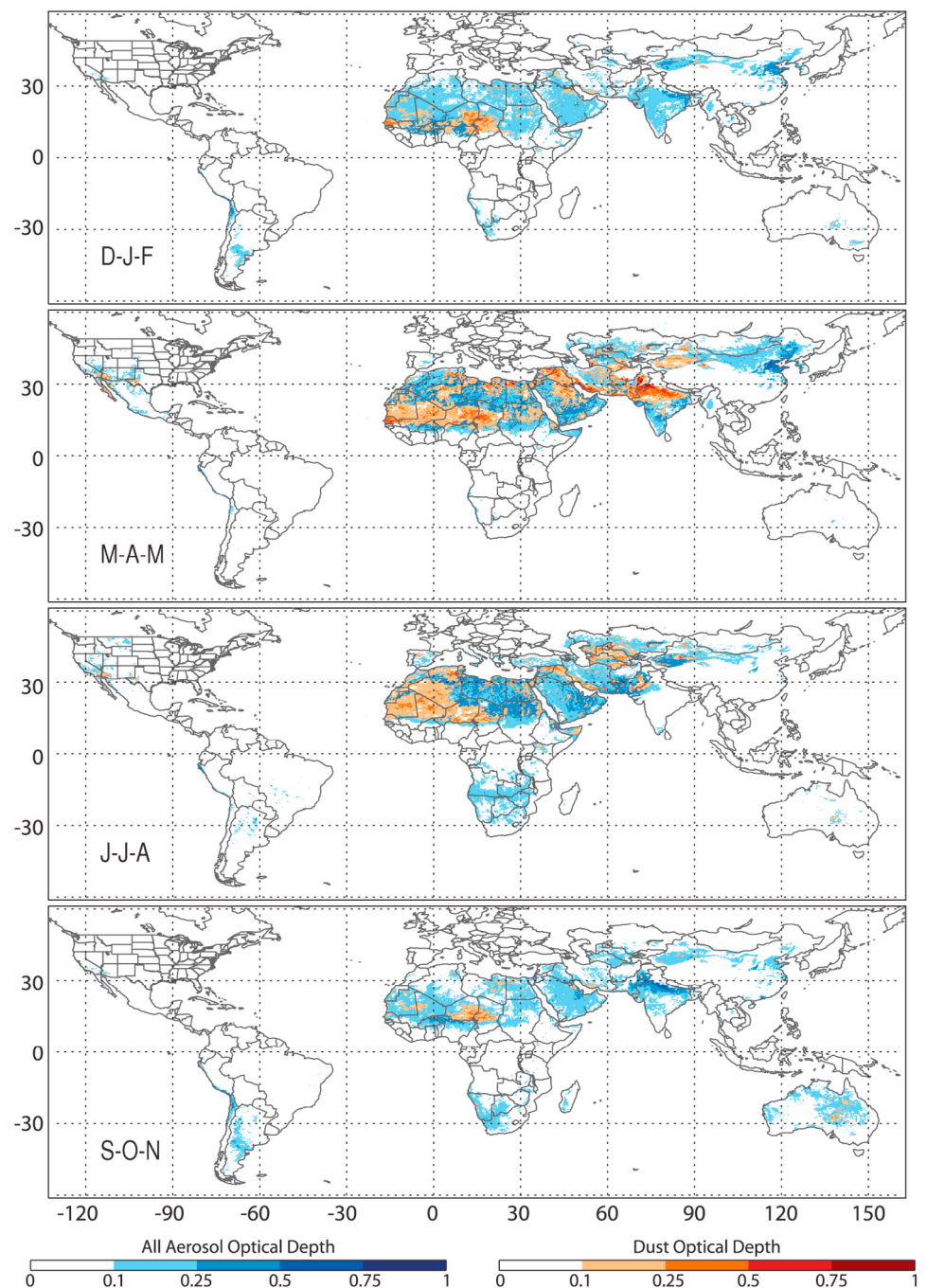


**Figure 4.** Global distribution of M-DB2 seasonal mean aerosol optical depth (blue) overplotted by dust optical depth (red).

[35] In Figure 4, India is characterized by a strong seasonal and latitudinal variation of DOD. The peak period for dust is March, April, and May (premonsoon), and the weakest period is in September, October, and November (postmonsoon). During the premonsoon period, DOD is  $>0.5$  over the Indo-Gangetic basin. During the monsoon period (June, July, and August), the number of retrievals is too low (cf. Figure 1) to make any conclusion about DOD or AOD in Figure 4. But after the monsoon period and in winter, the region appears free of a significant amount of dust.

[36] Recently, *Dey and Di Girolamo* [2010] derived a climatology of nonspherical aerosol optical depth over India using MISR data. For the most part, the seasonal variation and latitudinal gradients are similar, but the absolute values of DOD are more than a factor of 5 lower in their study. As shown above (Figure 3), we overestimate AOD by a factor of 2 in Kanpur in May and June, while in their study they underestimate AERONET AOD by a factor of 2 at Kanpur.

**TABLE 2.** Domain of the Continental Regions Considered in This Study

Region	Longitude Range	Latitude Range
North America	125°W–70°W	20°N–50°N
South America	85°W–60°W	55°S–0°N
North Africa	20°W–35°E	5°N–40°N
South Africa	5°E–50°E	35°S–5°N
West Asia	35°E–60°E	5°S–50°N
Central Asia	60°E–100°E	5°N–30°N
East Asia	60°E–140°E	30°N–50°N
Australia	110°E–155°E	45°S–10°S

[37] Data are only consistently obtained in NW and NE China where the AOD and DOD distributions show a significant seasonal and spatial variation. DOD coverage and amplitude are at a maximum in spring, in agreement with previous studies [Sun *et al.*, 2001; Wang *et al.*, 2004]. DOD makes a significant contribution to total AOD only during this most active dust season and only in the NW region. It is notable that in NE China, AOD dominates DOD in spring, despite the fact that intense, large-scale dust events are common throughout the region. This is most likely related to the large contribution of fine-pollutant aerosol to optical depth and the low frequency of dust events, as discussed in the next section. The intense and widespread dust activity seen in NW China in MAM is mostly associated with basins that have been previously identified: Tarim, Qaidam, Junggar, and Turpan [Prospero *et al.*, 2002]. Over these regions, the seasonal mean DOD varies between 0.1 and 0.5 in MAM but drops below 0.1 in most areas during the other seasons. In JJA, some areas of the Tarim and Qaidam basins are still dusty; in the Tarim, there are two strong sources (DOD maxima > 0.5), one in the NE and one in the SW of the basin. Ge *et al.* [2010] showed that M-DB2 retrievals agree relatively well with ground-based data during dust events in northwest China. They observed AOD varying from 0.07 to 2.5 during dust events, with M-DB2 performance improving with increasing AOD. Christopher and Wang [2004] showed similar daily variations (from 0.2 to 1.5) during dust events over Dunhuang (40.1°N, 94.4°E), which is located near the Tarim Basin and Gobi dust sources.

[38] In North America, DOD > 0.1 are seen around Baja California and the southern high plains in Texas. Some hot spots with DOD > 0.25 are observed in MAM over the Salton Basin of southern California, the Gila Valley in southwest Arizona, along the Pecos River of southwest Texas, the Vizcano Desert of the central part of the Baja California, and the Playa de San Nicolas in the southern part of the Sonoran Desert in Mexico. In Europe, the only two regions with DOD > 0.1 are located in Spain's Meseta Central and Anatolia in Turkey, but only in JJA.

[39] In the Southern Hemisphere, Australia is the only continent that yields substantial areas with DOD > 0.1; dust activity is greatest in SON, Austral spring. Over some ephemeral lakes within the Lake Eyre Basin, DOD is higher than 0.25 from September to February. But, as seen in Figure 3, M-DB2 AOD and DOD are largely overestimated in Australia. The other regions in the Southern Hemisphere

with DOD > 0.1 are mostly areas within deserts, e.g., the Namib (Namibia), Kalahari (Namibia), Atacama (Chile), and Sechura (Peru) Deserts.

#### 4.3. Frequency Distribution

[40] In this section, we analyze the FoO of optical depth by region and season with the objective of developing a procedure to identify major dust storm days based on the relative frequency of magnitude of DOD and AOD. To this end we divided the continents into seven regions defined in Table 2. The number of samples per region is large and varies between  $10^5$  to  $10^7$  depending on the season. Table 3 provides the percent cumulative frequency for three values of optical depths (0.25, 0.5, and 1) and for each region and season.

[41] In all regions, for all seasons, and for all three optical depth values in Table 3, the cumulative frequencies of AOD are much greater than those of DOD. The frequency of AOD > 0.25 is generally lower than 50%, except during MAM in west and central Asia, while DOD is most frequently greater than 0.25 for all regions. Therefore, a DOD threshold  $DOD_{thresh} = 0.2$  is selected to distinguish dust events from background aerosols.

[42] The global distribution of the number of days  $DOD > 0.2$  for each season is shown in Figure 5. The global distribution of dust event days with  $DOD > 0.2$  shown in Figure 5 is broadly similar to that of the mean M-DB2 AOD and DOD shown in Figure 4. The most widespread occurrence and the highest frequencies are seen in North Africa. Within the Sahel, events with  $DOD > 0.2$  occur at least seven times per season and more than 75% of the time in certain areas (e.g., Mauritania, Niger, and the Bodélé depression). Engelstaedter *et al.* [2003] used visibility data to develop a global map of annual dust storm frequency which shows distributions in the Sahel that are remarkably similar to those in Figure 5, taking into consideration that our results are based on seasons. Other areas with frequent events are Mesopotamia in summer, the Iranian coastal region all seasons, eastern Uzbekistan and Turkmenistan in summer, and the Indo-Gangetic basin during premonsoon season. On the other hand, the number of dust events in Inner Mongolia and Mongolia appears to be low. Ground-based visibility data appear to support this low frequency of dust outbreaks in China. Using visibility data from 1988 to 2004 over the entire east Asian continent, Kurosaki and Mikami [2005] showed that the frequency of dust outbreaks in China is greater than 4% (corresponding to 4 days per season in Figure 5) only in the Tarim Basin, the Gobi Desert, and the Loess Plateau. These are the regions in Figure 5 where M-DB2 frequencies are greater than 7 days in MAM and JJA.

[43] In North America, the highest frequency of dust events is found in the southwestern U.S. and northern Mexico. Along the border between the U.S. and northern Mexico, events with  $DOD > 0.2$  appear as frequently as 30% of the time in MAM. This is in agreement with the long-term record of visibility data at El Paso (Texas), where there is high frequency of blowing dust in spring [Novlan *et al.*,

**TABLE 3. Cumulative Frequency Distribution (Expressed in Percentage) of M-DB2 DOD and AOD (in Parentheses)  $\leq 0.25$ ,  $0.5$ , and  $1$  Over Five Continental Regions for Each Season<sup>a</sup>**

Region Name	DJF			MAM			JJA			SON		
	$\leq 0.25$	$\leq 0.5$	$\leq 1$	$\leq 0.25$	$\leq 0.5$	$\leq 1$	$\leq 0.25$	$\leq 0.5$	$\leq 1$	$\leq 0.25$	$\leq 0.5$	$\leq 1$
North America	21 (89)	78 (97)	98 (100)	9 (67)	53 (84)	90 (97)	11 (75)	55 (88)	90 (98)	23 (95)	78 (99)	98 (100)
South America	12 (69)	57 (85)	92 (98)	21 (92)	71 (97)	97 (99)	17 (86)	72 (94)	96 (99)	8 (60)	49 (79)	90 (96)
North Africa	13 (49)	51 (77)	91 (96)	3 (23)	25 (60)	84 (94)	4 (27)	27 (66)	89 (96)	23 (72)	71 (91)	97 (99)
South Africa	18 (72)	63 (88)	95 (99)	21 (90)	71 (97)	97 (100)	14 (77)	65 (88)	95 (98)	13 (65)	61 (83)	94 (97)
West Asia	12 (63)	52 (86)	90 (98)	4 (40)	31 (68)	82 (94)	12 (53)	46 (78)	88 (96)	18 (75)	69 (93)	97 (99)
Central Asia	9 (60)	58 (79)	90 (95)	4 (40)	32 (59)	76 (87)	8 (58)	52 (77)	87 (92)	14 (72)	71 (86)	95 (97)
East Asia	9 (60)	57 (75)	87 (91)	4 (52)	32 (66)	71 (85)	9 (69)	55 (83)	88 (94)	16 (76)	72 (87)	96 (96)
Australia	20 (90)	71 (96)	96 (99)	33 (99)	84 (100)	99 (100)	26 (96)	80 (99)	98 (100)	20 (79)	69 (92)	97 (99)

<sup>a</sup>DJF, December, January, and February; MAM, March, April, and May; JJA, June, July, and August; SON, September, October, and November.

2007]. There is also considerable dust activity in the western great plains in MAM.

## 5. MODIS DUST SOURCES

### 5.1. Detection

[44] After emission, dust concentration decreases by gravitational settling, dry deposition at the surface, and wet removal in and below clouds [Ginoux et al., 2001]. As long as the sources are active, DOD retrieved from instantaneous satellite measurement will be at a maximum over the sources. But dust emission is generally episodic, and subsequently, the maximum DOD will move with the plume. Nonetheless, as meteorological conditions change from day to day, maxima of DOD distribution will be more frequently located over the sources. This relationship seems to apply even over regions with quasi-permanent wind direction. For example, Ginoux et al. [2010] showed that within the Bodélé depression, the DOD maximum lies precisely over some ephemeral lakes, although the wind direction over the depression flows consistently from the northeast.

[45] Other satellite products have been used previously to detect dust sources [Prospero et al., 2002; Legrand et al., 2001; Schepanski et al., 2007]. But of these, only Prospero et al. [2002] attempted to identify dust sources on a global scale. Here we first compare our results with theirs.

### 5.2. Comparison With TOMS and OMI Aerosol Indexes

[46] One of the most comprehensive studies of dust sources was realized by Prospero et al. [2002] using near-ultraviolet (nUV) measurements by TOMS between 1980 to 1992. Herman et al. [1997] defined the TOMS aerosol index (AI) as a function of the ratio of the backscattering radiances at two wavelengths in the nUV. They showed that the TOMS AI can be used to detect dust events. Prospero et al. [2002] associated dust sources with the most frequent occurrence of TOMS AI greater than 0.7 over North Africa and 0.2 elsewhere. The difficulties in using TOMS AI to identify dust include the interference of other nUV absorbing aerosols, the sensitivity of TOMS to the aerosol vertical profile, and the presence of subpixel or underlying clouds. By restricting the use of TOMS AI to arid regions, the interference of clouds and other absorbing aerosols (e.g.,

black carbon) was minimized, and consequently, TOMS AI would be expected to be a good indicator of the presence of dust. Outside arid regions dust sources could not be unambiguously detected. M-DB2 does not suffer from these limitations, although it has its own limitations, in particular, it provides data only over bright surfaces. But the major advantage of M-DB2 products is that it can be used to make quantitative measurements of AOD, while TOMS AI cannot.

[47] Nonetheless the frequency of dust occurrence derived from TOMS AI and M-DB2 DOD should yield similar distributions over regions with overlapping retrievals. Although most dust sources identified by Prospero et al. [2002] are associated with paleolakes and depressions characterized by a deep layer of sediment, Zender and Kwon [2005] have shown that they can be subdivided depending on their response to precipitation anomalies. Some of these sources are supply limited, and their activity will depend on interannual alluvial recharge or modification of their surface crust. In making this performance comparison, we also use OMI in order to account for natural change of sources distribution over the decade that has elapsed between TOMS and M-DB2 recording dates. The OMI instrument was launched in 2004, and aerosol products are available up to 2006. The OMI aerosol index is calculated using the same wavelengths as for TOMS AI (see Torres et al. [2007] for details).

[48] Figure 6 shows the global distribution of the mean annual frequency of occurrence of M-DB2 DOD  $> 0.2$ , TOMS AI  $\geq 0.5$ , and OMI AI  $\geq 0.5$ . The frequency for M-DB2 DOD is calculated as previously described, but for the entire year rather than for each season. The TOMS and OMI AI FoO are calculated similarly by counting the number of days each year that AI  $> 0.5$ , divided by the total number of days with data, and converting into a percentage. The mean values are obtained by averaging the yearly FoO between 1980 and 1992 for TOMS AI, between 2004 and 2006 for OMI AI, and between 2003 and 2009 for M-DB2 DOD. In Figure 6, the overlap of different FoO for TOMS AI and OMI AI is informative considering that 2 decades separate their measurements. One major exception is over east China, where the 50% FoO isoline of OMI AI (lighter green isocontour) covers most of it, while the same isoline for TOMS AI (lighter blue isocontour) is limited to the Beijing area.

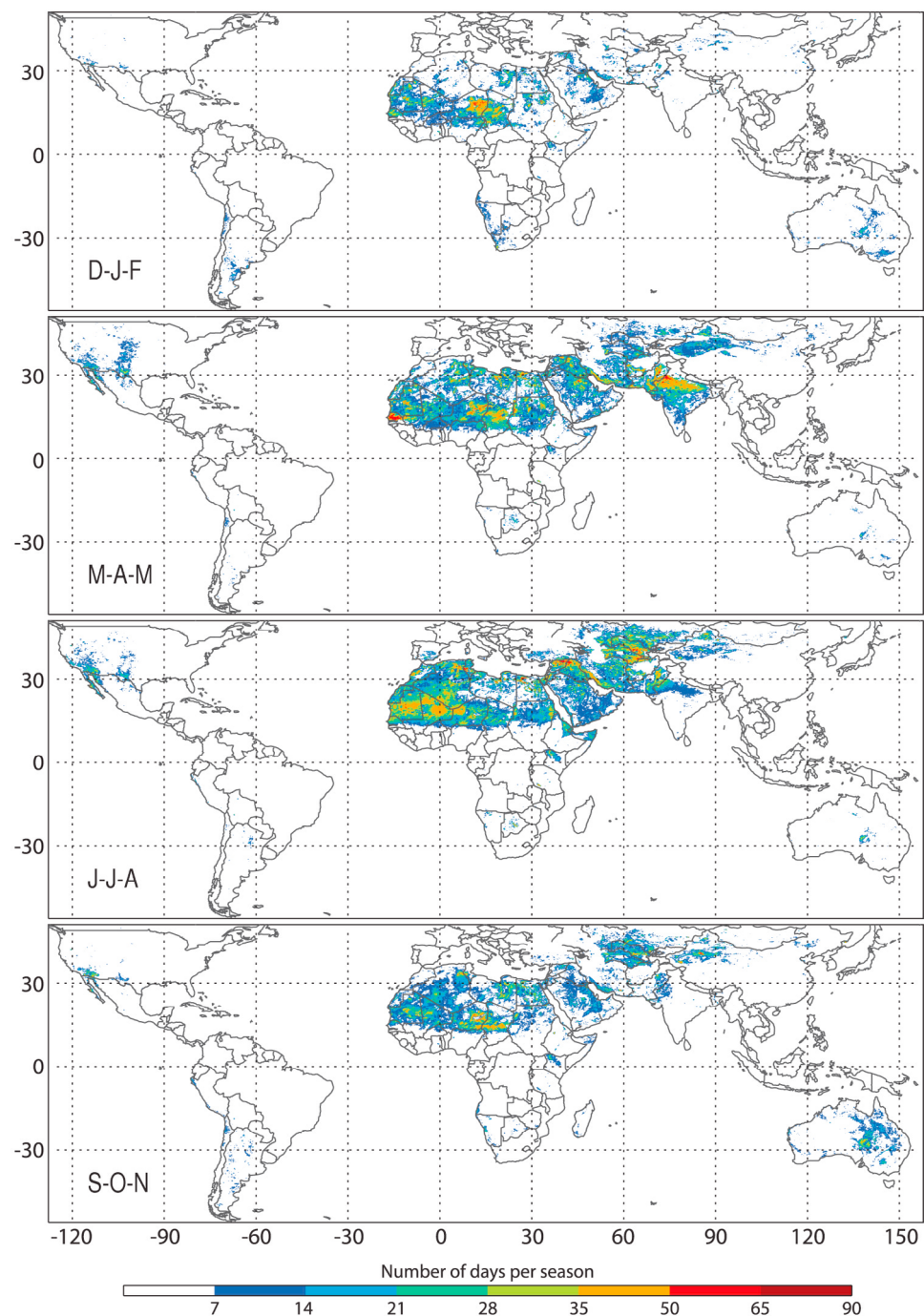


**Figure 5.** Global distribution of the mean (2003–2009) number of days per season M-DB2 DOD > 0.2.

This difference might be linked to the increasing trend of dust emission in some areas of eastern China as reported by *Zhang et al.* [2003]. They associated the trend in these areas to desertification of anthropogenic origin. More recently, *Igarashi et al.* [2011] indicate that the increasing trend of dust emission in east China is due to an adverse combination of anthropogenic grassland degradation and drought. Another region with increasing AI is along the border of Uzbekistan and Kazakhstan. This may be associated with intense irrigation along the Syr Darya and Amu Darya [Micklin, 2007].

Conversely, in Botswana and northern Australia, AI > 0.5 was observed more frequently by TOMS than OMI instruments. This decreased frequency is contrary to a study of dust storms in Australia by *Ekström et al.* [2004]. They showed an increasing trend in the annual number of dust storms in continental and coastal regions of Australia in the last 20 years of the twentieth century that they attributed to increased drought. However, the dependency of AI on factors such as elevation, layer thickness, and the absorption properties of dust is as strong as the mass load [Ginoux and

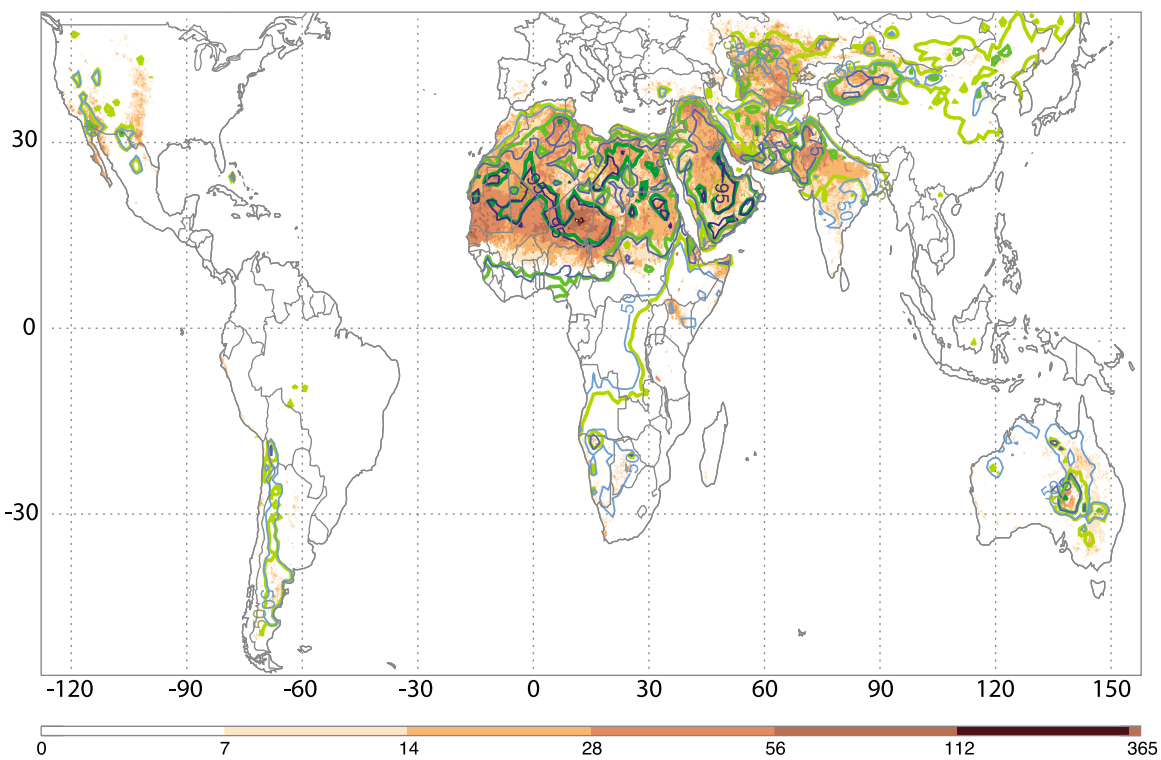


**Figure 6.** Annual mean frequency distribution of M-DB2 (2003–2009) DOD > 0.2 (red), TOMS (1980–1991) aerosol index  $\geq 0.5$  (blue), and OMI (2004–2006) aerosol index  $\geq 0.5$  (green). The isocontours of TOMS and OMI have been removed over oceans for clarity.

Torres, 2003]. These factors may be responsible for this apparent discrepancy between TOMS and OMI AI.

[49] Concerning M-DB2 dust sources, the TOMS and OMI AI envelop most of M-DB2 DOD shading. The regions where M-DB2 coverage is larger than OMI and TOMS are the high plains of the United States, the Baja California Peninsula, the Mediterranean basin, Kirghiz steppe of Kazakhstan, and the Australian Riverina. We might have also added to the list the southeast coast of India if the number of retrievals were not so low (cf. Figure 1). In 2007, the period not covered by OMI data, the western North American plains were particularly wet, but 2008 and 2009 were marked by dry-to-drought conditions [Cayan *et al.*, 2010]. The drought in East Australia in 2009 has been linked to a very pronounced El Niño phase over the Pacific [Webb *et al.*, 2006].

[50] On the other hand, some areas of TOMS AI  $> 0.5$  do not overlap with M-DB2 FoO DOD  $> 0.2$ , most notably the region south of the Sahel in North Africa. These differences occur most frequently in the tropics where there is no M-DB2 retrieval (cf. Figure 1). In Botswana, both OMI and M-DB2 have much lower frequency of dust events than TOMS because the 1980s were much drier in southern Africa [Morishima and Akasaka, 2010]. In east China, OMI AI covers a larger area than M-DB2 shading, which in turn covers a much larger region than the TOMS AI 50% isoline. As the number of dust events detected from M-DB2 is quite low (cf. Figure 5), it is difficult to reach firm conclusions about these differences.

### 5.3. Attribution

[51] Prospero *et al.* [2002] have shown that dust sources are usually associated with topographical lows in arid regions where runoff and flooding have created lacustrine and alluvial sediments. Only the most prominent topographic features were characterized in their study because of the coarse TOMS resolution. With M-DB2 0.1° resolution, it is possible to make more precise attributions, in particular the linking of sources to land use and ephemeral water bodies.

[52] To link dust sources to hydrologic features, we use MODIS 0.01° resolution database (E. Vermote, personal communication, 2010), which provides data on shorelines, ephemeral water, and shallow and deep inland water features. We identify a dust source as “hydrologic” when there is at least one of these types of water bodies within a M-DB2 0.1° grid cell. Our method excludes any hydrologic feature less than 1 km wide. As most rivers, ponds, and lakes have smaller scale, we may be underestimating the amount of sources directly related to hydrology.

[53] We label a dust source as “anthropogenic” if it is associated with some form of land use (agriculture). We use the data set developed by Klein Goldewijk [2001] (henceforth KG01) which provides globally the fraction of agriculture within every 0.1° grid cell relative to the end of the twentieth century. To determine the relative importance of climate and land use in dust emission, Tegen *et al.* [2004] considered a source to be natural if there is less than 5% land use. A similar threshold was used by Ginoux *et al.* [2010]. However, most desertic areas in the KG01 data set

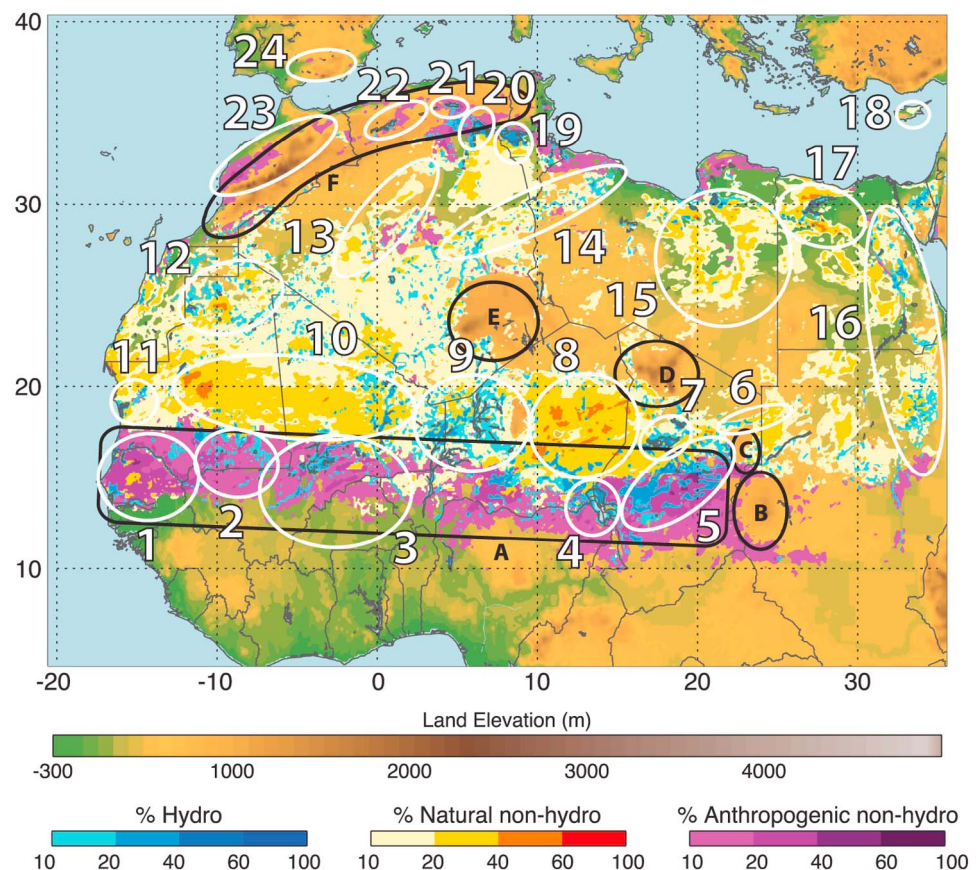


**Figure 7.** Distribution of the percentage number of days per year M-DB2 DOD  $> 0.2$  over North Africa overplotted on shaded orography. The frequencies associated with (hydro) and without (nonhydro) ephemeral water bodies and with less (natural) and more (anthropogenic) than 30% land use are shaded in blue; yellow, red, and orange; and magenta, respectively. The frequency levels are 10%, 20%, 40%, 60%, and 100%. The topography shading varies from dark green ( $-300\text{ m}$ ) to brown ( $1000\text{--}4000\text{ m}$ ), then to grey for high elevation up to  $8000\text{ m}$ . Some source areas, discussed in the text, are contoured in white and are numbered as follows: 1, Senegal River Basin; 2, Aoukar depression; 3, upper Niger River Basin; 4, Lake Chad; 5, river drainage basin of the Ennedi and Ouaddaï highlands; 6, Mourdi depression; 7, Bodélé depression; 8, Grand Erg of Bilma; 9, river drainage basin of the Aïr; 10, Erg El Djouf; 11, Sebkhet te-n-Dgämcha; 12, Tiris Zemmour region; 13, Grand Erg Occidental; 14, Grand Erg Oriental; 15, Libyan Desert; 16, Nile River Basin; 17, Qattarah depression; 18, Mesaoria plain in Cyprus; 19, Chott el Jerid; 20, Chott Melrhir; 21, Chott el Hodma; 22, Chott ech Chergui; 23, Morocco coastal plains; and 24, Andalusia in Spain. Some geographic features are contoured in black and are labeled as follows: A, the Sahel; B, the Ouaddaï Highlands; C, Ennedi; D, Tibesti; E, Ahaggar; and F, Atlas Mountains.

have 5% land use, and it is not realistic to assume that most desertic sources are anthropogenic. On the other hand, above 30% land use the spatial distribution is relatively similar. This may be explained by the fact that once an area is found to be suitable for agriculture, most of the land will be rapidly developed for such use. Therefore, we adopt a value of 30% as the threshold land use to separate natural and anthropogenic sources. The sensitivity of our computed dust emissions to land use percentage is discussed in section 6.

[54] In the following eight figures the relative frequency of  $\text{DOD} > 0.2$  on a seasonal or annual basis is shown for different continental regions. The selection of a particular season is based on the maximum intensity of the sources over that region. It should be noted that the scaling of FoO varies between figures to improve clarity. In addition, dust sources

may vary considerably between seasons. Because of space limitations, we only show the peak seasons of dust activity. The exception is North Africa, for which we show the annual distribution.

[55] The figures show the associations with three source types: hydrologic, dust linked to various water features as discussed above; natural, dust emitted from land surfaces where land use is less than 30%; and anthropogenic, sources where land use exceeds 30%. The dominant source designation is carried out as follows: If there is a hydrographic feature in the grid cell, it is designated as “hydro” source. If it is not “hydro” and if land use is less than 30%, it is “natural.” If it is not “hydro” and land use is greater than 30%, it is “anthropogenic.”

#### 5.4. North Africa and Europe

[56] The annual mean distribution of FoO AOD > 0.2 over North Africa is shown in Figure 7. A major difference from the results of Prospero *et al.* [2002] is the large source of dust throughout much of the southern Sahel (black contour labeled A in Figure 7). However, Prospero *et al.* [2002] removed the Sahel region from their study because TOMS AI could not distinguish between biomass burning aerosols and dust. We also note in Figure 7 the southern Sahel sources are overwhelmingly anthropogenic, and there is a clear separation between natural dust sources in the Sahara and anthropogenic dust in the southern Sahel. The sources in the Atlas Mountains (zone F in Figure 7) and along the Mediterranean coast are also mostly anthropogenic.

[57] There are limited in situ data over the Sahel, but they all suggest that dust emissions are related to land use. Gill [1996] reported measurements in the 1950s showing that playas and ephemeral lakes were reactivated by overgrazing and cultivation in Senegal (location 1 in Figure 7), as well as from Lake Faguibine in Mali (blue spot in location 3 at the border with Mauritania). Analyzing thousands of years of dust deposition in the mouth of the Senegal River, Mulitza *et al.* [2010] found a sharp increase after the advent of commercial agriculture in the Sahel, about 200 years ago. Gillies *et al.* [1996] have studied intense dust haze events emitted from alluvial sediments of the Inland Delta of the Niger River (location 3) near Mopti in Mali. These sediments are deposited by seasonal flooding from the Niger River. These sediments have a large percentage of silt and clay and are generally heavily crusted except where disturbed by herds [Nickling and Gillies, 1993]. Using surface visibility data, N'Tchayi Mbourou *et al.* [1997] reported a continually increasing presence of dust in the Sahel since the 1950s, particularly in the western Sahel. A recent analysis of this data set by Klose *et al.* [2010] suggests that dust observed in the Sahel is primarily windborne dust transported from the Sahara. On the other hand, Bou Karam *et al.* [2008] studied several cases of dust storms generated within the monsoon flow over the Sahel, and Lyngsie *et al.* [2011] found that dust collected in northern Ghana had a local origin.

[58] The Senegal River Basin (location 1 in Figure 7) appears as an anthropogenic source with FoO up to 60% of days per year. Niang *et al.* [2008] analyzed 50 years of visibility data and aerial photos along the Senegal River. They found a continuous disappearance of forest from 1954 to 1992, a time span that included the severe droughts of the 1970s and 1980s. During the following years precipitation was closer to normal; water erosion increased, which produced gullying, bank erosion, and badlands, which in turn resulted in increased dust production. These observations are consistent with those of Mulitza *et al.* [2010], who associated increased offshore sediment deposition with the onset of agriculture in the region. We lack similar information for the Niger River, but we would expect the same sequence of conditions: deforestation followed by water and wind erosion. If confirmed, it would suggest that dust

sources in the Sahel are largely controlled by river streamflow and soil disturbance.

[59] Outside the Sahel, major sources in Figure 7 have been identified and described by Prospero *et al.* [2002]. These include major depressions (Bodélé, location 7, and Qattarah, location 17), large basins with sand seas (Erg of Bilma, location 8; Erg el Djouf, location 10; Grand Erg Occidental, location 13; Grand Erg Oriental, location 14; and Libyan Desert, location 15), ephemeral lakes (Sebkhet te-n-Dgâmcha, location 11; Chott el Jerid, location 19; Chott Melrhir, location 20; and lakes in the Tiris Zemmour region, location 12), and the Nile River Basin (location 16), all of which are essentially natural sources. Additional sources associated with ephemeral lakes can be identified in Figure 7, such as Chott el Hodma (location 21) and Chott ech Chergui (location 22) in the Atlas Mountains (location F). Mahowald *et al.* [2003] have shown the importance of the hydrological cycle on modulating dust emission in the zone of Chotts. In addition to these large natural sources, smaller anthropogenic sources can be identified in coastal Morocco (location 23), Tunisia, Libya, and Egypt.

[60] The Bodélé depression (location 7 in Figure 7) has been studied extensively, including during the BoDEx field campaign [Washington *et al.*, 2006; Todd *et al.*, 2007]. Prospero *et al.* [2002] described it as one of the most intense dust sources in the world. The frequency and intensity of dust emissions from the Bodélé has been related to a Venturi effect of the Harmattan winds passing between the Ennedi (location C) and Tibesti (location D) mountains [Washington *et al.*, 2006]. In Figure 7, we see additional sources (location 5) associated with alluvial fans and wadis on the flanks of the Ennedi (location C) and Ouaddai highlands (location B). The alluvial fans in this region are the sources of weathered sedimentary material which is carried down to the Bodélé (location 7) and even the Erg of Bilma (location 8), constantly replenishing these sources with fine soil particles [Wright, 2001]. Schepanski *et al.* [2009] also identified these flanking fans as dust sources. Alluvial sediments (location 9) are also clearly identified on the southern flank of the Air and the Ahaggar (location E) mountains. These sources are sensitive to the hydrological cycle as well as to effects of mesoscale winds intensified by the orography.

[61] Dust activity is seen in Figure 7 along the Mediterranean basin in Andalusia (location 24) and Cyprus (location 18). These sources reach a maximum activity in summer, with maximum FoO over the fluvial plains of the Guadalquivir and Segura Rivers in southern Spain. Dust from these sources is mainly associated with agriculture, and dust tends to channel through and flow down the river valley [Fernandez *et al.*, 2000]. Desertification in the western Mediterranean basin has been documented for quite some time and appears to have been triggered by climatic variability and demographic disequilibrium and the associated changes in agricultural practice [Puigdefàbregas and Mendizabal, 1998]. In summer, dust sources are also apparent in the Konya plain (cf. third panel in Figure 4), which were previously identified as the hot spot of wind erosion in Turkey [Berkay *et al.*, 2006; Avci, 2011].

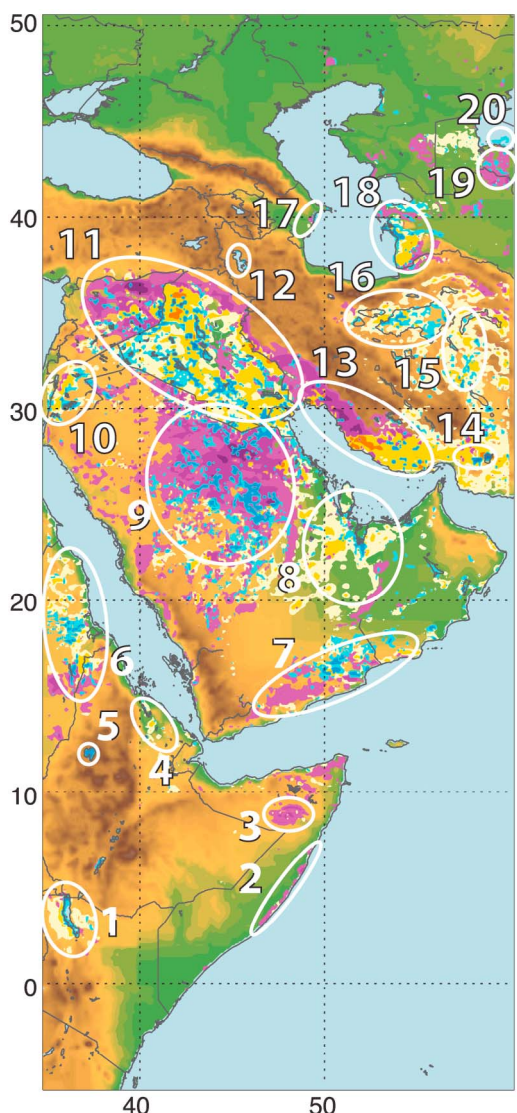


**Figure 8.** Distribution of the percentage number of days per season (March, April, and May) M-DB2 DOD  $> 0.2$  over the Middle East with color code as in Figure 6. The white circled sources are numbered as follows: 1, Chalbi Desert of Kenya; 2, coastal desert of Somalia; 3, Nogal Valley of Somalia; 4, Danakil Desert of Ethiopia; 5, Lake Tana of Ethiopia; 6, northeast Sudan; 7, Hadramawt region; 8, Empty Quarter; 9, highlands of Saudi Arabia; 10, Jordan River Basin of Jordan; 11, Mesopotamia; 12, Urumia Lake of Iran; 13, coastal desert of Iran; 14, Hamun-i-Mashkel; 15, Dasht-e Lut Desert of Iran; 16, Dasht-e Kavir Desert of Iran; 17, Qobustan in Azerbaijan; 18, Atrek delta of Turkmenistan; 19, Turan plain of Uzbekistan; and 20, Aral Sea.

### 5.5. Middle East

[62] The distribution of FoO with DOD  $> 0.2$  for the Middle East is shown in Figure 8 for MAM. FoO is higher than 20% over most of Mesopotamia (location 11) and is composed of a mixture of anthropogenic, natural, and hydrologic sources. As far back as the 1980s, the region was described as a major source of dust [Middleton, 1986]. The dust from the region between the Tigris and Euphrates is

mostly natural in Iraq but anthropogenic in Syria. There is also a distinct contrast at the border of Iraq with Saudi Arabia and Iran where dust is anthropogenic. The maximum frequency ( $\text{FoO} > 60\%$ ) is located over the farmland region northeast of the city of Ar Raqqah (Syria) in the northwest of region location 11, which was described by *Walker et al.* [2009] as generating anthropogenic dust plumes. The highest frequency along the border of Syria and Iraq corresponds to several sabkhas (Arabic for salt flat): Albu Gharz, al Burghuth, and Ar-Rawda. In Saudi Arabia (location 9), there is a mixture of anthropogenic and hydrologic sources, but they are essentially aggregated around three wadis (Arabic for dry riverbed): Al Batin, Al-Rimah, and Al Sahba. *Fryberger et al.* [1983] described eolian erosion from these wadis, as well as from the sabkhas, with a peak emission in June. In the Rub' al Khali sandy desert (location 8), the sources are sparse, except for the very large Sabkha Matti in the United Arab Emirates, which extends from the Emirates into Saudi Arabia. The sabkha interfingers into sand dunes, offering a source of sand which efficiently sandblasts the sabkha surface to generate dust emission as observed by *Alsharhan and ElSammak* [2004]. Dust storms in the area are becoming an environmental problem [Abdelfattah, 2009].

[63] There are many other sources in the Middle East. We note in particular a cluster of anthropogenic and hydrologic sources along the Jordan River, particularly on the east side (location 10) which corresponds to the Wadi Araba Desert characterized by *Saqqa and Atallah* [2004]. Several studies have indicated that the diversion of water from the Jordan River has induced wind erosion of desiccated sediments in the Paleolake Lisan basin [Gill, 1996; Ghazleh et al., 2011]. In Yemen, large dust sources are associated with river fans at the base of the coastal escarpment in the Hadramawt (location 7).

[64] One prominent source is situated along the west coast of Iran (location 13), as previously noted by *Middleton* [1986] and *Littmann* [1991]. The northwestern part is anthropogenic, and the southeastern part is natural. The other major sources in Iran are associated with large salty lakes, such as the southern shore of the Urumia Lake (location 12), or in the Hamun-i-Mashkel (location 14) and the Dasht-e Kavir (location 16) Deserts. These deserts have been previously identified as dust sources by *Middleton* [1986]. More recently, *Rashki et al.* [2012] have indicated that due to land use change and desiccation of lakes in the Hamun-i-Mashkel, the frequency and severity of dust storms have been significantly increased. Because of water diversions, Urumia Lake is becoming a new source of salt dust [Golabian, 2011; Zarghami, 2011] much like the Aral Sea today.

[65] The plains between the Caspian and Aral Seas are largely irrigated for agriculture and thus qualify as active anthropogenic dust sources. Specific sources are the delta of the Atrek River (location 18) and the Turan plain (location 19). The dramatic decrease in the size of the Caspian Sea because of water diversions has lead to rapid exposures of formerly inundated land [Dickerson, 2000] which have now become dust sources. The diversion of river water for irrigation has greatly reduced river flow and is the

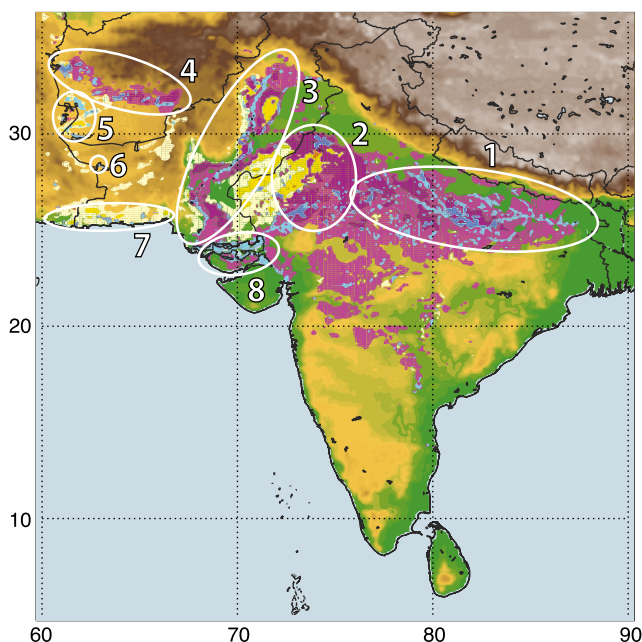


**Figure 9.** Distribution of the percentage number of days per season (March, April, and May) M-DB2 DOD  $> 0.2$  over the Indian subcontinent with color code as in Figure 6, except the percentage levels are 20%, 40%, 60%, 80%, and 100%. The white circled sources are numbered as follows: 1, Ganges basin in India; 2, desert of Rajasthan in India; 3, Indus basin of Pakistan; 4, southern drainage basin of the Hindu Kush in Afghanistan; 5, ephemeral lakes around the city of Zabol; 6, Hamun-i-Mashkel of Pakistan; 7, Makran coast of Pakistan; and 8, Rann of Kutch in India.

fundamental cause of the desiccation of the Aral Sea [Micklin, 2007, 2010]. The Aral Sea was formerly one of the largest lakes in the world (area 68,000 km<sup>2</sup>) but is now reduced to 10% of its original size. Large areas of the Aral Sea are now active dust sources (location 20), in agreement with in situ measurements by Wiggs *et al.* [2003]. Darmenova and Sokolik [2007] showed the importance of feedbacks between dust emission and meteorology over the Aral Sea. The authors noted that such feedbacks add further complexity to the quantification of the anthropogenic dust fraction in the region. On the west side of the Caspian Sea, the sources are limited to small sections along the coastal region in the Qobustan area (location 17), south of Baku. The region has the largest concentration of mud volcanoes in the world, which emit mineral aerosols with large amounts of gases [Kopf *et al.*, 2010].

## 5.6. East Africa

[66] In northeast Africa, the dust sources are aggregated into six arid or semiarid areas (Figure 8): the Chalbi Desert and semiarid northeastern province of Kenya (location 1), the coastal desert of Somalia (location 2), the arid Nogal Valley (location 3), the Danakil Desert in the Dafar Depression of Ethiopia (location 4), Lake Tana of Ethiopia (location 5), and the coastal region of northeast Sudan (location 6). The Chalbi and Danakil Deserts were paleolakes at about the same time as the Bodélé depression was a lake [Abell and

Nyamweru, 1988]; with changing climate the lakes became dust sources [Nyamweru and Bowman, 1989], as previously noted by Parkinson [1939] and Hemming and Trapnell [1957].

## 5.7. Indian Subcontinent

[67] Figure 9 shows FoO distribution over the Indian subcontinent in MAM when DOD is high over all of northern India (Figure 4). The dust is largely attributed to land use with a widespread contribution associated with ephemeral water bodies ranging in scale from the major rivers to small lakes. Some seasonal lakes may be so dense as to occupy an entire region, such as in the Rann of Kutch (location 8). Dust sources occupy the entire Indo-Gangetic basin (locations 1, 2, and 3), which is characterized by intense agricultural activities as well as persistence of dust transported from desert regions of western India [Prasad *et al.*, 2007].

[68] The highest frequency is observed in the Rajasthan province (location 2) with maxima (FoO  $> 70\%$ ) along the Ghaggar River, which flows intermittently only during the monsoon season (June to September). The Rajasthan Desert is considered as a significant dust source of southwest Asia [Pandithurai *et al.*, 2008], and Ramachandran *et al.* [2012] indicate that increased wind speed over the Rajasthan Desert is a factor in increasing optical depth over parts of India over the past decade. Gill [1996] previously indicated that human-influenced desertification processes have resulted in wind erosion and deposition of sediments in saline lake basins in Rajasthan. Other agricultural areas include the Indian Plateau where FoO is in some areas greater than 20%.

[69] In Pakistan, the most pronounced maximum is in the Lakki Marwat district over the fluvial plain of the Karram River, a tributary of the Indus (location 3). Dust events yield FoO greater than 40% along the Makran coast of Pakistan (location 7) and more than 70% FoO in the fluvial plain of the Dasht River near the border with Iran. Using TOMS aerosol index, Goudie and Middleton [2001] classified the Makran coast as one of the major global dust sources. The Hamun-i-Mashkel ephemeral lake (location 6) was identified previously by Middleton [1986] as a dust source, and M-DB2 indicates up to 50% FoO during spring.

[70] In Afghanistan, there are two areas of dust activity. One occupies the front range of the Hindu Kush (location 4), which is strongly incised by many rivers feeding into the Helmand River with some irrigated agriculture along Highway 1 between Farah in the west to Kandahar. The other is formed by dust from seasonal lakes within the Sistan Basin (location 5): the Hamoun-i Sabari, Hamun-i Puza, and Gaud-i Zereh in Afghanistan and the Hamin-i Helmand in Iran. The extent and volume of the hamuns varies substantially from season to season and from year to year. They expand during the spring and reach a maximum size in late May and June and then shrink due to high evaporation and low inflow [Whitney, 2006]. On the basis of dust storm frequency, Middleton [1986] ranked Zabol among the dustiest places on Earth. The Helmand Basin has recently experienced an unusually prolonged series of droughts since 2000, and as one of the windiest deserts in the world, it produces dust plumes that are hundreds of kilometers long and which are

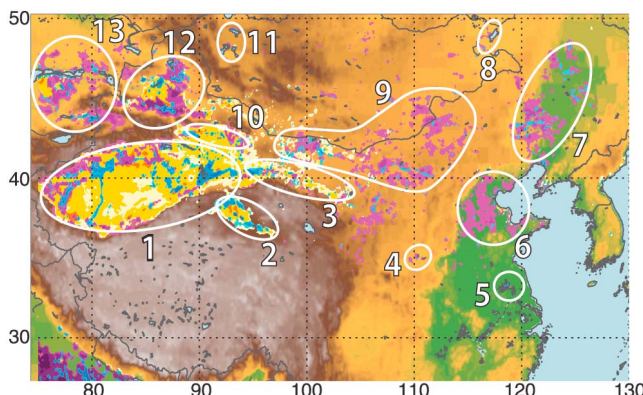


**Figure 10.** Distribution of the percentage number of days per season (March, April, and May) M-DB2 DOD  $> 0.2$  over East Asia with color code as in Figure 6, except the percentage levels are 5%, 10%, 25%, 50%, and 100%. The white circled sources are numbered as follows: 1, Tarim Pendi; 2, Qaidam Pendi; 3, Hexi corridor in Gansu Province; 4, Tongguan county; 5, Hongze and Gaoyou Lakes of eastern China; 6, North China Plains; 7, Horqin sandy land; 8, Hulun Buir plain; 9, Inner Mongolia deserts; 10, Turpan Pendi; 11, Great Lakes depression in Mongolia; 12, Junggar Pendi; and 13, Balkhash-Alakol depression.

frequently captured in spectacular satellite images [Whitney, 2006].

### 5.8. East Asia

[71] In China (Figure 10) the largest natural sources are associated with basins (“pendi” in Mandarin). They include the Taklamakan Desert of the Tarim Pendi (location 1), the Qaidam Pendi (location 2), and the Turpan Pendi (location 10). A long series of natural sources are stretched along the Hexi corridor, in the Gansu province (location 3) at the base of the Tibetan plateau; these sources are associated with fluvial fans [Derbyshire et al., 1998]. Except for some areas in the Gobi Desert of Inner Mongolia (location 9), all other sources are essentially anthropogenic. Xuan and Sokolik [2002] found that human activities, mainly farming, overgrazing, and water usage, have likely been responsible for the expansion of dust sources in northern China. Igarashi et al. [2011] add that drought has been also a contributing factor. Gong et al. [2004] showed that although desertification has increased by only a few percent in China, it has generated disproportionately large areas of enhanced dust emissions. In agreement with their study, Figure 10 shows anthropogenic sources mostly in the deserts of Inner Mongolia (location 9), on the Hulun Buir plain (location 8), on the northeast China plains (location 7), within the Junggar Pendi (location 12), and on the margins of the Tarim Pendi (location 1). The largest anthropogenic FoOs (between 10% and 25%) are distributed over the Junggar Pendi (location 12). Although there are scattered sources outside the identified areas in Figure 10, dust activity is relatively low with FoO less than 10%. Kurosaki and Mikami [2005] have established over East Asia the geographic distribution of dust outbreaks and floating dust FoO from visibility data. Our

results appear to agree with their study not only in the distribution of maxima but also in the values of FoO. The similarity of our results is also apparent in agricultural or industrialized areas, such as along the Wei and Yellow Rivers (location 4), in the north China plains (location 6), and around Hongze and Gaoyou Lakes in eastern China (location 5). This is also consistent with Wang et al. [2006], who find that dust storm frequency does not exceed 8 days per year in northern China, even where there are high levels of human activity.

[72] In Mongolia, there are dozens of small sources associated with pasture, lakes, or alluvial fans. The sources are generally small with low FoO except in the Great Lakes depression (location 11), where FoO  $> 10\%$  around Lakes Chjargas and Char Us. In the southern part, along the Gobi Desert, FoO varies between 5% and 10%. This seems to agree with the analysis of data from 47 meteorological stations in Mongolia by Natsagdorj et al. [2003]. They found that only in the southern Gobi Desert and semidesert areas could the frequency of dust storms reach 10%; elsewhere, it is less than 5%.

[73] The Balkhash-Alakol depression in eastern Kazakhstan (location 13) is a significant source of anthropogenic dust. Gill [1996] indicated that Lake Balkhash has been rapidly desiccating since 1970 after completion of a dam on the Ili River. Over the eastern part of Lake Balkhash and the entirety of nearby dry lakes, the FoO is greater than 50%. Abuduwaili et al. [2008] have studied Lake Ebinur located on the eastern part of the Dzungarian basin (location 12) in a narrow pass connecting with the Balkhash-Alakol depression (location 13). As a result of human-induced desiccation, the dry lake bed is now the source of intense dust storms with a peak frequency in spring. Chemical analyses of dust samples around Lake Ebinur indicate a high level of potentially toxic trace elements [Liu et al., 2011]. Within the depression, FoO is mostly anthropogenic with values between 10% and 25%. The impact of human activities in the area has been investigated by Kezer and Matsuyama [2006], who found that river runoff draining into Lake Balkhash has decreased by half since 1970 due to human activity. In fact, comparable reductions were found for most tail-end lakes in flat areas of central Asia [Bai et al., 2011].

### 5.9. North America

[74] Most dust activity over North America (Figure 11) is centered in two western areas separated by the continental divide. One area occupies the high plains (location 11) on the east side of Rockies and is essentially anthropogenic. On the west side of the divide, the anthropogenic and natural sources are intertwined. In the Sonoran Desert (location 1), sources on the west side of the Gulf of California are mostly natural, and on the east side, sources are anthropogenic.

[75] The high plains (location 11 in Figure 11), which extend from Montana to southern Texas, are the largest dust source in North America, and the dust is almost entirely anthropogenic in origin except for a few ephemeral lakes. This semiarid and subhumid region accounts for 60% of wind erosion in the U.S., with the highest frequency located

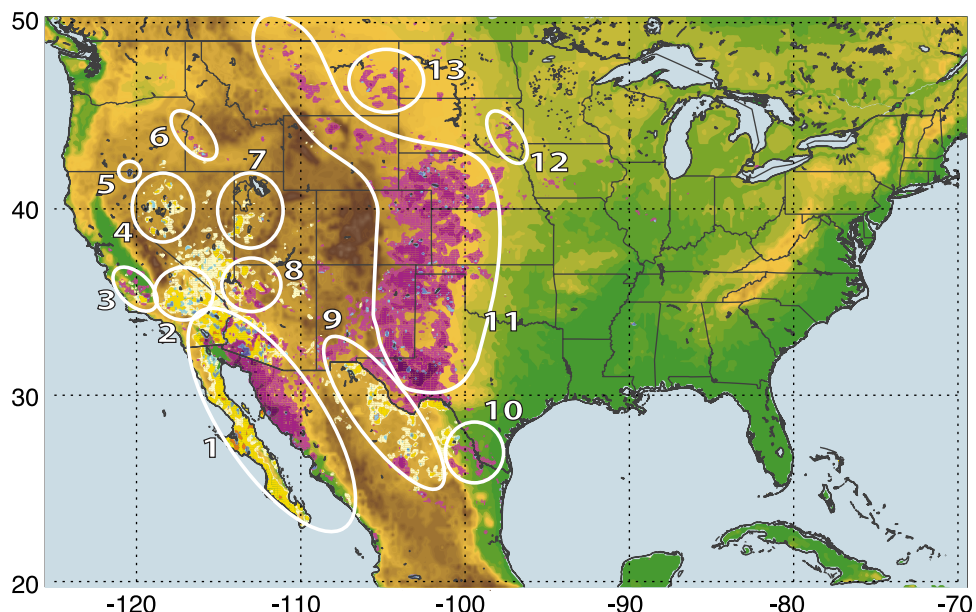


**Figure 11.** Distribution of the percentage number of days per season (March, April, and May) M-DB2 DOD  $> 0.2$  over North America with color code as in Figure 6. The white circled sources are numbered as follows: 1, Sonoran Desert; 2, Mojave Desert; 3, San Joaquin Valley; 4, Black Rock-Smoke Creek deserts; 5, Goose Lake; 6, Snake River; 7, Great Salt Lake Desert; 8, Colorado River; 9, Chihuahuan Desert; 10, Rio Grande; 11, High Plains; 12, Big Sioux River; and 13, lower Yellowstone Valley.

in the southern plains of Texas, which experience 50 dust days per year, the national maximum [Hagen and Woodruff, 1973]. Our result differs from Prospero *et al.* [2002], who did not find any significant dust activity in the high plains from TOMS data covering the 1980s. But an earlier study based on visibility data from 1940 to 1970 by Orgill and Sehmel [1976] did show a maximum reduction of visibility along the high plains, with a peak in the southern great plains. Cook *et al.* [2007] have reconstructed drought cycles over North America from tree rings. They reported severe drought in the midwest and high plains for the 1930s, 1950s, and 2000s, while the 1980s were not particularly dry or wet. This suggests that dust source activity in the high plains is modulated by precipitation variability. Such a dependency has been previously shown to exist in the southern part of the high plains by Stout and Lee [2003]. With projected increase of severe drought in the southwest [Seager and Vecchi, 2010], this region may experience an increase in dust events in the future.

[76] An interesting result drawn from Figure 11 is that major river basins are potential dust sources, although relatively weak. These include the Snake (location 6), Colorado (location 8), Pecos and Rio Grande (location 10), and Big Sioux (location 12) Rivers and the lower Yellowstone Valley (location 13). Dust activity in some of these basins has been previously reported [Lee *et al.*, 2009; Munson *et al.*, 2011]. In fact, there is a remarkable similarity between Figure 11 and the figure presented by Nordstrom and Hotta [2004] showing the locations of cropland in the U.S. that have the greatest potential for wind erosion.

[77] In the Columbia plateau, Nordstrom and Hotta [2004] indicated that dust is related to dry conditions and agricultural

practice. Each fall after harvest, half of the dryland soils are bare due to the 2 year crop rotation system, while the other half is mostly dry and sparsely vegetated rangelands [Claiborn *et al.*, 1998].

[78] Some anthropogenic dust sources are observed along the Coast Ranges in the southwest part of the San Joaquin Valley, California. M-DB2 sources in the valley (location 3) are essentially anthropogenic and localized in the southernmost part near Bakersfield. There is one natural hot spot over the Carrizo Plain, which includes Soda Lake, shown as a hydrologic source in Figure 11. Nordstrom and Hotta [2004] indicated that much of the dust produced from soil erosion in California comes from desert environments, but cropland is also prone to dust generation, such as in the same region of the Central Valley where agriculture is industrialized and the climate is semiarid Mediterranean type with a long, dry summer and fall. Fugitive dust from intense agricultural activities is the primary constituent of aerosols in the southern San Joaquin Valley [Chow *et al.*, 1992, 2003].

[79] Our results reinforce the conclusions of previous studies in which it was shown that anthropogenic dust is significant in North America [e.g., Neff *et al.*, 2008]. But there are also many natural sources in North America. Many are distributed within the Black Rock and Smoke Creek Deserts (location 4), Great Salt Lake Desert (location 7), Mojave Desert (location 2), and Chihuahuan Desert (location 9). The Black Rock Desert was part of Lake Lahontan in the Pleistocene, and the depression is now composed of multiple ephemeral lakes. Similarly, the Great Salt Lake Desert was part of Lake Bonneville in the Pleistocene. In these deserts, FoO maxima are localized on or near the playas, with values greater than 20% covering Sand Spring

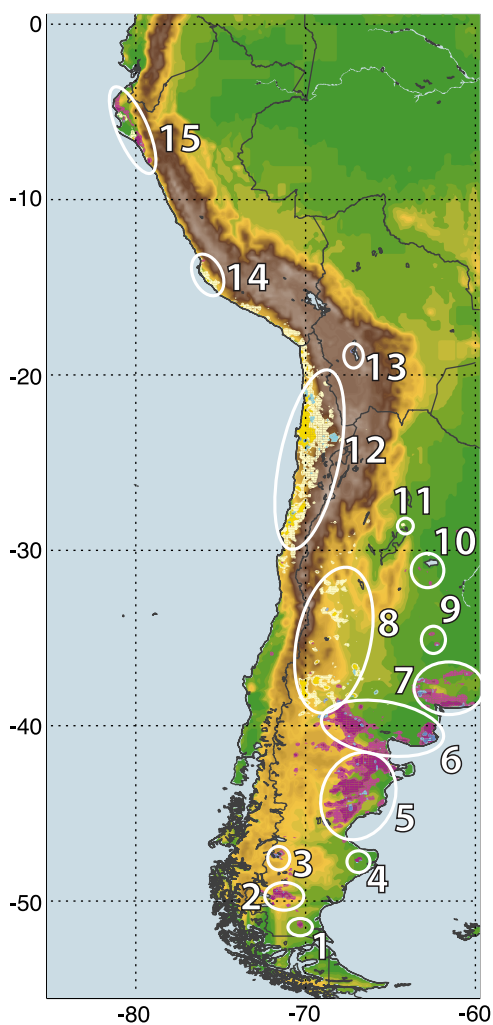


**Figure 12.** Distribution of the percentage number of days per season (December, January, and February) M-DB2 DOD  $> 0.2$  over South America with color code as in Figure 6. The white circled sources are numbered as follows: 1, Gallegos River; 2, San Martin and Viedna lakes; 3, Lake Pueyrredon; 4, ephemeral lakes in the Deseado district of Santa Cruz Province; 5, coastal plains of Chubut Province; 6, Rio Negro plain; 7, Buenos Aires Province; 8, eastern flank of the Andes; 9, Laguna Salada; 10, Laguna Mar Chiquita; 11, Salinas Grandes Desert in Argentina; 12, Atacama Desert of Chile; 13, Lake Poopo of Bolivia; 14, Nazca Desert of Peru; and 15 Sechura Desert of Peru.

Salt Flat and the southern part of Lakes Winnemucca and Pyramid. Peak activities are in spring. The generation of dust storms from these playas has been mentioned by Gill [1996] and studied in detail by Lewis *et al.* [2011] and Hahnenberger and Nicoll [2012].

[80] The source characteristics of Chihuahuan Desert (location 9) dust outbreaks have been studied by Rivera Rivera *et al.* [2010]. They showed that although playa deposits and alluvial deposits dominate the dust sources, about 23% of them are agricultural lands. This partitioning corresponds to our results.

[81] Figure 11 shows many sources, either natural or anthropogenic, related to ephemeral water bodies. An example is Owens Lake in California (location 2) which was desiccated by water diversions of the Owens River into Los Angeles Aqueduct since 1913 [Gill, 1996]. Goose Lake (location 5) at the border between Oregon and California is a quasi-permanent dust source in M-DB2 data. Gill [1996] found that the desiccation of Goose Lake, among others, has lead to blowing plumes of salt dust. Similarly ephemeral lakes in the Great Salt Lake Desert (location 7), the Mojave Desert (location 2), and the Sonoran Desert (location 1) are sources of dust.

### 5.10. South America

[82] The FoO distribution DOD  $> 0.2$  for DJF over South America is shown in Figure 12. The largest natural sources of dust are located in the Atacama Desert of Chile (location 12), followed by the Nazca (location 14) and Sechura (location 15) Deserts of Peru. In Argentina, the FoO distribution matches remarkably well the zones of aeolian landforms described by Zárate and Tripaldi [2012]; all sources are of anthropogenic origin, except on the eastern flank of the Andes (location 8).

[83] The dust sources in Patagonia are often associated with major river basins: sections of the Rio Negro from Neuquén to the Atlantic in the Rio Negro province (location 6), most of the Chubut (from Lake Colhue Huapi) and Chico Rivers in the Chubut province (location 5), and the lower section of the Deseado River in the Santa Cruz province (location 4). Pasquini and Depetris [2006] studied the discharge trends and flow dynamics of South American rivers from the early 20th century to the beginning of the 21st century. They found a significant decrease in the discharge of all the rivers that we identify as dust sources; in contrast, they found increasing flow trends for the rivers not appearing as dust sources in Figure 12 (e.g., the Santa Cruz in Santa Cruz province). This would seem to suggest an influence of climate variability on dust sources in Patagonia. However, it has been suggested that sheep ranching is largely responsible for the desertification of Patagonia and is the cause of the observed doubling of dust in Antarctic Peninsula ice cores during the twentieth century [McConnell *et al.*, 2007]. Due to the tendency of herds to concentrate around water sources, riparian areas and wetlands are heavily impacted by grazing. Consequently, dust sources in Patagonia may be characterized as being anthropogenic both by direct disturbance of soil cover and by the indirect effect of climate change. Similarly, in the Magellan region (location 1), ranching is important, and again, dust sources are observed along the Gallegos River.

[84] Patagonia is also a region of known glaciogenic dust sources [Li *et al.*, 2008, 2010]. Sugden *et al.* [2009] suggest that glacial lakes San Martin, Viedna (location 2), and Pueyrredon (location 3) are linked to the variability of dust concentration in Antarctic ice cores over 80,000 years. Gassó and Stein [2007] report on a dust event originating from this region that was subsequently traced to the Antarctic 48 h later. It is remarkable to observe in Figure 12 that

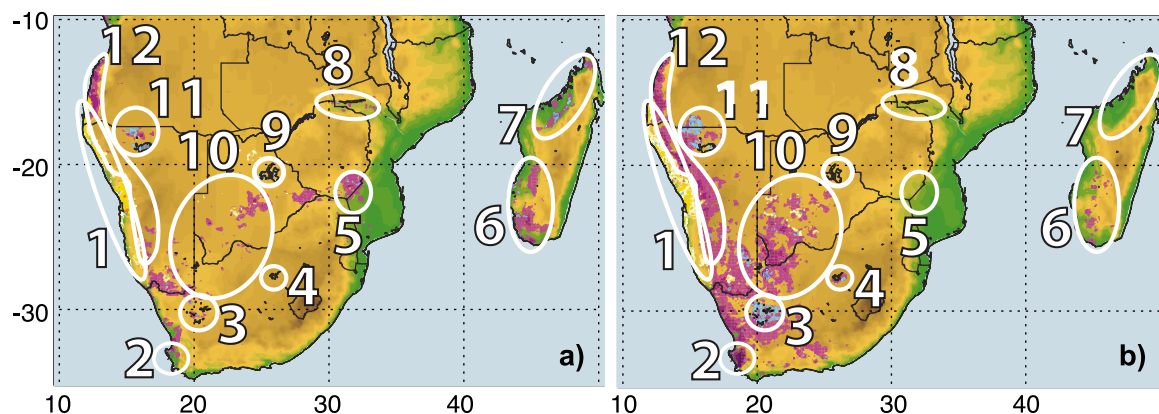


**Figure 13.** Distribution of the percentage number of days per season ((a) September, October, and November and (b) December, January, and February) M-DB2 DOD  $> 0.2$  over South Africa with color code as in Figure 6. The white circled sources are numbered as follows: 1, Namib Desert; 2, croplands near Cape Town in South Africa; 3, South African Bushmanland; 4, Bloemhof Dam of South Africa; 5, Hippo Valley of Zimbabwe; 6, southern Madagascar; 7, northern Madagascar; 8, Cahora Bassa reservoir of Mozambique; 9, Makgadikgadi Pans of Botswana; 10, Kalahari Desert; 11, Etosha Pan; and 12, Great Escarpment of Namibia.

these small sources have apparently been active over such a long period.

[85] Other sources of dust in Argentina are associated with salt lakes: Laguna Salada (location 9), Laguna Mar Chiquita (location 10), and lakes in the Salinas Grandes Desert (location 11). The water level of the Laguna Mar Chiquita varies considerably, and during low-level stages the development of dust storms has been observed [Troin *et al.*, 2010]. Prospero *et al.* [2002] found a weak but persistent source of dust in the Bolivian Altiplano. Here we find much reduced activity. Indeed, the only place with FoO  $> 10\%$  is over the northern half of Lake Poopo (location 13). A possible explanation is that Figure 12 corresponds to austral summer, the only period with precipitation over the Altiplano [Garreaud and Aceituno, 2001]. In austral spring, M-DB2 shows a dozen more sources associated with ephemeral lakes over the Altiplano.

### 5.11. Southern Africa

[86] The FoO distributions of DOD  $> 0.2$  over southern Africa are shown for austral spring and summer in Figure 13. The figures show considerable variation between seasons. Activity develops weakly on the western regions in austral spring and increases strongly in summer, spreading into central regions. The major exception is the Namib Desert (location 1), which is active during most seasons. Using Sea-viewing Wide Field-of-view Sensor (SeaWiFS), Eckardt and Kuring [2005] have shown that dust sources of the Namib Desert are associated with either salt pans or dry river beds, and their supply of dust is maintained by fluvial landforms and associated hydrology.

[87] Silty deposits are widespread on the eastern margin of the escarpment bordering the Namib Desert. These deposits are locally produced weathering detritus and allochthonous dust blown in from the western Kalahari (location 10) [Eitel *et al.*, 2001]. These deposits appear as an elongated dust source (location 12) in Figure 13a, activated by easterly winds in December, January, and February. During that

season, FoO is greater than 20% in some areas. In other seasons, this elongated source is inactive.

[88] Bryant *et al.* [2007] have shown that the Kalahari Desert (location 10), including the Makgadikgadi Pans (location 9), is influenced by the extent and frequency of lake inundation, sediment inflows, and surface wind speed variability. They suggested that TOMS aerosol optical depth was unreliable because it showed peaked activity over the Makgadikgadi from August to October. But our results also indicate a maximum FoO over the Makgadikgadi (location 9) from September to October. On the other hand, dust activity over the Etosha Pans (location 11) and the Kalahari (location 10) is greatest in the December–February period, in agreement with their study. An explanation of this discrepancy may be related to the strong interannual variability of inundation, which shuts down dust emission [Mahowald *et al.*, 2003], and the fact that we analyze different periods.

[89] The other significant source areas in South Africa are the ephemeral lakes in Bushmanland (location 3), the Swartland north of Cape Town (location 2 in Figure 13), the Highveld region around the Bloemhof Dam (location 4), and the Namaqualand Desert (between the Namib Desert (location 1) and Cape Town (location 2)). The anthropogenic nature of these sources has been studied elsewhere [Soderberg and Compton, 2007]. Meadows [2003] has documented the wind erosion of sandy agricultural soils of the Swartland; Wiggs and Holmes [2011] have studied wind erosion in the Highveld; and Botha *et al.* [2008] have shown that the combination of dry climate, strong winds, and especially land degradation have contributed to wind erosion in the Namaqualand.

[90] We also found active anthropogenic dust sources in Zimbabwe (Hippo Valley, location 5) and Mozambique (Cahora Bassa reservoir, location 8). But these sources are only active in austral spring.

[91] Dust sources in Madagascar have not been studied previously, although extensive soil erosion due to deforestation

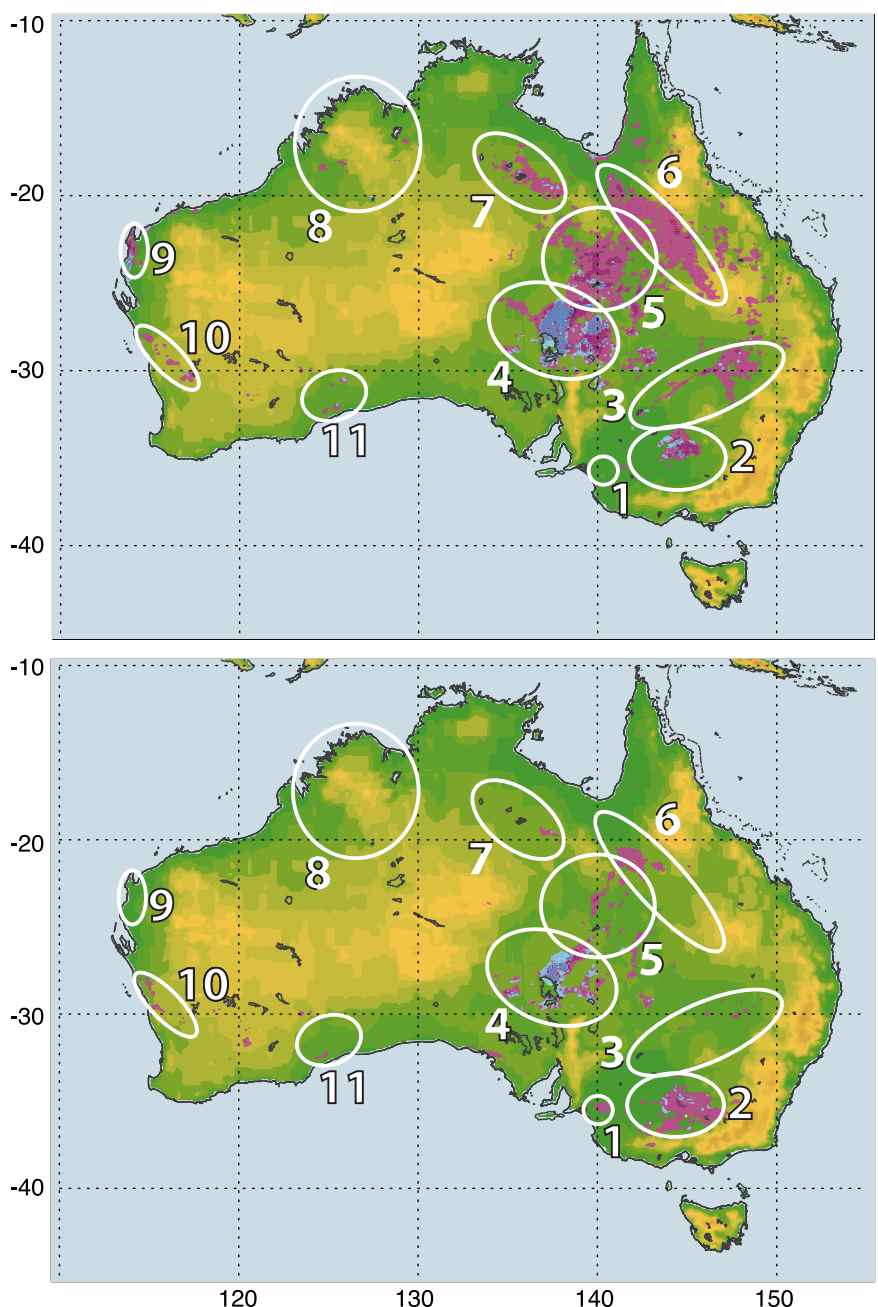


**Figure 14.** Distribution of the percentage number of days per season ((top) September, October, and November and (bottom) December, January, and February) M-DB2 DOD  $> 0.2$  over Australia with color code as in Figure 6. The white circled sources are numbered as follows: 1, Victorian Big Desert; 2, Riverina; 3, Barwon-Darling Basin; 4, Lake Eyre Basin; 5, Simpson Desert; 6, lee side of Great Dividing Range; 7, Barkly Tableland; 8, Kimberley Plateau; 9, North West Cape; 10, Darling Front Range; and 11, Nullarbor Plain.

has been documented [Goudie and Boardman, 2010], and wind erosion has been suggested in southern Madagascar (location 6) by Feddema [1998]. December through February is the rainy season, but rainfall is essentially concentrated in the east and north, such that dust activity is located in the semiarid southwest of Madagascar (location 6). Before the rainy season some areas of northern Madagascar (location 7) appear as active dust sources.

## 5.12. Australia

[92] In Figure 14, Australia shows a large spatial change in dust source activity between austral spring, when northern sources are most active, and summer, when there is less activity and it is centered in the southeast. Dust sources in Australia are associated with either hydrologic features or land use. Based on the KG01 land use data set, the percentage of land use in Australia is generally higher than 50% everywhere

and often reaches 75% or more. The land use is for pasture except in the SW and SE (Murray region), where cropland is more intensive.

[93] The dust sources are mainly located in eastern Australia: Queensland, Northern Territory, South Australia, New South Wales, and Victoria.

[94] The most active sources are located within the Lake Eyre Basin (location 4), as previously shown by *Prospero et al.* [2002]. *Bullard et al.* [2008] found that in the basin 60% of dust plumes originate from hydrologic features with 30% from ephemeral lakes. From Figure 14, it appears that the Eyre Lakes (north and south) themselves are weakly active dust sources compared to the feeding creeks on the north and east sides where  $FOO > 20\%$ . On an annual basis, the largest source with the highest frequency over the entire Australian continent is in channel country, at the mouth of the Warburton River feeding North Lake Eyre. Dust emission in the channel country has been described by multiple studies [*Nickling et al.*, 1999; *Butler et al.*, 2001, 2005], and *Prospero et al.* [2002] have described Warburton Creek as a major dust source in Australia. In the Lake Eyre Basin, there are dozens of smaller lakes, some of them active while others are not. Some are active all year long (e.g., Lake Yamma Yamma), while others are active for one or two seasons (e.g., Lake Frome, active in SON). The difference may be linked to their geomorphology and to river discharge. The soils around Lake Yamma Yamma are composed of clay and fine sediments and are transected with wide expanses of braided fluvial channels [*Fagan and Nanson*, 2004]. In contrast, Lake Frome is only occasionally fed through the Bullow Overflow during austral summer flooding [*McTainsh*, 1989]. In the Lake Eyre Basin dust activity is greatest and most widespread in austral spring. In the Simpson Desert (location 5 in Figure 14) dust activity is most frequent in austral spring and summer but is limited to only a few spots for the remainder of the year. The Simpson Desert is a sand desert where dust is produced by abrasion of the sand mantle composed of fine clays and iron oxides, not by ejection of fine particles by sandblasting of alluvium [*Bullard et al.*, 2007]. Although the amount of erodible material is limited, the Simpson Desert can yield very large amounts of dust during major events [*Knight et al.*, 1995].

[95] The dust sources of the Murray-Darling are aggregated in three clusters: the Victorian Big Desert (location 1 in Figure 14), the irrigated farmland of Riverina (location 2), and the Barwon-Darling Basin (location 3). The Murray-Darling River systems erode fine particles from the uplands and carry them downriver into the arid zone where they served as one of the major Australian dust sources in the present and geological past [*Hesse and McTainsh*, 2003; *Li et al.*, 2008; *Marx et al.*, 2009]. In the Miocene, the Victorian Big Desert was a shallow sea which since has been slowly filled with sediments. Since European settlement began in the region, the hydrological regime has been disrupted by the increasing demand of water for agriculture and clearing of land, which has led to significant increase in dust deposition on a millennial scale [*Marx et al.*, 2011]. As a consequence of diversion, the ephemeral lakes within the region were last filled in 1976

[*Wevill and Read*, 2010]. The area is now part of a network of parks, including the Wyperfeld National Park. Within the Murray-Darling basin, dust events are more widespread in the southern part in austral summer and in the Barwon-Darling basin in austral spring.

[96] It should be noted that the period of M-DB2 data overlaps the 2001–2007 Australian drought. During this drought, the inflow into the Murray-Darling River system was reduced by a factor of 3, reaching a historical low [*Cai and Cowan*, 2008]. As a consequence of frequent dust events the Darling River from the Barwon Basin to the Victorian Big Desert appears as a long narrow strip (location 3 in Figure 14). In general, the spatial distribution of rainfall in Australia is controlled by El Niño/La Niña–Southern Oscillation (ENSO) and monsoon variability [*Marx et al.*, 2009]. Using the Australian Land Erodibility Model, *Webb et al.* [2006] have shown that during El Niño conditions, there is increased wind erosion in central and southeastern Australia, while during La Niña years the sources are shifted to the southwestern regions. They provided maps of wind erosion susceptibility for dry and wet years. In dry years, their results are quite similar to Figure 14, with high susceptibility in the Lake Eyre basin and the Murray-Darling basin and low susceptibility in the west.

[97] In Northern Territory and Queensland, dust events are most frequent in spring. Their frequency decreases in summer, and only Lakes Tarrabol and Sylvester in the Barkly Tableland (location 7 in Figure 14) are still active from June to August. This was shown previously by *Prospero et al.* [2002]. The M-DB2 period covers two pronounced El Niño periods (2002–2004 and 2009–2010), years which favor dust activity in Northern Territory and Queensland [*Webb et al.*, 2006]. This may explain why this large source area location 6 is located on the lee side of the Great Dividing Range. However, if we had included the strong La Niña 2010–2011 years, the results may have shown much reduced mean dust activities in the east and more in the west, based on the results of *Webb et al.* [2006]. Indeed, *Bullard and McTainsh* [2003] have shown a strong relationship between ENSO cycles and dust emissions and sediment supply.

## 6. DUST EMISSION

[98] Dust emission is mainly initiated by saltation and sandblasting processes which have been parameterized based on laboratory measurements and field studies. The main parameters include the soil granulometry, cohesion, moisture, and the surface roughness. These parameters are implicitly expressed in a threshold velocity of wind erosion, which is the minimum velocity to initiate dust emission. Different parameterizations are available, and we use the simple expression of *Ginoux et al.* [2001] where the dust emission  $F_p$  is calculated as follows:

$$F_p = CSu_{10m}^2(u_{10m} - u_t), \quad (1)$$

where  $C$  a dimensional factor,  $S$  is the fraction of dust source,  $u_{10m}$  is the horizontal wind speed at 10 m, and  $u_t$  is the

threshold velocity for wind erosion. The fraction of dust source  $S$  is assumed to be proportional to the seasonal M-DB2 FoO.

[99] Dust emission is calculated using the 3-hourly instantaneous 10 m wind speed resulting from a 1 year simulation (2005) with the Geophysical Fluid Dynamics Laboratory C360 High Resolution Atmospheric Model (HIRAM) described by *Zhao et al.* [2009]. The C360 configuration consists of  $360 \times 360$  grid points on each face of a cubed sphere grid topology covering the Earth [*Putman and Lin*, 2007]. The size of the model grid varies from 20 to 30 km. Compared to 10 other general circulation models, HIRAM has the lowest root-mean-square errors for several meteorological fields including winds [*Zhao et al.*, 2009].

[100] The dynamical processes generating  $u_{10m}$  intense enough to overcome  $u_t$  cover a large range of scales: synoptic depressions, low-level jets and cold pools of mesoscale convective systems, and microscale dust devils and dusty plumes [*Knippertz and Todd*, 2012]. Most global dust models have a spatial resolution of the order of 100 km; consequently, they can only explicitly resolve synoptic systems but not smaller-scale processes. The simulation of dust storms associated with cold pool outflows from moist convection (so called “haboobs”) necessitates resolution of downdrafts within convective clouds. Resolving such small-scale processes can only be achieved in regional models. Global models with coarser resolution can attempt to simulate them through parameterizations, but such an approach introduces uncertainties associated with each introduced parameter. In addition, *Marsham et al.* [2011] have shown that the inclusion of parameterized moist convection into a regional model produces substantially fewer haboobs than when solved explicitly. For microscale dust devils, *Koch and Renno* [2005] have developed a parameterization which appears to lift significant amounts of dust, but the results have only been tested over a limited area in Arizona. Considering the difficulty of parameterizing these small-scale processes and the lack of data to constrain these parameters globally, we do not include any parameterization of convective vertical downdraft. This means that we are not able to include dust emission from haboobs which have been studied in West Africa [*Bou Karam et al.*, 2009; *Marsham et al.*, 2011], the Arabian Peninsula [*Miller et al.*, 2008], Iraq and northwest Iran [*Abdi Vishkaee et al.*, 2012], Australia [*Strong et al.*, 2011], and North America [*Idso et al.*, 1972; *Chen and Fryrear*, 2002]. The estimated contribution of these haboobs to dust emissions varies from 9% in Australia [*Strong et al.*, 2011] up to 67% in West African monsoon [*Bou Karam et al.*, 2009].

[101] Another uncertainty in equation (1) is associated with the threshold friction velocity,  $u_t$ . Combining M-DB2 data with results from a high-resolution mesoscale model, *Draxler et al.* [2010] showed typical values of  $u_t$  over the United States to be around  $60 \text{ cm s}^{-1}$  over deserts and  $100 \text{ cm s}^{-1}$  over cultivated areas, such as the high plains. These results correspond to the values suggested by *Gillette and Passi* [1988] for mixed barren lands ( $65 \text{ cm s}^{-1}$ ) and

pasture and range in good conditions ( $100 \text{ cm s}^{-1}$ ). Converting these surface friction velocities to wind speed at 10 m, we impose  $u_t = 6$  and  $10 \text{ m s}^{-1}$  for smooth (natural and hydrologic sources) and vegetated (agriculture or range) surfaces, respectively. These values correspond to the range of values ( $6.5$  to  $13 \text{ m s}^{-1}$ ) reported by *Helgren and Prospero* [1987] for western Sahara. In the next section, we will test the sensitivity of dust emission to  $u_t$  over vegetated surfaces.

## 6.1. Emission and Vegetation

[102] *Ginoux et al.* [2001] have developed a  $1^\circ$  resolution dust source inventory with preferential locations in topographic depressions (TOPO). The inventory includes a vegetation mask that excludes all sources for all ecosystems except bare ground. This inventory has been extensively used and evaluated [e.g., *Cakmur et al.*, 2005]. As discussed in *Ginoux et al.* [2001], a value of  $C = 1 \mu\text{g s}^2 \text{ m}^{-5}$  provides the best agreement with observations. Here we use their inventory to calculate the annual dust emission using HIRAM wind speed  $u_{10m}$ . This yields an annual global emission of  $1223 \text{ Tg yr}^{-1}$  from bare ground. This value is lower than the value of *Ginoux et al.* [2001] but close to the median value ( $1123 \text{ Tg yr}^{-1}$ ) derived by *Huneeus et al.* [2011] in the comparison of 15 global dust models. By considering relative emission between continents, we obtain similar results to those calculated by *Ginoux et al.* [2004] using *Ginoux et al.*'s [2001] sources.

[103] We then scale the  $C$  value to obtain also  $1223 \text{ Tg yr}^{-1}$  when using M-DB2 FoO as source fraction  $S$  and the vegetation mask of *Ginoux et al.* [2001]. This calculation gives  $C = 1.9 \mu\text{g s}^2 \text{ m}^{-5}$ , which is double the  $C$  value determined by *Ginoux et al.* [2001].

[104] Figure 15a shows the global distribution of annual emission using TOPO ( $C = 1 \mu\text{g s}^2 \text{ m}^{-5}$ ,  $u_t = 6 \text{ m s}^{-1}$ , and  $S$  from *Ginoux et al.* [2001]). Figure 15b shows also the global distribution of annual emission but using the M-DB2 FoO for  $S$ ,  $C = 1.9 \mu\text{g s}^2 \text{ m}^{-5}$ , and  $u_t = 6 \text{ m s}^{-1}$  over natural sources and  $10 \text{ m s}^{-1}$  over land use sources. With the introduction of vegetated surfaces (Figure 15b, blue shading), many new sources appear. The most intense are located in Kazakhstan near the Aral Sea, along the Indus and Ganges Rivers, over the Riverina of Australia, and in the northern provinces of Argentina. We have previously identified significant source areas linked to land use practices in the Sahel, Australia, east China, and the high plains of the United States, but because of weaker mean surface winds emissions are weak in these areas. There are also substantial changes in emissions rates from bare surfaces, most notably increases in SE South America, Inner Mongolia, and NE China. In North Africa, the general pattern of dust emissions is retained, but there are substantial changes in some areas, e.g., eastern Mauritania and western Mali, southeastern Algeria and western Libya, and eastern Iraq.

[105] Table 4 summarizes the emission values obtained for each continental region. Agreement is good for all regions except South Africa and South America, where M-DB2 emissions are much lower. On the other hand, there are

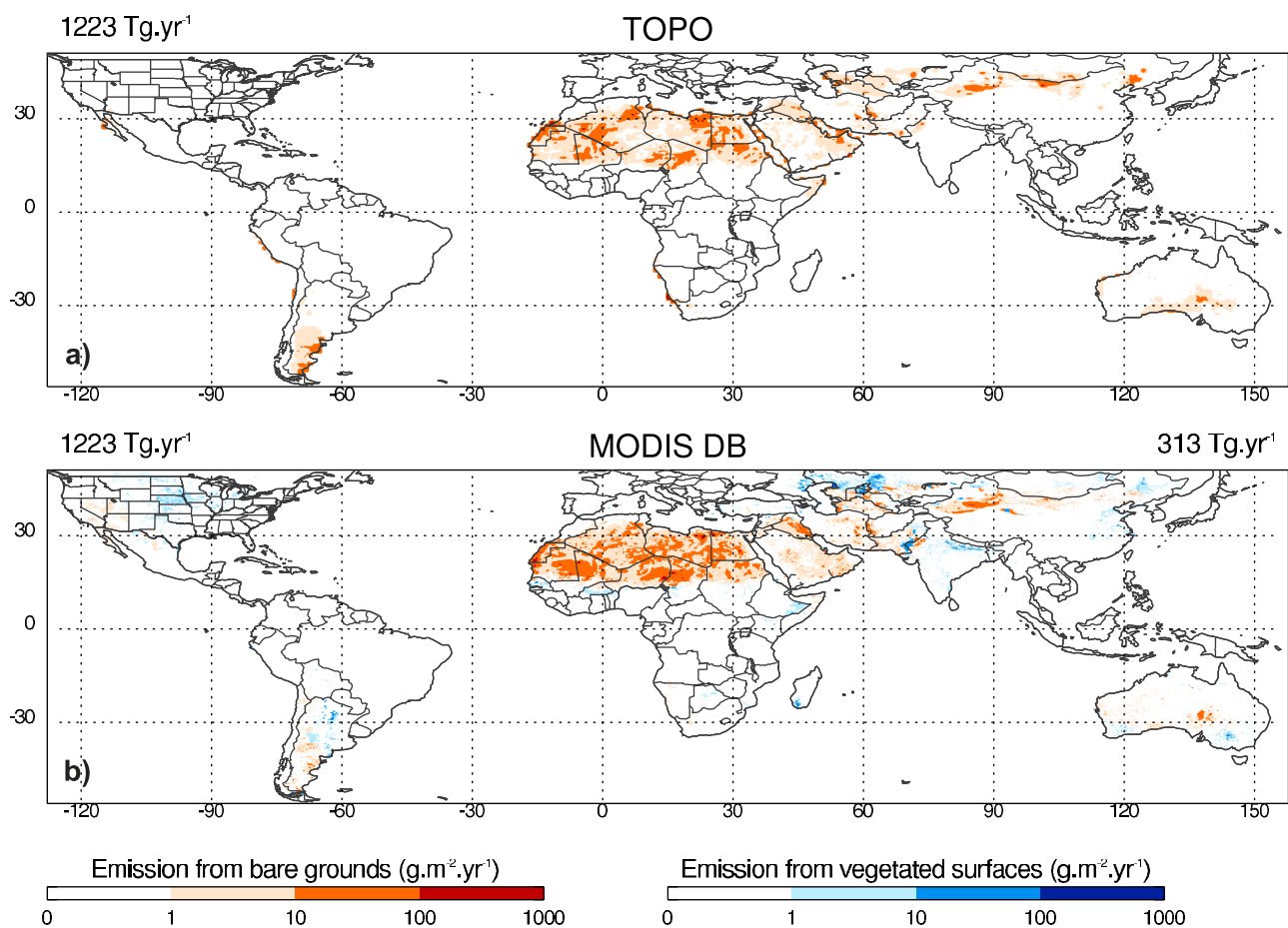


**Figure 15.** Annual mean dust emission using (a) topographic depression sources and (b) M-DB2 FoO that DOD > 0.2. The M-DB2 emissions are colored in blue or red shadings if they are within or outside topographic depression coverage, respectively.

strong regional differences in the contribution of vegetated areas, as seen in Table 4. The lowest contribution is in North Africa (4%), and the highest is in North America (78%). Globally, vegetated areas contribute 20%.

## 6.2. Emission and Hydrography

[106] The global distribution of dust emissions according to source type is shown in Figure 16. In Figure 16a sources

associated with the ephemeral water bodies are shown in blue shading (“hydro”), and all other sources (“nonhydro”) are shown in red shading, independently of their natural or anthropogenic origin. The contribution of these two types of source (“HYD” and “NHYD”) for each region is shown in Table 4.

[107] Dust emission from grid cells with ephemeral water bodies represents ~30% of global dust emission, with a

**TABLE 4. Annual Dust Emission (Tg yr<sup>-1</sup>) Over Eight Continental Regions (Domain Defined in Table 2) and for the Sum of the Eight Regions (Global) Using 1° × 1° Topographic Sources of *Ginoux et al.* [2001] (TOPO), Using M-DB2 0.1° × 0.1° Sources (M-DB2), and for M-DB2 the Contributions From Bare (BARE), Vegetated (VEGET), Nonhydrological (NHYD), Hydrological (HYD), Land Use < 30% (NAT), Land Use > 30% (ANT), Land Use < 30% and Water Bodies > 10% (NAT-H), and Land Use > 30% and Water Bodies > 10% (ANT-H) Surfaces**

Region	TOPO	M-DB2	BARE	VEGET	NHYD	HYD	NAT	ANT	NAT-H	ANT-H
North America	12	63	14	49	37	26	29	34	2	25
South America	79	54	25	28	38	15	32	22	2	14
North Africa	659	840	807	32	684	156	771	69	94	63
South Africa	51	25	7	18	19	6	11	13	1	5
West Asia	210	225	170	55	119	106	158	67	43	64
Central Asia	17	62	22	40	35	26	34	28	1	27
East Asia	146	202	137	65	106	96	121	80	25	71
Australia	47	63	39	24	17	45	15	47	4	42
Global	1223	1536	1223	313	1056	479	1172	363	169	310

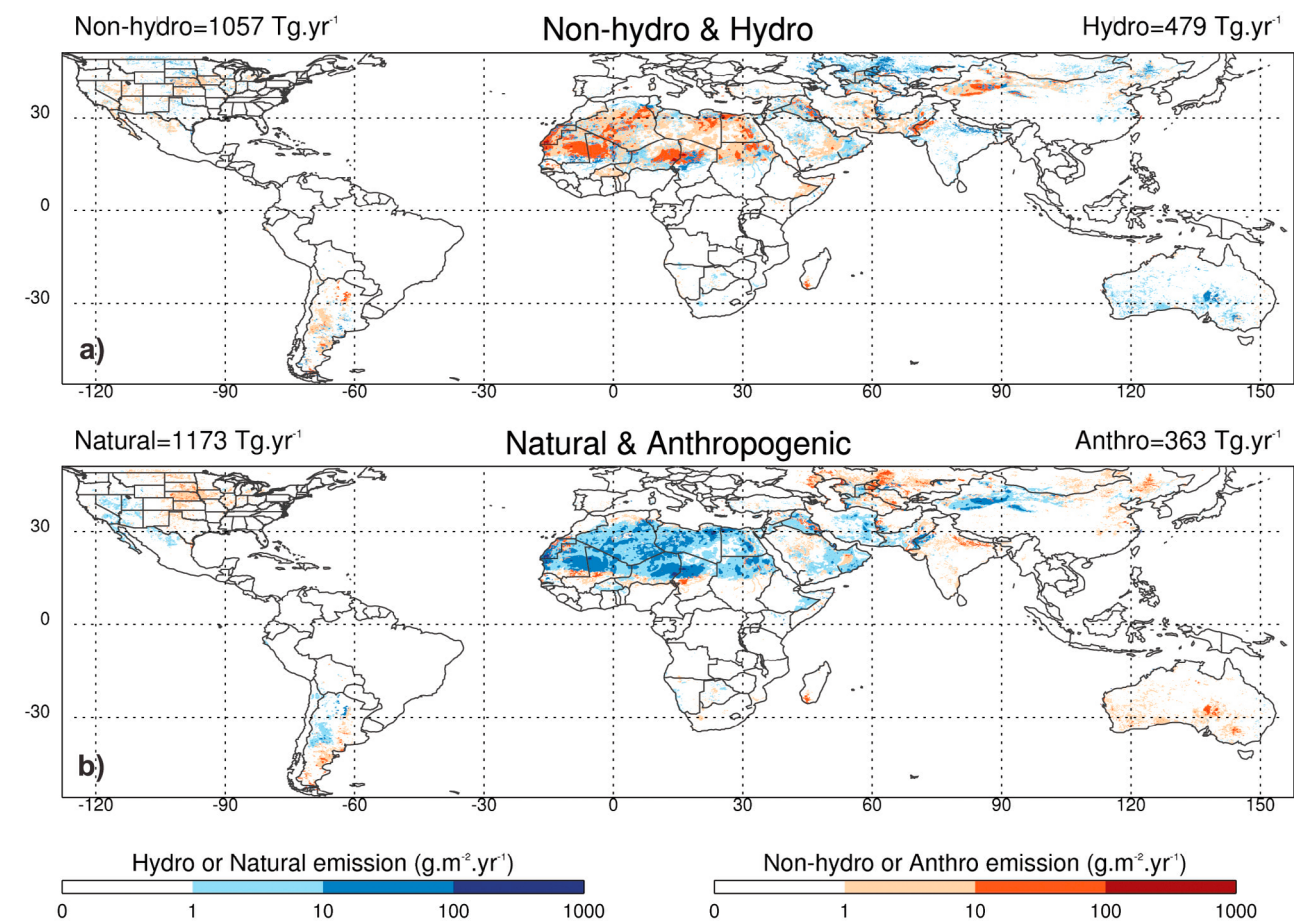


**Figure 16.** Annual mean dust emission (a) from ephemeral water bodies and (b) from land use. The M-DB2 emissions are colored in blue for hydrologic and natural sources and in red for nonhydrologic and anthropogenic sources.

maximum contribution of 71% in Australia and a minimum of 18% in North Africa. Outside North Africa, ephemeral water bodies contribute at least 25% to dust emission. The predominance of hydrological sources in Australia is linked to the absence of paleolakes with deep layers of accumulated alluvium, making them supply limited [Bullard *et al.*, 2011]. As indicated by Prospero *et al.* [2002], the most active sources in North Africa are characterized by the presence of a deep layer of sediments laid down during the Pleistocene and Holocene. In contrast, such deposits are not widely distributed in Australia, and hence, the only strong sources are dependent on the accumulation of recently deposited weathering products. It should be noted that the water body data set only captures features larger than 1 km wide; thus, it may miss a significant number of smaller lakes. This means that their contribution as shown in Table 4 should be considered as a lower limit.

### 6.3. Emission and Land Use

[108] Figure 16b presents the distribution of natural (“natural,” blue shading) and anthropogenic (“anthropogenic,” red shading) sources, independently of their relation with ephemeral water bodies. The contribution of these two types (“NAT” and “ANT”) of source for each region is shown in

Table 4. In addition, dust emissions from natural and anthropogenic sources from grid cells which contain more than 10% ephemeral water bodies are also provided in Table 4 and are designated as “NAT-H” and “ANT-H,” respectively.

[109] The global annual NAT and ANT dust emissions are 1172 and 363 Tg yr<sup>-1</sup>, respectively. ANT emission represents 25% of total emission. Table 4 indicates that over North Africa ANT emission represents only 8% of African emissions, but globally, they represent 20% of anthropogenic emissions. Most anthropogenic sources in North Africa are located in the Sahel and the western Sahara. In other regions, the anthropogenic contribution to the regional emissions is much larger and varies from 30% in the Middle East and west Asia to 75% in Australia.

[110] The global annual NAT and ANT dust emissions, as well as their hydrologic contributions (NAT-H and ANT-H), are shown in Figure 17a. The percentage contributions of ephemeral water bodies to natural and anthropogenic emissions are shown in Figure 17b. In Australia, the hydrologic sources account for nearly 90% of the Australian anthropogenic emissions. In the Indian subcontinent, it reaches 96% because of increasing agriculture in the Indo-Gangetic floodplain. In general, anthropogenic sources related to

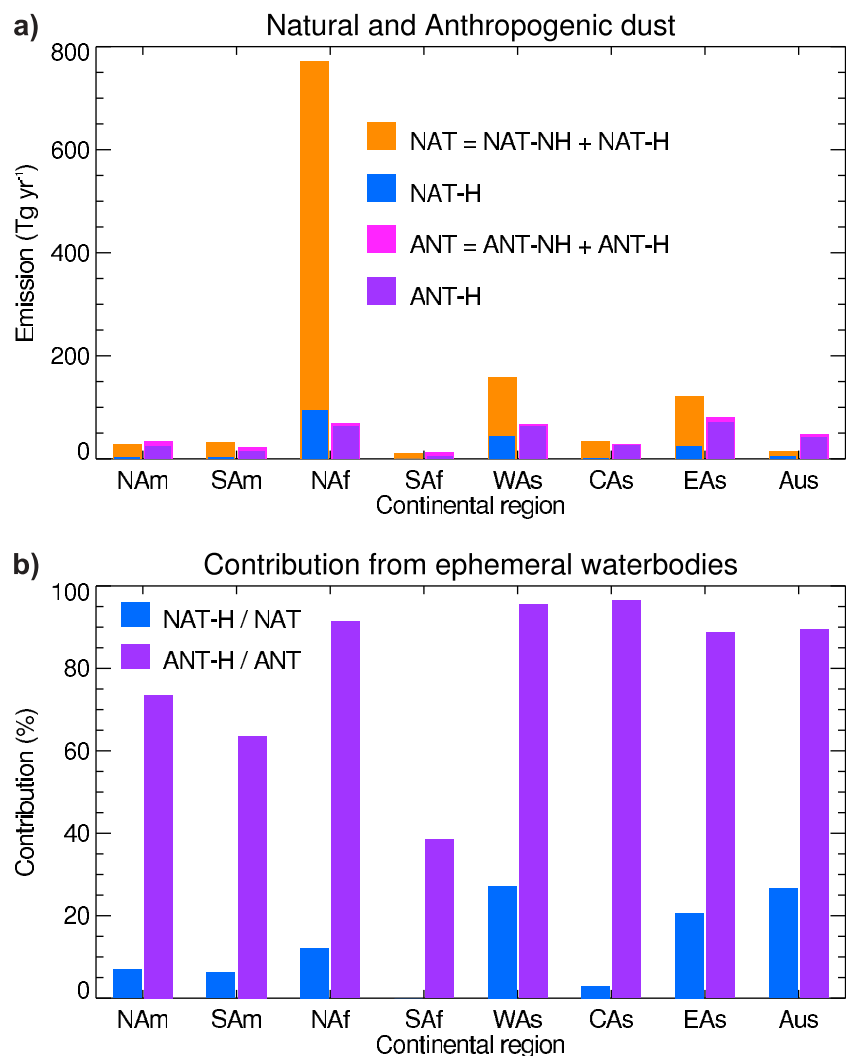


**Figure 17.** (a) Annual mean emission ( $\text{Tg yr}^{-1}$ ) over North America (NAm), South America (SAm), North Africa (NAf), South Africa (SAf), West Asia-Middle East (WAs), Central Asia (CAs), East Asia (EAs), and Australia (Aus) from natural (NAT-H + NAT-NH), anthropogenic (ANT-H + ANT-NH), and natural (NAT-H) and anthropogenic (ANT-H) sources with more than 10% ephemeral water bodies per grid cell. (b) The percentage contribution of ephemeral water bodies to natural and anthropogenic emissions for each continental region.

ephemeral water bodies contribute to 85% of anthropogenic dust emission globally and regionally. The exception is South Africa with the largest contribution from nonhydrologic sources, 36%. Conversely, only 15% of natural dust sources are associated with ephemeral lakes (Table 4). North Africa accounts for 92% natural dust sources, only 11% of which are associated with ephemeral water bodies. This confirms the work of Bullard *et al.* [2011] showing that about 95% of the Sahara dust plume frequency is from nonanthropogenic sources because 54% are from paleolakes.

[111] In the previous sections we selected a 30% threshold of land use fraction to identify anthropogenic sources and a  $10 \text{ m s}^{-1}$  threshold of wind erosion to calculate dust emission from anthropogenic sources. To evaluate the sensitivity of dust emissions to these two parameters, we calculated annual emissions for different values of these parameters (Table 5). As seen in Table 5, the sensitivity to land use

**TABLE 5. Annual Anthropogenic Dust Emission ( $\text{Tg yr}^{-1}$ ) Over Eight Continental Regions (Domain Defined in Table 2) and Globally, for Two Different Values of the Threshold of Wind Erosion Over Land Use Area ( $u_t$ ) and Three Minimum Percentages of Land Use (LU) for Attributing a Source to Anthropogenic Origins**

Region	$u_t = 10 \text{ m s}^{-1}$			$u_t = 6 \text{ m s}^{-1}$		
	LU > 10	LU > 30	LU > 50	LU > 10	LU > 30	LU > 50
North America	39	34	28	146	137	124
South America	26	22	11	87	75	33
North Africa	87	69	51	192	158	115
South Africa	15	13	5	55	50	21
West Asia	86	67	46	195	154	104
Central Asia	31	28	23	77	68	59
East Asia	96	80	47	221	196	129
Australia	54	47	12	149	143	55
Global	437	363	225	1105	966	633

fraction is much smaller than to the threshold of wind erosion. Indeed, reducing land use threshold from 30% to 10% increases global anthropogenic dust by 20%, while increasing it to 50% reduces the emission by 38%. On the other hand, lowering  $u_t$  from 10 to 6 m s<sup>-1</sup> results in an increase of global emissions by a factor of 2–3. This is more or less true for each continental region. Thus, the threshold of wind erosion is the principal source of uncertainty in our results, and this is most likely true for all models. More robust values might be obtained by using a time-varying threshold of wind erosion which could be linked to vegetation cover and soil moisture. Another method is to use an inversion such as the one developed by *Draxler et al.* [2010] to retrieve the threshold of wind erosion.

[112] Other limitations of our work include uncertainties associated with the HIRAM wind speed and the lack of interannual variability. Due to the cubic dependency of dust emission to wind speed (cf. equation (1)), small variations in the high tail of the wind speed distribution between meteorological data sets can produce large differences in the resulting budget. Comparing HIRAM zonal winds with National Centers for Environmental Prediction (NCEP) reanalysis [Kalnay et al., 1996], *Zhao et al.* [2009] showed that the root-mean-square error is the lowest for HIRAM compared to 10 other models in the World Climate Research Program Coupled Model Intercomparison Project 3 database [*Meehl et al.*, 2007]. On the other hand, *Menut* [2008] found a factor of 3 difference between the emission fluxes calculated with NCEP and European Centre for Medium-Range Weather Forecasts meteorological fields, NCEP having the lowest emissions. In addition to this inherent variability between models, some subscale processes important for dust generation are not explicitly resolved because of model resolution. These processes include evaporationally driven, cold, near-surface outflows from organized moist convection and turbulent circulation in dry convective boundary layer [*Knippertz and Todd*, 2012]. To resolve these processes explicitly, a model would require a resolution of 10 km or finer [*Marsham et al.*, 2011], a capability not yet available for most global models. We have shown that anthropogenic sources are often located in regions influenced by monsoon winds, where such convective regimes often occur. Thus, we may underestimate dust emissions from these regions. This may also explain the apparent discrepancy between the high M-DB2 FoO sources seen in the Sahel (Figure 7) and in the southern high plains (Figure 11) but the low emissions calculated for these areas (Figure 16b).

## 7. RELATIONSHIP TO CLIMATE, AIR QUALITY, AND HUMAN HEALTH

[113] Our results indicate that up to 25% of dust is emitted from agriculture with 85% of it associated with hydrology. This implies that dust emission from these sources is particularly sensitive to land use practices and changes in the hydrological cycle. In an effort to mitigate the numerous negative effects of wind erosion, improved agricultural management practices have been developed [*Ravi et al.*,

2011]. Projections of total agricultural land (crop plus pasture) prepared for the Intergovernmental Panel on Climate Change Fifth Assessment Report [*Hurtt et al.*, 2011] yield a range of estimates, from a projected increase by 13% to a decrease by 24% by 2100, depending on the scenarios used. These changes are relatively small compared to expected precipitation changes. Indeed, there is a tendency for increased precipitation associated with monsoon flow but with large disparity between regions and major uncertainty in some areas [*Christensen et al.*, 2007]. Regions that are currently dusty areas and which are likely to experience a decrease in precipitation include most of Mediterranean Europe and Africa, northern Sahara, central Asia, southwest U.S., and southern Australia in spring [*Christensen et al.*, 2007]. Conversely, over currently dusty areas in east Africa and east Asia precipitation will likely increase [*Christensen et al.*, 2007]. Because of large model uncertainties, projections cannot be made for the Sahel-Sudan, the Gangetic basin, and the Lake Eyre region. As a consequence of these precipitation changes we might expect a reduction in low-latitude dust sources and an intensification of sources in the tropics, unless implementation of better agricultural practices could mitigate the expected increase in dust emissions with reduced rainfall.

[114] Such shifts in dust sources will modulate the effects of dust on climate by changing the distribution of dust and possibly affecting its composition. Because these new agricultural dust sources areas also emit ammonia [*Beusen et al.*, 2008] and because they are located close to fossil fuel sources of fine-mode acidic aerosols (e.g., sulfate and nitrate), dust will be increasingly mixed with such aerosols. This mixing changes the chemical and optical properties of dust, which will affect its interactions with radiation, cloud microphysics, and biogeochemical cycles. The mixing of dust with acidic species will decrease the absorption of solar radiation [*Bauer et al.*, 2007] and yield more efficient cloud condensation nuclei, but it will decrease the formation of ice nuclei [*Sullivan et al.*, 2010]. In addition, the presence of acidic species will increase the solubility of iron in dust particles; after deposition to the ocean, the release of iron, an essential micronutrient, can promote phytoplankton growth and consequently modulate the carbon cycle [*Jickells et al.*, 2005]. On the other hand, it has been suggested [*Mahowald et al.*, 2006] that natural dust loading may be reduced by 60% in a doubled carbon dioxide climate when the impacts of carbon dioxide fertilization on vegetation are included. These forcings on climate may be amplified or attenuated through positive or negative feedbacks, respectively. *Miller et al.* [2004] found negative feedbacks of dust emission by dust radiative forcing through the planetary boundary layer, but *Cook et al.* [2009] showed that the North American “Dust Bowl” drought was amplified through human-induced land degradation. A possible desertification feedback loop by dust suppressing precipitation has been suggested [*Rosenfeld et al.*, 2001].

[115] Dust, like any other aerosol, must be considered in the more general terms of its nature as particulate matter and implications for air quality. A substantial fraction of dust

mass is in the “respirable” size range as defined by the U.S. Environmental Protection Agency, particles under  $10\text{ }\mu\text{m}$  and under  $2.5\text{ }\mu\text{m}$  diameter. Although there have been few systematic studies of the air quality impact of dust in, or proximate to, major dust source regions [De Longueville *et al.*, 2010], it is clear that the concentrations of respirable particles in these regions can far exceed typical air quality standards [Gillies *et al.*, 1996; Rivera Rivera *et al.*, 2010]. Dust transported across ocean basins can have air quality impacts on receptor continents [Chin *et al.*, 2007]. For example, African dust transported to the Caribbean [Prospero and Lamb, 2003] and Florida [Prospero *et al.*, 2001], can rise to concentrations that challenge the U.S. air quality standard, and there is a growing recognition of the contribution of Asian dust to surface aerosol loadings in western North America [Van Curen and Cahill, 2002; Jaffe *et al.*, 2003; Fairlie *et al.*, 2007].

[116] Finally, we note that there have been relatively few studies assessing the human health impact of mineral dust as compared to other aerosols. Some investigations have evaluated health effects of dust advected from distant sources [De Longueville *et al.*, 2010] and suggest that impacts could be substantial [Liu *et al.*, 2009]. For example, epidemiological studies in Italy [Sajani *et al.*, 2011] and Spain [Jiménez *et al.*, 2010] found evidence of increased respiratory mortality among the elderly during Saharan dust events, and dust advected from mainland Asia was associated with increased risk of ischemic heart disease in Taiwan [Bell *et al.*, 2008]. Dust transported across ocean basins can have air quality impacts on receptor continents [Chin *et al.*, 2007]. Indeed, even in the Caribbean [Prospero and Lamb, 2003] and in Florida [Prospero *et al.*, 2001], the concentration of African dust can rise to levels that challenge the U.S. air quality standard. Closer to the source area, dust advecting into El Paso (Texas) from the surrounding Chihuahuan Desert was found to be associated with increased odds of hospitalization for asthma and bronchitis, especially in children [Grineski *et al.*, 2011].

[117] Dust storms have long been known as an exposure pathway for various fungal diseases including coccidioidomycosis [Williams *et al.*, 1979] and aspergillosis [Chao *et al.*, 2012]. Acute exposure to mineral dust can even, at its extreme, cause nonindustrial silicosis, recognized as “desert lung” syndrome in portions of the global dust belt [Derbyshire, 2007].

[118] It is clear that mineral dust can have a substantial impact on air quality and human health. Changing dust emissions with changing land use and land cover, especially where advected toward human populations, will have public policy implications with regards to compliance with air quality regulations. Consequently, it is important to develop a better understanding of the factors affecting source activity and how these might change with climate.

## 8. SUMMARY AND CONCLUSIONS

[119] The objective of this study was to develop a protocol based on the MODIS Deep Blue Level 2 (M-DB2) product

that could be used to estimate the contribution of anthropogenic and hydrologic dust sources to regional and global emissions. We identified each grid cell dust source as “anthropogenic” or “hydrologic” according to the areal extent of land use and of ephemeral water bodies in each grid cell. Based on a sensitivity analysis we attributed the source to anthropogenic activities when the land use fraction was over 30%; otherwise, the source was “natural.” Each source, whether “natural” or “anthropogenic,” was further classified as either “hydrologic” when ephemeral water bodies cover over 10% of a grid cell coverage or, if less, “nonhydrologic.” We used the M-DB2 algorithm to estimate total aerosol optical depth (AOD) and dust optical depth (DOD) over arid (i.e., bright, relatively vegetation-free) regions. There was good agreement between the M-DB2 product and measurements at AERONET sites located in arid regions using data over the period 2003–2009. We found that over large regions the M-DB2 DOD often composed a major fraction of AOD.

[120] We next developed a global seasonal picture of the most active dust source regions at  $0.1^\circ$  resolution based on the distribution of the frequency of occurrence (FoO) of  $\text{DOD} > 0.2$ . The M-DB2 product shows that the most active dust sources are located in a broad band that extends from the west coast of North Africa through the Middle East to central Asia. In contrast, there is remarkably little dust activity in the Southern Hemisphere. The M-DB2 distribution was compared to distributions derived previously using the Nimbus 7 TOMS aerosol index based on data from 1978 to 1991 [Prospero *et al.*, 2002] and also with the more recent OMI aerosol index which covers 2003 to 2006. These three data sets yield similar dust distributions over North Africa, the Middle East, and South America, thereby indicating that there have been no major changes in dust activity over these regions over 3 decades. In contrast, we found substantial changes in the U.S. high plains, central Asia, and Australia.

[121] An analysis of source attributions over different continental regions reveals consistent patterns and relationships. In North Africa, anthropogenic and hydrologic sources are mostly located within river basins in the Sahel and also along the Mediterranean coast. We also observed small but significant anthropogenic sources in southern Spain and Turkey. In Asia, major dust sources are linked to the Aral Sea, Lake Balkhash, and Urumia Lake, all of which have been desiccated as a result of water diversion. In the Middle East, the largest anthropogenic sources are observed in Mesopotamia and Saudi Arabia. Anthropogenic sources were dominant across the entire Gangetic Basin during the premonsoon. In China, large anthropogenic sources are found in the Horqin sandy region and in the north China plains. Some of these sources are in extensively industrialized areas. In South America Patagonia is a major anthropogenic source largely linked to livestock grazing. Major river basins are clearly apparent as dust sources in Mesopotamia, the Indo-Gangetic basin, North America, and Australia. A particularly good example of M-DB2 sensitivity is the detection of dust along the entire length of the Darling River in Australia whose course is made visible (Figure 14) as a long narrow dust source. Severe droughts appear to be

the cause of some of the observed source activities. In North America dust sources are observed in most of the high plains. In South Africa, we found anthropogenic sources north of Cape Town and Bloemhof reservoir. We found several sources of dust in southern Madagascar, which are most likely linked to intense deforestation followed by erosion.

[122] Finally, we calculated emissions from these sources using a high-resolution data set of wind speed for the year 2005. The global annual emissions are  $1536 \text{ Tg yr}^{-1}$ , which corresponds well to the mean value of multimodel comparison [Huneeus *et al.*, 2011]. We found that 20% of total emissions are from vegetated areas. These areas include the Sahel, Kazakhstan, Indo-Gangetic basin, east China, several states of Australia, Argentina, and the U.S. high plains.

[123] We found that 30% of global dust emission originates from terrains associated with ephemeral water bodies. In West Africa, they account for only 18% of regional emissions, while in all other regions they contribute over twice as much. These percentages might have been even larger had we been able to include hydrological features smaller than 1 km (e.g., ephemeral streams, small lakes, and ponds). It is notable that in Australia ephemeral water sources, natural and anthropogenic, make the largest contribution to total emissions, 71%.

[124] Although we found widespread examples of anthropogenic sources, they account for only 25% of global dust emissions. The reason is that North Africa contributes 55% of global emissions but only 8% to global anthropogenic emissions. In other regions, the percentages of anthropogenic emissions are much higher but have a small impact on global budgets. For example, Australia with 75% anthropogenic dust accounts for only 13% of the global anthropogenic emissions. About 85% of all anthropogenic emissions are associated with ephemeral water bodies. This relationship might be linked to the use of water resources for croplands, for urban use, and for grazing ranges for sheep and cattle. It also implies that because of this association, the activity of these sources could change greatly with changing climate. On the other hand, natural sources are weakly related to ephemeral water bodies with only 15% associated with presently ephemeral water bodies. This can be explained by the important role that paleolakes play as sources of aeolian dust.

[125] Our methodology based on M-DB2 is the first that enables us to estimate DOD. Because of the high resolution, we can more closely relate our product to land use and other features. This enables us for the first time to estimate emissions in a more systematic and quantitative way and, in particular, to characterize emissions from anthropogenic sources. The major source of uncertainty in the calculation of emissions is due to the uncertainties in the threshold of wind erosion. To reduce this uncertainty, it will be necessary to have a better estimate of these threshold velocities for different terrain conditions and to include the time varying dependency of the threshold on vegetation cover and soil moisture. This might be accomplished using satellite data sets or using values derived by the inversion technique developed by *Draxler et al.* [2010]. In

addition, the model used in this study could not resolve some subgrid-scale dynamical processes that could produce haboobs, downbursts, and dust devils. In the few cases where they have been simulated, they appear to generate significant dust loading, particularly in areas with anthropogenic sources. However, global model resolution continually improves, so we can expect that in the near future we will be able to evaluate their importance at the subcontinental and global scales.

[126] As stated above, we found that a large fraction of emissions, at least 30%, is related to the hydrological cycle. This association could be a source of strong interannual variability. To better address this issue, longer data records should be used. The 14 year record of aerosol products from the SeaWiFS instrument could be useful after detailed comparison of the dust inventories derived from the different satellite instruments with geomorphologic characterization such as that derived by *Bullard et al.* [2011].

[127] Projected precipitation changes with changing climate may increase dust emission from tropical dust sources at the expense of low-latitude and midlatitude sources. However, the projections of precipitation changes are highly uncertain in some regions (e.g., sub-Saharan Africa) which are known to be highly active sources today. Consequently, it is difficult to anticipate how dust source locations might change and how these changes might impact emissions. Nonetheless, any shifts in dust source location and emission will modify the effects of dust on climate. As a significant fraction of these subtropical sources are associated with agriculture, the coemission of ammonia and the proximity of fine-mode acidic aerosols (e.g., sulfate) from fossil fuel burning will increase their internal mixing with dust. Such mixing would change the chemical and optical properties of dust which, in turn, would affect its lifetime and the interactions with radiation, cloud microphysics, and biogeochemical cycles. While it is difficult to anticipate in detail such changes, it is clear that there is a highly complex linkage between climate, human activities, and dust emissions and that we need a better quantitative understanding of those relationships before we can assess possible feedbacks on climate, air quality, and public health. In presenting our results we focused for the most part on major dust sources and examples that illustrated various aspects of dust mobilization on a global scale. However, we hope that our results will stimulate research on specific dust source areas. For this purpose, the data presented in Figures 7–14 can be visualized with ultrahigh resolution on Google Earth by downloading files (KML or compressed KMZ format) from <http://www.gfdl.noaa.gov/atmospheric-physics-and-chemistry-data>. KML versions of Figures 7–14 are available in the auxiliary material.

[128] **ACKNOWLEDGMENTS.** The authors thank the AERONET program for establishing and maintaining the Sun photometer sites used in this study. We are grateful to the NASA TOMS and OMI science teams for providing the aerosol index. We are grateful to Catherine Raphael for helping with the figures. T. E. Gill acknowledges support via NOAA cooperative agreement

NA17AE1623, and J. M. Prospero was supported by grants from the U.S. National Science Foundation, OCE 0623189 and AGS 0962256.

[129] The Editor of this paper was Greg Okin. He thanks four anonymous reviewers.

## REFERENCES

- Abdelfattah, M. A. (2009), Land degradation indicators and management options in the desert environment of Abu Dhabi, United Arab Emirates, *Soil Surv. Horizons*, *50*, 3–10.
- Abdi Vishkaee, F., C. Flamant, J. Cuesta, L. Oolman, P. Flamant, and H. R. Khalesifard (2012), Dust transport over Iraq and northwest Iran associated with winter Shamal: A case study, *J. Geophys. Res.*, *117*, D03201, doi:10.1029/2011JD016339.
- Abell, P. I., and C. K. Nyamweru (1988), Paleoenvironments in the Chalbi Basin of Kenya, *Chem. Geol.*, *72*, 283–291.
- Abuduwaili, J., M. V. Gabchenko, and X. Junrong (2008), Eolian transport of salts—A case study in the area of Lake Ebinur (Xinjiang, northwest China), *J. Arid Environ.*, *72*, 1843–1852, doi:10.1016/j.aredenv.2008.05.006.
- Alsharhan, A., and A. A. El-Sammak (2004), Grain-size analysis and characterization of sedimentary environment of the United Arab Emirates coastal area, *J. Coastal Res.*, *20*, 464–477.
- Avci, M. (2011), Conservation tillage in Turkish dryland research, *Agron. Sustain. Dev.*, *31*, 299–307, doi:10.1051/agro/2010022.
- Bai, J., X. Chen, J. Li, L. Yang, and H. Fang (2011), Changes in the area of inland lakes in arid regions of central Asia during the past 30 years, *Environ. Monit. Assess.*, *178*, 247–256, doi:10.1007/s10661-010-1686-y.
- Bauer, S. E., M. I. Mishchenko, A. A. Lacis, S. Zhang, J. Perlitz, and S. M. Metzger (2007), Do sulfate and nitrate coatings on mineral dust have important effects on radiative properties and climate modeling?, *J. Geophys. Res.*, *112*, D06307, doi:10.1029/2005JD006977.
- Bell, M. L., J. K. Levy, and Z. Lin (2008), The effect of sandstorms and air pollution on cause-specific hospital admissions in Taipei, Taiwan, *Occup. Environ. Med.*, *65*, 104–111, doi:10.1136/oem.2006.031500.
- Berkay, A., B. Nas, and A. Demirbas (2006), Contribution of Konya plain projects to the national development in Turkey's water-related energy, *Energy Explor. Exploit.*, *24*, 87–94.
- Beusen, A. H. W., A. F. Bouwman, P. S. C. Heuberger, G. Van Drecht, and K. W. Van Der Hoek (2008), Bottom-up uncertainty estimates of global ammonia emissions from global agricultural systems, *Atmos. Environ.*, *42*, 6067–6077, doi:10.1016/j.atmosenv.2008.03.044.
- Botha, S., P. J. Carrick, and N. Allsopp (2008), Capturing lessons from land-users to aid the development of ecological restoration guidelines for lowland Namaqualand, *Biol. Conserv.*, *141*, 885–895, doi:10.1016/j.biocon.2007.12.005.
- Bou Karam, D., C. Flamant, P. Knippertz, O. Reitebuch, J. Pelon, M. Chong, and A. Dabas (2008), Dust emissions over the Sahel associated with the West African monsoon intertropical discontinuity region: A representative case-study, *Q. J. R. Meteorol. Soc.*, *134*, 621–634, doi:10.1002/qj.244.
- Bou Karam, D., C. Flamant, P. Tulet, J.-P. Chaboureau, A. Dabas, and M. C. Todd (2009), Estimate of Sahelian dust emissions in the intertropical discontinuity region of the West African monsoon, *J. Geophys. Res.*, *114*, D13106, doi:10.1029/2008JD011444.
- Bryant, R. G. (2003), Monitoring hydrological controls on dust emissions: Preliminary observations from Etosha Pan, Namibia, *Geogr. J.*, *169*, 131–141, doi:10.1111/1475-4959.04977.
- Bryant, R. G., G. R. Bigg, N. M. Mahowald, F. D. Eckardt, and S. G. Ross (2007), Dust emission response to climate in southern Africa, *J. Geophys. Res.*, *112*, D09207, doi:10.1029/2005JD007025.
- Bullard, J. E., and G. H. McTainsh (2003), Aeolian-fluvial interactions in dryland environments: Examples, concepts and Australia case study, *Prog. Phys. Geog.*, *27*, 471–501.
- Bullard, J. E., G. H. McTainsh, and C. Pudmenzky (2007), Factors affecting the nature and rate of dust production from natural sand dunes, *Sedimentology*, *54*, 169–182, doi:10.1111/j.1365-3091.2006.00827.x.
- Bullard, J., M. Baddock, G. H. McTainsh, and J. Leys (2008), Sub-basin scale dust source geomorphology detected using MODIS, *Geophys. Res. Lett.*, *35*, L15404, doi:10.1029/2008GL033928.
- Bullard, J. E., S. P. Harrison, M. Baddock, N. A. Drake, T. E. Gill, G. H. McTainsh, and Y. Sun (2011), Preferential dust sources: A geomorphological classification designed for use in global dust-cycle models, *J. Geophys. Res.*, *116*, F04034, doi:10.1029/2011JF002061.
- Butler, H. J., W. L. Hogarth, and G. H. McTainsh (2001), Effects of spatial variations in source areas upon dust concentration profiles during three wind erosion events in Australia, *Earth Surf. Processes Landforms*, *26*, 1039–1048, doi:10.1002/esp.235.
- Butler, H. J., G. H. McTainsh, W. L. Hogarth, and J. F. Leys (2005), Kinky profiles: Effects of soil surface heating upon vertical dust concentration profiles in the Channel Country of western Queensland, Australia, *J. Geophys. Res.*, *110*, F04025, doi:10.1029/2004JF000272.
- Cachorro, V. E., P. Durán, R. Vergz, and A. M. de Frutos (2000), Measurements of the atmospheric turbidity of the north-centre continental area in Spain: Spectral aerosol optical depth and Angström turbidity parameters, *J. Aerosol Sci.*, *31*, 687–702.
- Cai, W., and T. Cowan (2008), Evidence of impacts from rising temperature on inflows to the Murray-Darling Basin, *Geophys. Res. Lett.*, *35*, L07701, doi:10.1029/2008GL033390.
- Cakmur, R. V., R. L. Miller, J. Perlitz, I. V. Geogdzhayev, P. Ginoux, D. Koch, K. E. Kohfeld, I. Tegen, and C. S. Zender (2005), Constraining the magnitude of the global dust cycle by minimizing the difference between a model and observations, *J. Geophys. Res.*, *111*, D06207, doi:10.1029/2005JD005791.
- Cayan, D. R., T. Das, D. W. Pierce, T. P. Barnett, M. Tyree, and A. Gershunov (2010), Future dryness in the southwest US and the hydrology of the early 21st century drought, *Proc. Natl. Acad. Sci. U. S. A.*, *107*, 21,271–21,276, doi:10.1073/pnas.0912391107.
- Chao, H. J., C. C. Chan, C. Y. Rao, C. T. Lee, Y. C. Chuang, Y. H. Chiu, H. H. Hsu, and Y. H. Wu (2012), The effects of transported Asian dust on the composition and concentration of ambient fungi in Taiwan, *Int. J. Biometeorol.*, *56*, 211–219, doi:10.1007/s00484-011-0413-x.
- Chen, W., and D. W. Fryrear (2002), Sedimentary characteristics of a haboob dust storm, *Atmos. Res.*, *61*(1), 75–85.
- Cheng, T., H. Wang, Y. Xu, H. Li, and L. Tian (2006), Climatology of aerosol optical properties in northern China, *Atmos. Environ.*, *40*, 1495–1509, doi:10.1016/j.atmosenv.2005.10.047.
- Chin, M., T. Diehl, P. Ginoux, and W. Malm (2007), Intercontinental transport of pollution and dust aerosols: implications for regional air quality, *Atmos. Chem. Phys.*, *7*, 5501–5517.
- Chow, J. C., J. G. Watson, D. H. Lowenthal, P. A. Solomon, K. L. Magliano, S. D. Ziman, and L. W. Richards (1992), PM10 source apportionment in California's San Joaquin Valley, *Atmos. Environ. Part A*, *26*(18), 3335–3354.
- Chow, J. C., J. G. Watson, L. L. Ashbaugh, and K. L. Magliano (2003), Similarities and differences in PM10 chemical source profiles for geological dust from San Joaquin Valley, California, *Atmos. Environ.*, *37*(9–10), 1317–1340.
- Christensen, J. H., et al. (2007), Regional climate projections, in *Climate Change 2007: The Physical Science Basis. Contribution of Working Group I to the Fourth Assessment Report of the Intergovernmental Panel on Climate Change*, edited by S. Solomon et al., pp. 847–940, Cambridge Univ. Press, Cambridge, U. K.
- Christopher, S. A., and J. Wang (2004), Intercomparison between multi-angle imaging spectroradiometer (MISR) and sunphotometer aerosol optical thickness in dust source regions over China: Implications for satellite aerosol retrievals and radiative forcing calculations, *Tellus, Ser. B*, *56*, 451–456.

- Claiborn, C., B. Lamb, A. Miller, J. Beseda, B. Clode, J. Vaughan, L. Kang, and C. Newvine (1998), Regional measurements and modeling of windblown agricultural dust: The Columbia Plateau PM10 Program, *J. Geophys. Res.*, 103(D16), 19,753–19,767.
- Cook, B. I., R. L. Miller, and R. Seager (2009), Amplification of the North American “Dust Bowl” drought through human-induced land degradation, *Proc. Natl. Acad. Sci. U. S. A.*, 106, 4997–5001, doi:10.1073/pnas.08102000106.
- Cook, E. R., R. Seager, M. A. Cane, and D. W. Stahle (2007), North American drought: Reconstructions, causes, and consequences, *Earth Sci. Rev.*, 81, 93–134, doi:10.1016/j.earscirev.2006.12.002.
- Crusius, J., A. W. Schroth, S. Gassó, C. M. Moy, R. C. Levy, and M. Gatica (2011), Glacial flour dust storms in the Gulf of Alaska: Hydrologic and meteorological controls and their importance as a source of bioavailable iron, *Geophys. Res. Lett.*, 38, L06602, doi:10.1029/2010GL046573.
- Crutzen, P. J., and M. O. Andreae (1990), Biomass burning in the tropics: Impact on atmospheric chemistry and biogeochemical cycles, *Science*, 21, 1669–1678, doi:10.1126/science.250.4988.1669.
- Cuesta, J., et al. (2008), Multiplatform observations of the seasonal evolution of the Saharan atmospheric boundary layer in Tamanrasset, Algeria, in the framework of the African Monsoon Multidisciplinary Analysis field campaign conducted in 2006, *J. Geophys. Res.*, 113, D00C07, doi:10.1029/2007JD009417.
- Darmenova, K., and I. N. Sokolik (2007), Assessing uncertainties in dust emission in the Aral Sea region caused by meteorological fields predicted with a mesoscale model, *Global Planet. Change*, 56, 297–310, doi:10.1016/j.gloplacha.2006.07.024.
- De Longueville, F., Y. C. Hountondji, S. Henry, and P. Ozer (2010), What do we know about effects of desert dust on air quality and human health in West Africa compared to other regions?, *Sci. Total Environ.*, 409, 1–8.
- Derbyshire, E. (2007), Natural mineralogenic dust and human health, *Ambio*, 36, 73–77.
- Derbyshire, E., X. Meng, and R. A. Kemp (1998), Provenance, transport and characteristics of modern aeolian dust in western Gansu Province, China, and interpretation of the Quaternary loess record, *J. Arid Environ.*, 39, 497–516, doi:10.1006/jare.1997.0369.
- Dey, S., and L. Di Girolamo (2010), A climatology of aerosol optical and microphysical properties over the Indian subcontinent from 9 years (2000–2008) of Multiangle Imaging Spectroradiometer (MISR) data, *J. Geophys. Res.*, 115, D15204, doi:10.1029/2009JD013395.
- Dickerson, P. W. (2000), A Caspian chronicle: Sea level fluctuations between 1982 and 1997, in *Dynamic Earth Environments: Remote Sensing Observations from Shuttle-Mir Missions*, edited by K. P. Lulla and L. V. Dessinov, pp. 145–148, John Wiley, New York.
- Draxler, R. R., P. Ginoux, and A. F. Stein (2010), An empirically derived emission algorithm for wind-blown dust, *J. Geophys. Res.*, 115, D16212, doi:10.1029/2009JD013167.
- Dubovik, O., and M. D. King (2000), A flexible inversion algorithm for retrieval of aerosol optical properties from Sun and sky radiance measurements, *J. Geophys. Res.*, 105, 20,673–20,696.
- Dubovik, O., B. Holben, T. F. Eck, A. Smirnov, Y. J. Kaufman, M. D. King, D. Tanré, and I. Slutsker (2002), Variability of absorption and optical properties of key aerosol types observed in worldwide locations, *J. Atmos. Sci.*, 59, 590–608.
- Eck, T. F., B. N. Holben, J. S. Reid, O. Dubovik, A. Smirnov, N. T. O’Neill, I. Slutsker, and S. Kinne (1999), Wavelength dependence of the optical depth of biomass burning, urban, and desert dust aerosols, *J. Geophys. Res.*, 104(D24), 31,333–31,349.
- Eckhardt, F. D., and N. Kuring (2005), SeaWiFS identifies dust sources in the Namib Desert, *Int. J. Remote Sens.*, 26, 4159–4167, doi:10.1080/01431160500113112.
- Eitel, B., W. D. Blümel, K. Hüser, and B. Mauz (2001), Dust and loessic alluvial deposits in northwestern Namibia (Damaraland, Kaokoveld): Sedimentology and palaeoclimatic evidence based on luminescence data, *Quat. Int.*, 76–77, 57–65.
- Ekström, M., G. H. McTainsh, and A. Chappell (2004), Australian dust storms: temporal trends and relationships with synoptic pressure distributions (1960–99), *Int. J. Climatol.*, 24, 1581–1599, doi:10.1002/joc.1072.
- Engelstaedter, S., K. E. Kohfeld, I. Tegen, and S. P. Harrison (2003), Controls of dust emissions by vegetation and topographic depressions: An evaluation using dust storm frequency data, *Geophys. Res. Lett.*, 30(6), 1294, doi:10.1029/2002GL016471.
- Fagan, S. D., and G. C. Nanson (2004), The morphology and formation of floodplain-surface channels, Cooper Creek, Australia, *Geomorphology*, 60, 107–126, doi:10.1016/j.geomorph.2003.07.009.
- Fairlie, T. D., D. J. Jacob, and R. J. Park (2007), The impact of transpacific transport of mineral dust in the United States, *Atmos. Environ.*, 41, 1251–1266.
- Feddema, J. J. (1998), Estimated impacts of soil degradation on the African water balance and climate, *Clim. Res.*, 10, 127–141.
- Fernandez, A. J., M. Ternero, F. J. Barragan, and J. C. Jimenez (2000), An approach to characterization of sources of urban airborne particles through heavy metal speciation, *Chemosphere*, 2, 123–136, doi:10.1016/S1465-9972(00)00002-7.
- Forster, P., et al. (2007), Changes in atmospheric constituents and in radiative forcing, in *Climate Change 2007: The Physical Science Basis. Contribution of Working Group I to the Fourth Assessment Report of the Intergovernmental Panel on Climate Change*, edited by S. Solomon et al., pp. 129–234, Cambridge Univ. Press, Cambridge, U. K.
- Fryberger, S. G., A. M. Al-Sari, and T. J. Clisham (1983), Eolian dune, interdune, sand sheet, and siliciclastic sabkha sediments of an offshore prograding sand sea, Dhahran area, Saudi Arabia, *AAPG Bull.*, 67, 280–312.
- Garreaud, R. D., and P. Aceituno (2001), Interannual rainfall variability over the South American Altiplano, *J. Clim.*, 14, 2779–2789.
- Gassó, S., and A. F. Stein (2007), Does dust from Patagonia reach the sub-Antarctic Atlantic Ocean?, *Geophys. Res. Lett.*, 34, L01801, doi:10.1029/2006GL027693.
- Ge, J. M., J. Su, T. P. Ackerman, Q. Fu, J. P. Huang, and J. S. Shi (2010), Dust aerosol optical properties retrieval and radiative forcing over northwestern China during the 2008 China-US joint field experiment, *J. Geophys. Res.*, 115, D00K12, doi:10.1029/2009JD013263.
- Ghazleh, A., S. Abed, and A. M. Kempe (2011), The dramatic drop of the Dead Sea: Background, rates, impacts and solutions, in *Macro-engineering Seawater in Unique Environments*, edited by V. Badescu and R. B. Cathcart, pp. 77–105, Springer, Heidelberg, Germany, doi:10.1007/978-3-642-14779-1\_4.
- Gill, T. E. (1996), Eolian sediments generated by anthropogenic disturbance of playas: Human impacts on the geomorphic system and geomorphic impacts on the human system, *Geomorphology*, 17, 207–228, doi:10.1016/0169-555X(95)00104-D.
- Gillette, D. A. (1999), A qualitative geophysical explanation for “hot spot” dust emitting source regions, *Contrib. Atmos. Phys.*, 72, 67–77.
- Gillette, D. A., and R. Passi (1988), Modeling dust emission caused by wind erosion, *J. Geophys. Res.*, 93(D11), 14,233–14,242, doi:10.1029/JD093iD11p14233.
- Gillette, D. A., D. W. Fryrear, T. E. Gill, T. Ley, T. A. Cahill, and E. A. Gearhart (1997), Relation of vertical flux of particles smaller than 10  $\mu\text{m}$  to total aeolian horizontal mass flux at Owens Lake, *J. Geophys. Res.*, 102(D22), 26,009–26,015, doi:10.1029/97JD02252.
- Gillies, J. A., W. G. Nickling, and G. H. McTainsh (1996), Dust concentrations and particle-size characteristics of an intense dust haze event: Inland Delta Region, Mali, West Africa, *Atmos. Environ.*, 30, 1081–1090, doi:10.1016/1352-2310(95)00432-7.
- Ginoux, P., and O. Torres (2003), Empirical TOMS index for dust aerosol: Applications to model validation and source

- characterization, *J. Geophys. Res.*, 108(D17), 4534, doi:10.1029/2003JD003470.
- Ginoux, P., M. Chin, I. Tegen, J. M. Prospero, B. Holben, O. Dubovik, and S.-J. Lin (2001), Sources and distributions of dust aerosols simulated with the GOCART model, *J. Geophys. Res.*, 106, 20,255–20,274.
- Ginoux, P., J. M. Prospero, O. Torres, and M. Chin (2004), Long-term simulation of global dust distribution with the GOCART model: Correlation with the North Atlantic Oscillation, *Environ. Model. Software*, 19, 113–128, doi:10.1016/S1364-8152(03)00114-2.
- Ginoux, P., D. Garbuзов, and H. C. Hsu (2010), Identification of anthropogenic and natural dust sources using Moderate Resolution Imaging Spectroradiometer (MODIS) Deep Blue level 2 data, *J. Geophys. Res.*, 115, D05204, doi:10.1029/2009JD012398.
- Golabian, H. (2011), Urumia Lake: Hydro-ecological stabilization and permanence, in *Macro-engineering Seawater in Unique Environments*, edited by V. Badescu and R. B. Cathcart, pp. 365–397, Springer, Heidelberg, Germany, doi:10.1007/978-3-642-14779-1\_18.
- Gong, S. L., X. Y. Zhang, T. L. Zhao, and L. A. Barrie (2004), Sensitivity of Asian dust storm to natural and anthropogenic factors, *Geophys. Res. Lett.*, 31, L07210, doi:10.1029/2004GL019502.
- Goudie, A. S., and J. Boardman (2010), Soil erosion, in *Geomorphological hazards and disaster prevention*, edited by I. Alcántara-Ayala and A. S. Goudie, pp. 177–184, Cambridge Univ. Press, Cambridge, U. K.
- Goudie, A. S., and N. J. Middleton (2001), Saharan dust storms: Nature and consequences, *Earth Sci. Rev.*, 56, 179–204, doi:10.1016/S0012-8252(01)00067-8.
- Grineski, S. E., J. G. Staniswalis, P. Bulathsinhala, Y. Peng, and T. E. Gill (2011), Hospital admissions for asthma and acute bronchitis in El Paso, Texas: Do age, sex, and insurance status modify the effects of dust and low wind events?, *Environ. Res.*, 111, 1148–1155.
- Guelle, W., Y. Balkanski, M. Schulz, B. Marticorena, G. Bergametti, C. Moulin, R. Arimoto, and K. Perry (2000), Modeling the atmospheric distribution of mineral aerosol: Comparison with ground measurements and satellite observations for yearly and synoptic timescales over the North Atlantic, *J. Geophys. Res.*, 105(D2), 1997–2012.
- Hagen, L. J., and N. P. Woodruff (1973), Air pollution from dust storms in the Great Plains, *Atmos. Environ.*, 7, 323–332.
- Hahnberger, M., and K. Nicoll (2012), Meteorological characteristics of dust transport events in the Eastern Great Basin of Utah, USA, *Atmos. Environ.*, doi:10.1016/j.atmosenv.2012.06.029, in press.
- Haustein, K., et al. (2012), Atmospheric dust modeling from meso to global scales with the online NMMB/BSC-Dust model—Part 2: Experimental campaigns in northern Africa, *Atmos. Chem. Phys.*, 12, 2933–2958, doi:10.5194/acp-12-2933-2012.
- Helgren, D. M., and J. M. Prospero (1987), Wind velocities associated with dust deflation events in the Western Sahara, *J. Clim. Appl. Meteorol.*, 26, 1147–1151.
- Hemming, C. F., and C. G. Trapnell (1957), A reconnaissance classification of the soils of the South Turkana Desert, *J. Soil Sci.*, 8, 167–183.
- Herman, J., P. K. Bhartia, O. Torres, N. C. Hsu, C. Seftor, and E. Celarier (1997), Global distribution of UV-absorbing aerosols from Nimbus 7/TOMS data, *J. Geophys. Res.*, 102(D14), 16,911–16,922.
- Hesse, P. P., and G. H. McTainsh (2003), Australian dust deposits: Modern processes and the Quaternary record, *Quat. Sci. Rev.*, 22, 2007–2035.
- Holben, B. N., et al. (1998), AERONET—A federated instrument network and data archive for aerosol characterization, *Remote Sens. Environ.*, 66(1), 1–16.
- Hsu, N. C., S.-C. Tsay, M. King, and J. R. Herman (2004), Aerosol properties over bright-reflecting source regions, *IEEE Trans. Geosci. Remote Sens.*, 42, 557–569.
- Hsu, N. C., S.-C. Tsay, M. King, and J. R. Herman (2006), Deep Blue retrievals of Asian aerosol properties during ACE-Asia, *IEEE Trans. Geosci. Remote Sens.*, 44, 3180–3195.
- Huneeus, N., et al. (2011), Global dust model intercomparison in AeroCom phase I, *Atmos. Chem. Phys.*, 11, 7781–7816, doi:10.5194/acp-11-7781-2011.
- Hurt, G. C., et al. (2011), Harmonization of land-use scenarios for the period 1500–2100: 600 years of global gridded annual land-use transitions, wood harvest, and resulting secondary lands, *Clim. Change*, 109, 117–161, doi:10.1007/s10584-011-0153-2.
- Idso, S. B., R. S. Ingram, and J. M. Pritchard (1972), An American haboob, *Bull. Am. Meteorol. Soc.*, 53, 930–935.
- Igarashi, Y., H. Fujiwara, and D. Jugder (2011), Change of the Asian dust source region deduced from the composition of anthropogenic radionuclides in surface soil in Mongolia, *Atmos. Chem. Phys.*, 11, 7069–7080, doi:10.5194/acp-11-7069-2011.
- Jaffe, D., J. Snow, and O. Cooper (2003), The 2001 Asian dust events: Transport and impact on surface aerosol concentrations in the U.S., *Eos Trans. AGU*, 84(46), 501, doi:10.1029/2003EO460001.
- Jickells, T. D., et al. (2005), Global iron connections between desert dust, ocean biogeochemistry, and climate, *Science*, 308, 67–71, doi:10.1126/science.1105959.
- Jiménez, E., C. Linares, D. Martínez, and J. Díaz (2010), Role of Saharan dust in the relationship between particulate matter and short-term daily mortality among the elderly in Madrid (Spain), *Sci. Total Environ.*, 408, 5729–5736.
- Kalnay, E., et al. (1996), The NCEP/NCAR 40-year reanalysis project, *Bull. Am. Meteorol. Soc.*, 77, 437–471.
- Kezer, K., and H. Matsuyama (2006), Decrease of river runoff in the Lake Balkhash basin in central Asia, *Hydrol. Processes*, 20, 1407–1423, doi:10.1002/hyp.6097.
- Klein Goldewijk, K. (2001), Estimating global land use change over the past 300 years: The HYDE database, *Global Biogeochem. Cycles*, 15, 417–433.
- Klose, M., Y. Shao, M. K. Karremann, and A. H. Fink (2010), Sahel dust zone and synoptic background, *Geophys. Res. Lett.*, 37, L09802, doi:10.1029/2010GL042816.
- Knight, A. W., G. H. McTainsh, and R. W. Simpson (1995), Sediment loads in an Australian dust storm: Implications for present and past dust processes, *Catena*, 24, 195–213.
- Knippertz, P., and M. C. Todd (2012), Mineral dust aerosols over the Sahara: Meteorological controls on emission and transport and implications for modeling, *Rev. Geophys.*, 50, RG1007, doi:10.1029/2011RG000362.
- Koch, J., and N. O. Renno (2005), The role of convective plumes and vortices on the global aerosol budget, *Geophys. Res. Lett.*, 32, L18806, doi:10.1029/2005GL023420.
- Kopf, A., G. Delisle, E. Faber, B. Panahi, C. S. Aliyev, and I. Guliyev (2010), Long-term in situ monitoring at Dashgil mud volcano, Azerbaijan: A link between seismicity, pore-pressure transients and methane emission, *Int. J. Earth Sci.*, 99, 227–240, doi:10.1007/s00531-009-0487-4.
- Koren, I., Y. J. Kaufman, R. Washington, M. C. Todd, Y. Rudich, J. V. Martins, and D. Rosenfeld (2006), The Bodélé depression: A single spot in Sahara that provides most of the mineral dust in the Amazon forest, *Environ. Res. Lett.*, 1, 014005, doi:10.1088/1748-9326/1/1/014005.
- Kurosaki, Y., and M. Mikami (2005), Regional difference in the characteristics of dust event in East Asia: Relationship among dust outbreak, surface wind, and land surface condition, *J. Meteorol. Soc. Jpn.*, 83A, 1–18.
- Lee, J. A., T. E. Gill, K. R. Mulligan, M. Dominguez Acosta, and A. E. Perez (2009), Land use/land cover and point sources of the 15 December 2003 dust storm in southwestern North America, *Geomorphology*, 105, 18–27, doi:10.1016/j.geomorph.2007.12.016.
- Lee, J. A., M. C. Baddock, M. J. Mbuh, and T. E. Gill (2012), Geomorphic and land cover characteristics of aeolian dust sources in

- West Texas and eastern New Mexico, USA, *Aeolian Res.*, 3(4), 459–466, doi:10.1016/j.aeolia.2011.08.001.
- Legrand, M., A. Plana-Fattori, and C. N'doumé (2001), Satellite detection of dust using the IR imagery of Meteosat: 1. Infrared difference dust index, *J. Geophys. Res.*, 106(D16), 18,251–18,274.
- Lelieveld, J., et al. (2002), Global air pollution crossroads over the Mediterranean, *Science*, 298, 794–799, doi:10.1126/science.1075457.
- Lewis, J. M., M. L. Kaplan, R. Vellore, R. M. Rabin, J. Hallett, and S. A. Cohn (2011), Dust storm over the Black Rock Desert: Larger-scale dynamic signatures, *J. Geophys. Res.*, 116, D06113, doi:10.1029/2010JD014784.
- Li, F., P. Ginoux, and V. Ramaswamy (2008), Distribution, transport, and deposition of mineral dust in the Southern Ocean and Antarctica: Contribution of major sources, *J. Geophys. Res.*, 113, D10207, doi:10.1029/2007JD009190.
- Li, F., P. Ginoux, and V. Ramaswamy (2010), Transport of Patagonian dust to Antarctica, *J. Geophys. Res.*, 115, D18217, doi:10.1029/2009JD012356.
- Littmann, T. (1991), Dust storm frequency in Asia: Climatic control and variability, *Int. J. Climatol.*, 11, 393–412, doi:10.1002/joc.3370110405.
- Liu, D., J. Abduwaili, J. Lei, and G. Wu (2011), Deposition rate and chemical composition of the Aeolian dust from a bare saline playa, Ebinur Lake, Xinjiang, China, *Water Air Soil Pollut.*, 218, 175–184, doi:10.1007/s11270-010-0633-4.
- Liu, J., D. L. Mauzerall, and L. W. Horowitz (2009), Evaluating inter-continental transport of fine aerosols: (2) Global health impact, *Atmos. Environ.*, 43, 4339–4347.
- Lyngsie, G., T. Awadzi, and H. Breuning-Madsen (2011), Origin of Harmattan dust settled in Northern Ghana—Long transported or local dust?, *Geoderma*, 167–168, 351–359, doi:10.1016/j.geoderma.2011.07.026.
- Ma, R., H. Duan, C. Hu, X. Feng, A. Li, W. Ju, J. Jiang, and G. Yang (2010), A half-century of changes in China's lakes: Global warming or human influence?, *Geophys. Res. Lett.*, 37, L24106, doi:10.1029/2010GL045514.
- Mahowald, N. M., and C. Luo (2003), A less dusty future?, *Geophys. Res. Lett.*, 30(17), 1903, doi:10.1029/2003GL017880.
- Mahowald, N. M., R. G. Bryant, J. del Corral, and L. Steinberger (2003), Ephemeral lakes and desert dust sources, *Geophys. Res. Lett.*, 30(2), 1074, doi:10.1029/2002GL016041.
- Mahowald, N. M., D. R. Muhs, S. Levis, P. J. Rasch, M. Yoshioka, C. Z. Zender, and C. Luo (2006), Change in atmospheric mineral aerosols in response to climate: Last glacial period, preindustrial, modern, and doubled carbon dioxide climates, *J. Geophys. Res.*, 111, D10202, doi:10.1029/2005JD006653.
- Mahowald, N. M., et al. (2010), Observed 20th century desert dust variability: Impact on climate and biogeochemistry, *Atmos. Chem. Phys.*, 10, 10,875–10,893, doi:10.5194/acp-10-10875-2010.
- Marsham, J. H., P. Knippertz, N. S. Dixon, D. J. Parker, and G. M. S. Lister (2011), The importance of the representation of deep convection for modeled dust-generating winds over West Africa during summer, *Geophys. Res. Lett.*, 38, L16803, doi:10.1029/2011GL048368.
- Marx, S. K., H. A. McGowan, and B. S. Kamber (2009), Long-range dust transport from eastern Australia: A proxy for Holocene aridity and ENSO-type climate variability, *Earth Planet. Sci. Lett.*, 282, 167–177, doi:10.1016/j.epsl.2009.03.013.
- Marx, S. K., B. S. Kamber, H. A. McGowan, and J. Denholm (2011), Holocene dust deposition rates in Australia's Murray-Darling Basin record the interplay between aridity and the position of the mid-latitude westerlies, *Quat. Sci. Rev.*, 30, 3290–3305, doi:10.1016/j.quascirev.2011.07.015.
- Maurer, T., L. Herrmann, and K. Stahr (2009), The effect of surface variability factors on wind-erosion susceptibility: A field study in SW Niger, *J. Plant. Nutr. Soil Sci.*, 172, 789–807.
- McConnell, J. R., A. J. Aristarain, J. R. Banta, P. R. Edwards, and J. C. Simões (2007), 20th-century doubling in dust archived in an Antarctic Peninsula ice core parallels climate change and desertification in South America, *Proc. Natl. Acad. Sci. U. S. A.*, 104, 5743–5748.
- McTainsh, G. H. (1989), Quaternary aeolian dust processes and sediments in the Australian region, *Quat. Sci. Rev.*, 8, 235–253.
- Meadows, M. E. (2003), Soil erosion in the Swartland, Western Cape Province, South Africa: Implications of past and present policy and practice, *Environ. Sci. Policy*, 6, 17–28, doi:10.1016/S1462-9011(02)00122-3.
- Meehl, G., C. Covey, T. Delworth, M. Latif, B. McAvaney, J. Mitchell, R. Stouffer, and K. Taylor (2007), The WCRP CMIP3 multimodel dataset: A new era in climate change research, *Bull. Am. Meteorol. Soc.*, 88, 1383–1394.
- Menut, L. (2008), Sensitivity of hourly Saharan dust emissions to NCEP and ECMWF modeled wind speed, *J. Geophys. Res.*, 113, D16201, doi:10.1029/2007JD009522.
- Micklin, P. (2007), The Aral Sea disaster, *Annu. Rev. Earth Planet. Sci.*, 35, 47–72.
- Micklin, P. (2010), The past, present, and future Aral Sea, *Lakes Reservoirs Res. Manage.*, 15(3), 193–213, doi:10.1111/j.1440-1770.2010.00437.x.
- Middleton, N. (1986), A geography of dust storms in south-west Asia, *Int. J. Climatol.*, 6, 183–196.
- Miller, R. L., J. Perlitz, and I. Tegen (2004), Feedback upon dust emission by dust radiative forcing through the planetary boundary layer, *J. Geophys. Res.*, 109, D24209, doi:10.1029/2004JD004912.
- Miller, S. D., A. P. Kuciauskas, M. Liu, Q. Ji, J. S. Reid, D. W. Breed, A. L. Walker, and A. A. Mandoos (2008), Haboob dust storms of the southern Arabian Peninsula, *J. Geophys. Res.*, 113, D01202, doi:10.1029/2007JD008550.
- Morishima, W., and I. Akasaka (2010), Seasonal trends of rainfall and surface temperature over southern Africa, *Afr. Study Monogr. Suppl.*, 40, 67–76.
- Mulitza, S., et al. (2010), Increase in African dust flux at the onset of commercial agriculture in the Sahel region, *Nature*, 466, 226–228, doi:10.1038/nature09213.
- Munson, S. M., J. Belnap, and G. S. Okin (2011), Responses of wind erosion to climate-induced vegetation changes on the Colorado Plateau, *Proc. Natl. Acad. Sci. U. S. A.*, 108, 3854–3859, doi:10.1073/pnas.1014947108.
- National Research Council (1983), *Environmental Change in the West African Sahel*, Natl. Acad. Press, Washington, D. C.
- Natsagdorj, L., D. Jugder, and Y. S. Chung (2003), Analysis of dust storms observed in Mongolia during 1937–1999, *Atmos. Environ.*, 37, 1401–1411, doi:10.1016/S1352-2310(02)01023-3.
- Neff, J. C., et al. (2008), Increasing eolian dust deposition in the western United States linked to human activity, *Nat. Geosci.*, 1, 189–195, doi:10.1038/ngeo133.
- Niang, A. J., A. Ozer, and P. Ozer (2008), Fifty years of landscape evolution in southwestern Mauritania by means of aerial photos, *J. Arid Environ.*, 72, 97–107, doi:10.1016/j.jaridenv.2007.04.009.
- Nickling, W. G., and J. A. Gillies (1993), Dust emission and transport in Mali, West Africa, *Sedimentology*, 40, 859–868.
- Nickling, W. G., G. H. McTainsh, and J. F. Leys (1999), Dust emissions from the Channel Country of western Queensland, Australia, *Z. Geomorphol. Suppl.*, 116, 1–17.
- Nordstrom, K. F., and S. Hotta (2004), Wind erosion from cropland in the USA: A review of problems, solutions and prospects, *Geoderma*, 12(3–4), 157–167.
- Novlan, D. J., M. Hardiman, and T. E. Gill (2007), A synoptic climatology of blowing dust events in El Paso, Texas from 1932–2005, paper presented at 16th Conference on Applied Climatology, Am. Meteorol. Soc., San Antonio, Tex.
- N'Tchayi Mbourou, G., J. J. Bertrand, and S. E. Nicholson (1997), The diurnal and seasonal cycles of wind-borne dust over Africa north of the equator, *J. Appl. Meteorol.*, 36, 868–882, doi:10.1175/1520-0450(1997)036.

- Nyamweru, C. K., and D. Bowman (1989), Climatic changes in the Chalbi desert, north Kenya, *J. Quat. Sci.*, 4, 131–139, doi:10.1002/jqs.3390040204.
- Okin, G. S., J. E. Bullard, R. L. Reynolds, J.-A. C. Ballantine, K. Schepanski, M. C. Todd, J. Belnap, M. C. Baddock, T. E. Gill, and M. E. Miller (2011), Dust: Small-scale processes with global consequences, *Eos Trans. AGU*, 92(29), 241–242, doi:10.1029/2011EO290001.
- Orgill, M. M., and G. A. Sehmel (1976), Frequency and diurnal variation of dust storms in the contiguous U.S.A., *Atmos. Environ.*, 10, 813–825.
- Orlove, B. (2005), Human adaptation to climate change: A review of three historical cases and some general perspectives, *Environ. Sci. Policy*, 8, 589–600.
- Osborne, S. R., B. T. Johnson, J. M. Haywood, A. J. Baran, M. A. J. Harrison, and C. L. McConnell (2008), Physical and optical properties of mineral dust aerosol during the Dust and Biomass-burning Experiment, *J. Geophys. Res.*, 111, D00C03, doi:10.1029/2007JD009551.
- Pandithurai, G., S. Dipu, K. K. Dani, S. Tiwari, D. S. Bisht, P. C. S. Devara, and R. T. Pinker (2008), Aerosol radiative forcing during dust events over New Delhi, India, *J. Geophys. Res.*, 113, D13209, doi:10.1029/2008JD009804.
- Parkinson, J. (1939), Notes on the Northern Frontier Province, Kenya, *Geogr. J.*, 94, 162–166.
- Pasquini, A. I., and P. J. Depetris (2006), Discharge trends and flow dynamics of South American rivers draining the southern Atlantic seaboard: An overview, *J. Hydrol.*, 333, 385–399, doi:10.1016/j.jhydrol.2006.09.005.
- Prasad, A. K., S. Singh, S. S. Chauhan, M. K. Srivastava, R. P. Singh, and R. Singh (2007), Aerosol radiative forcing over the Indo-Gangetic plains during major dust storms, *Atmos. Environ.*, 41, 6289–6301.
- Prospero, J. M. (1999), Long-term measurements of the transport of African mineral dust to the southeastern United States: Implications for regional air quality, *J. Geophys. Res.*, 104(D13), 15,917–15,927.
- Prospero, J. M., and P. J. Lamb (2003), African droughts and dust transport to the Caribbean: Climate change implications, *Science*, 7, 1024–1027, doi:10.1126/science.108915.
- Prospero, J. M., I. Olmez, and M. Ames (2001), Al and Fe in PM 2.5 and PM 10 suspended particles in south-central Florida: The impact of the long range transport of African mineral dust, *Water Air Soil Pollut.*, 125, 291–317.
- Prospero, J. M., P. Ginoux, O. Torres, S. E. Nicholson, and T. E. Gill (2002), Environmental characterization of global sources of atmospheric soil dust identified with the Nimbus 7 Total Ozone Mapping Spectrometer (TOMS) absorbing aerosol product, *Rev. Geophys.*, 40(1), 1002, doi:10.1029/2000RG000095.
- Prospero, J. M., J. E. Bullard, and R. Hodgkins (2012), High-latitude dust over the North Atlantic: Inputs from Icelandic proglacial dust storms, *Science*, 335, 1078–1082, doi:10.1126/science.1217447.
- Puigdefàbregas, J., and T. Mendizabal (1998), Perspectives on desertification: Western Mediterranean, *J. Arid Environ.*, 39, 209–224.
- Putman, W. M., and S.-J. Lin (2007), Finite-volume transport on various cubed-sphere grids, *J. Comput. Phys.*, 227, 55–78, doi:10.1016/j.jcp.2007.07.022.
- Radhi, M., et al. (2010), Optical, physical and chemical characteristics of Australian continental aerosols: Results from a field experiment, *Atmos. Chem. Phys.*, 10, 5925–5942, doi:10.5194/acp-10-5925-2010.
- Rajot, J. L., et al. (2008), AMMA dust experiment: An overview of measurements performed during the dry season special observation period (SOP0) at the Banizoumbou (Niger) supersite, *J. Geophys. Res.*, 113, D00C14, doi:10.1029/2008JD009906.
- Ramachandran, S., S. Kedia, and R. Srivastava (2012), Aerosol optical depth trends over different regions of India, *Atmos. Environ.*, 49, 338–347.
- Rashki, A., D. G. Kaskaoutis, C. J. deW. Rautenbach, P. G. Eriksson, M. Qiang, and P. Gupta (2012), Dust storms and their horizontal dust loading in the Sistan region, Iran, *Aeolian Res.*, 5, 51–62, doi:10.1016/j.aeolia.2011.12.001.
- Ravi, S., et al. (2011), Aeolian processes and the biosphere, *Rev. Geophys.*, 49, RG3001, doi:10.1029/2010RG000328.
- Reynolds, R. L., J. C. Yount, M. Reheis, H. Goldstein, P. Chavez Jr., R. Fulton, J. Whitney, C. Fuller, and R. M. Forester (2007), Dust emission from wet and dry playas in the Mojave Desert, USA, *Earth Surf. Processes Landforms*, 32, 1811–1827, doi:10.1002/esp.1515.
- Rivera Rivera, N. I., T. E. Gill, M. P. Bleiweiss, and J. L. Hand (2010), Source characteristics of hazardous Chihuahuan desert dust outbreaks, *Atmos. Environ.*, 44, 2457–2468, doi:10.1016/j.atmosenv.2010.03.019.
- Rosenfeld, D., Y. Rudich, and R. Lahav (2001), Desert dust suppressing precipitation: A possible desertification feedback loop, *Proc. Natl. Acad. Sci. U. S. A.*, 98, 5975–5980.
- Rudich, Y., O. Khersonsky, and D. Rosenfeld (2002), Treating clouds with a grain of salt, *Geophys. Res. Lett.*, 29(22), 2060, doi:10.1029/2002GL016055.
- Sabbah, I., and F. M. Hassan (2008), Remote sensing of aerosols over the Solar Village, Saudi Arabia, *Atmos. Res.*, 90, 170–179.
- Sajani, S. Z., R. Miglio, P. Bonasoni, P. Cristofanelli, A. Marinoni, C. Sartini, C. A. Goldoni, G. De Girolamo, and P. Lauriola (2011), Saharan dust and daily mortality in Emilia-Romagna (Italy), *Occup. Environ. Med.*, 68, 446–451.
- Saqqqa, W., and M. Atallah (2004), Characterization of the aeolian terrain facies in Wadi Araba Desert, southwestern Jordan, *Geomorphology*, 62, 286–304, doi:10.1016/j.geomorph.2004.02.002.
- Schepanski, K., I. Tegen, B. Laurent, B. Heinold, and A. Macke (2007), A new Saharan dust source activation frequency map derived from MSG-SEVIRI IR-channels, *Geophys. Res. Lett.*, 34, L18803, doi:10.1029/2007GL030168.
- Schepanski, K., I. Tegen, M. C. Todd, B. Heinold, G. Bönisch, B. Laurent, and A. Macke (2009), Meteorological processes forcing Saharan dust emission inferred from MSG-SEVIRI observations of subdaily dust source activation and numerical models, *J. Geophys. Res.*, 114, D10201, doi:10.1029/2008JD010325.
- Schuster, G. L., O. Dubovik, and B. N. Holben (2006), Angstrom exponent and bimodal aerosol size distributions, *J. Geophys. Res.*, 111, D07207, doi:10.1029/2005JD006328.
- Seager, R., and G. A. Vecchi (2010), Greenhouse warming and the 21st century hydroclimate of southwestern North America, *Proc. Natl. Acad. Sci. U. S. A.*, 107, 21,277–21,282, doi:10.1073/pnas.0910856107.
- Singh, S., S. Nath, R. Kohli, and R. Singh (2005), Aerosols over Delhi during pre-monsoon months: Characteristics and effects on surface radiation forcing, *Geophys. Res. Lett.*, 32, L13808, doi:10.1029/2005GL023062.
- Smirnov, A., B. N. Holben, T. F. Eck, I. Slutsker, B. Chatenet, and R. T. Pinker (2002), Diurnal variability of aerosol optical depth observed at AERONET (Aerosol Robotic Network) sites, *Geophys. Res. Lett.*, 29(23), 2115, doi:10.1029/2002GL016305.
- Soderberg, K., and J. S. Compton (2007), Dust as a nutrient source for Fynbos ecosystems, South Africa, *Ecosystems*, 10, 550–561, doi:10.1007/s10021-007-9032-0.
- Stout, J. E. (2001), Dust and environment in the Southern High Plains of North America, *J. Arid Environ.*, 47, 425–441, doi:10.1006/jare.2000.0732.
- Stout, J. E., and J. A. Lee (2003), Indirect evidence of wind erosion trends on the Southern High Plains of North America, *J. Arid Environ.*, 55, 43–61.
- Strong, C. L., K. Parsons, G. H. McTainsh, and A. Sheehan (2011), Dust transporting wind systems in the lower Lake Eyre Basin, Australia: A preliminary study, *Aeolian Res.*, 2, 205–214, doi:10.1016/j.aeolia.2010.11.001.

- Sugden, D. E., R. D. McCulloch, A. J.-M. Bory, and A. S. Hein (2009), Influence of Patagonian glaciers on Antarctic dust deposition during the last glacial period, *Nat. Geosci.*, 2, 281–285, doi:10.1038.NGEO474.
- Sullivan, R. C., et al. (2010), Irreversible loss of ice nucleation active sites in mineral dust particles caused by sulphuric acid condensation, *Atmos. Chem. Phys.*, 10, 11,471–11,487, doi:10.5194/acp-10-11471-2010.
- Sun, J., M. Zhang, and T. Liu (2001), Spatial and temporal characteristics of dust storms in China and its surrounding regions 1960–1999: Relations to source area and climate, *J. Geophys. Res.*, 106, 10,325–10,333, doi:10.1029/2000JD900665.
- Swap, R., M. Garstang, S. Greco, R. Talbot, and P. Kallberg (1992), Saharan dust in Amazon Basin, *Tellus, Ser. B*, 44, 133–149.
- Tegen, I., M. Werner, S. P. Harrison, and K. E. Kohfeld (2004), Relative importance of climate and land use in determining present and future global soil dust emission, *Geophys. Res. Lett.*, 31, L05105, doi:10.1029/2003GL019216.
- Tegen, I., B. Heinold, M. Todd, J. Helmert, R. Washington, and O. Dubovik (2006), Modelling soil dust aerosol in the Bodélé depression during the BoDEX campaign, *Atmos. Chem. Phys.*, 6, 4345–4359.
- Todd, M. C., R. Washington, J. V. Martins, O. Dubovik, G. Lizcano, S. M'Bainayel, and S. Engelstaedter (2007), Mineral dust emission from the Bodélé Depression, northern Chad, during BoDEX 2005, *J. Geophys. Res.*, 112, D06207, doi:10.1029/2006JD007170.
- Torres, O., A. Tanskanen, B. Veihelmann, C. Ahn, R. Braak, P. K. Bhartia, P. Veefkind, and P. Levelt (2007), Aerosols and surface UV products from Ozone Monitoring Instrument observations: An overview, *J. Geophys. Res.*, 112, D24S47, doi:10.1029/2007JD008809.
- Troin, M., C. Vallet-Couïlomb, F. Sylvestre, and E. Piovano (2010), Hydrological modelling of a closed lake (Laguna Mar Chiquita, Argentina) in the context of 20th century climatic changes, *J. Hydrol.*, 393, 233–244, doi:10.1016/j.jhydrol.2010.08.019.
- Van Curen, R. A., and T. A. Cahill (2002), Asian aerosols in North America: Frequency and concentration of fine dust, *J. Geophys. Res.*, 107, 4804(D24), doi:10.1029/2002JD002204.
- Walker, A. L., M. Liu, S. D. Miller, K. A. Richardson, and D. L. Westphal (2009), Development of a dust source database for mesoscale forecasting in southwest Asia, *J. Geophys. Res.*, 114, D18207, doi:10.1029/2008JD011541.
- Wang, X., Z. Dong, J. Zhang, and L. Liu (2004), Modern dust storms in China: An overview, *J. Arid. Environ.*, 58, 559–574, doi:10.1016/j.jaridenv.2003.11.009.
- Wang, X., Z. Zhou, and Z. Dong (2006), Control of dust emissions by geomorphic conditions, wind environments and land use in northern China: An examination based on dust storm frequency from 1960 to 2003, *Geomorphology*, 81, 292–308, doi:10.1016/j.geomorph.2006.04.015.
- Washington, R., M. C. Todd, S. Engelstaedter, S. M'bainayel, and F. Mitchell (2006), Dust and the low-level circulation over the Bodélé Depression, Chad: Observations from BoDEX 2005, *J. Geophys. Res.*, 111, D03201, doi:10.1029/2005JD006502.
- Webb, N. P., H. A. McGowan, S. R. Phinn, and G. H. McTainsh (2006), AUSLEM (AUStralian Land Erodibility Model): A tool for identifying wind erosion hazard in Australia, *Geomorphology*, 78, 179–200, doi:10.1016/j.geomorph.2006.01.012.
- Wevill, T., and J. Read (2010), Fine-scale patterns in the distribution of semi-arid tree species at Wyperfeld National Park, southeastern Australia—The potential roles of resource gradients vs disturbance, *J. Arid. Environ.*, 74, 482–490, doi:10.1016/j.jaridenv.2009.10.009.
- Whitney, J. W. (2006), Geology, water, and wind in the lower Helmand Basin, southern Afghanistan, *U.S. Geol. Surv. Sci. Invest. Rep.*, 2006-5182, 40 pp.
- Wiggs, G., and P. Holmes (2011), Dynamic controls on wind erosion and dust generation on west-central Free State agricultural land, South Africa, *Earth Surf. Processes Landforms*, 36, 827–838, doi:10.1002/esp.2110.
- Wiggs, G. F. S., S. O'Hara, J. Wegerdt, J. Van Der Meer, I. Small, and R. Hubbard (2003), The dynamics and characteristics of aeolian dust in dryland Central Asia: Possible impacts on human exposure and respiratory health in Aral Sea basin, *Geogr. J.*, 169, 142–157, doi:10.1111/1475-4959.04976.
- Williams, P. L., D. L. Sable, P. Mendez, and L. T. Smyth (1979), Symptomatic coccidioidomycosis following a severe natural dust storm. An outbreak at the Naval Air Station, Lemoore, Calif., *Chest*, 76, 566–570.
- Wright, J. (2001), Making loess-sized quartz silt: Data from laboratory simulations and implications for sediment transport pathways and the formation of desert loess deposits associated with the Sahara, *Quat. Int.*, 76–77, 7–9.
- Xin, J., S. Wang, Y. Wang, J. Yuan, W. Zhang, and Y. Sun (2005), Optical properties and size distribution of dust aerosols over the Tengger desert in northern China, *Atmos. Environ.*, 39, 5971–5978, doi:10.1016/j.atmosenv.2005.06.027.
- Xuan, J., and I. N. Sokolik (2002), Characterization of sources and emission rates of mineral dust in northern China, *Atmos. Environ.*, 36, 4863–4876, doi:10.1016/S1352-2310(02)00585-X.
- Zárate, M. A., and A. Tripaldi (2012), The aeolian system of central Argentina, *Aeolian Res.*, 3, 401–417, doi:10.1016/j.aeolia.2011.08.002.
- Zarghami, M. (2011), Effective watershed management: Case study of Urmia Lake, Iran, *Lake Reservoir Manage.*, 27(1), 87–94, doi:10.1080/07438141.2010.541327.
- Zender, C. S., and E. Y. Kwon (2005), Regional contrasts in dust emission responses to climate, *J. Geophys. Res.*, 110, D13201, doi:10.1029/2004JD005501.
- Zender, C. S., D. Newman, and O. Torres (2003), Spatial heterogeneity in aeolian erodibility: Uniform, topographic, geomorphic, and hydrologic hypotheses, *J. Geophys. Res.*, 108(D17), 4543, doi:10.1029/2002JD003039.
- Zhang, X. Y., S. L. Gong, T. L. Zhao, R. Arimoto, Y. Q. Wang, and Z. J. Zhou (2003), Sources of Asian dust and role of climate change versus desertification in Asian dust emission, *Geophys. Res. Lett.*, 30(24), 2272, doi:10.1029/2003GL018206.
- Zhao, M., I. M. Held, S.-J. Lin, and G. A. Vecchi (2009), Simulations of global hurricane climatology, interannual variability, and response to global warming using a 50 km resolution GCM, *J. Clim.*, 22, 6653–6678.